Blue Hydrogen in a flexible multi-commodity energy system for ammonia production

A dynamic numerical model of blue hydrogen production in a multi-commodity energy system to produce ammonia for conceptual design and simulation purposes

MSc Thesis: Mechanical Engineering

Nicole Eulderink

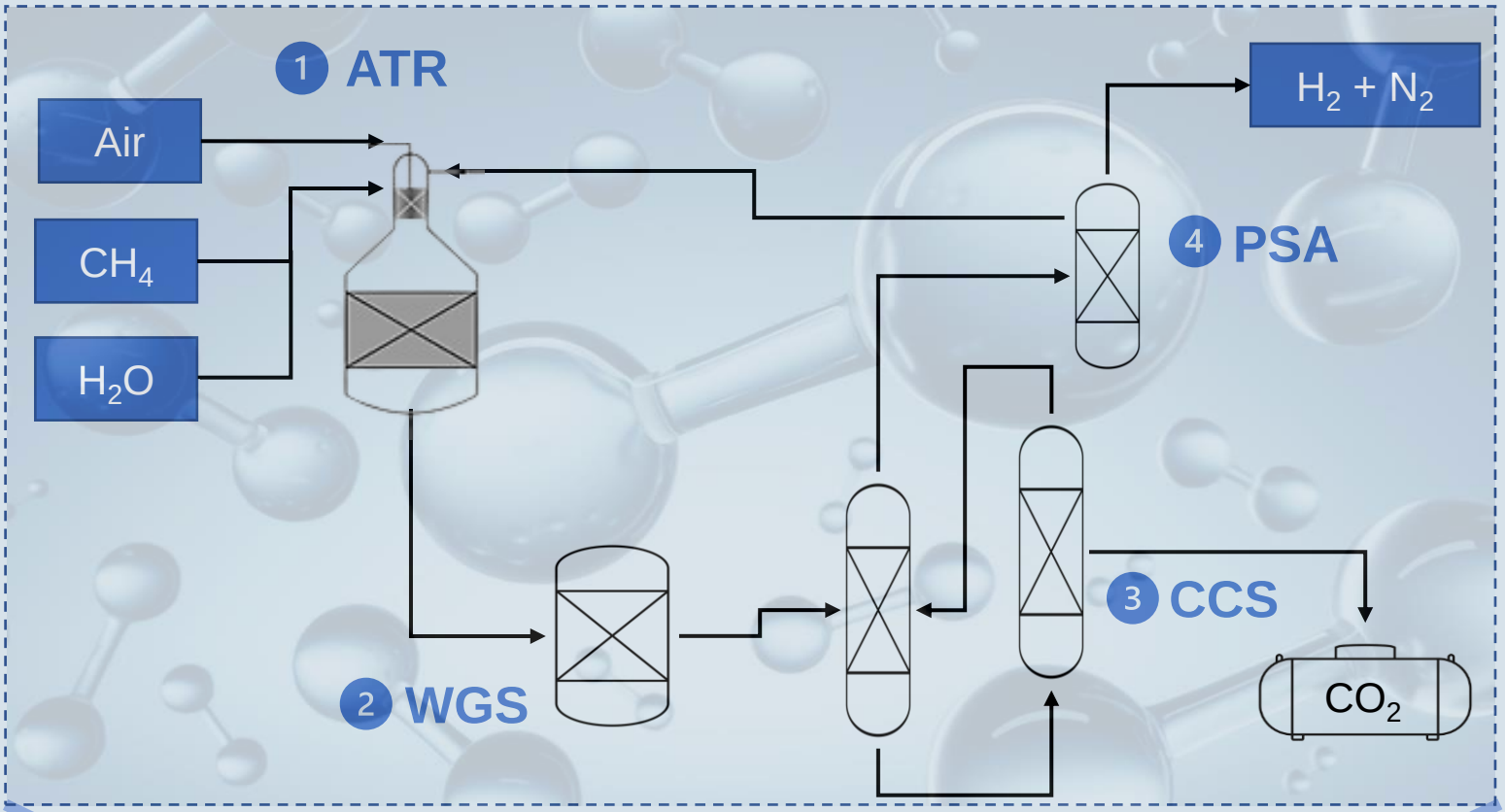

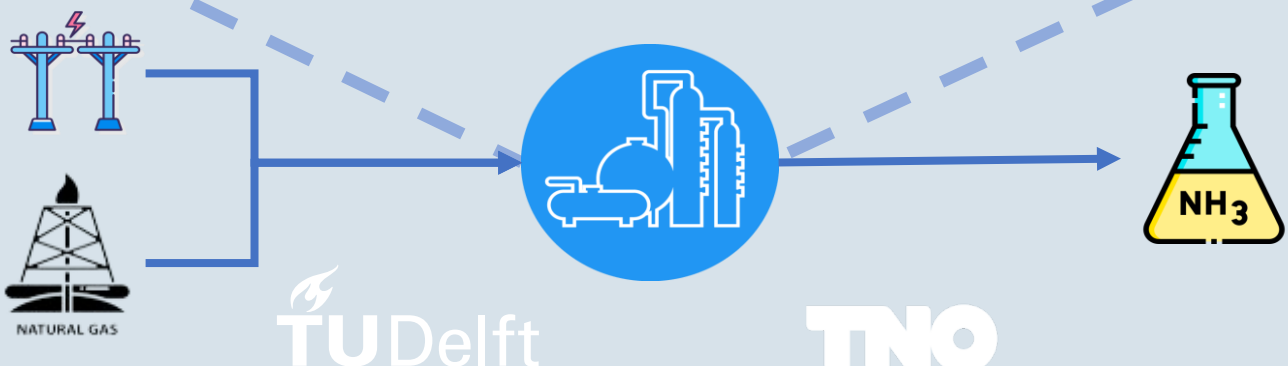

TU Delft

TNO

Blue Hydrogen in a flexible multi-commodity energy system for ammonia production

A dynamic numerical model of blue hydrogen production in a multi-commodity energy system to produce ammonia for conceptual design and simulation purposes

by

Nicole Eulderink

To obtain the degree of Master of Science
at the Delft University of Technology,
to be defended publicly on Thursday November 30, 2023.

Student Number:	4593073
TU Delft Supervisor:	Asst. Prof. Dr. Ir. M. Ramdin
TNO Supervisor:	Ir. J. Fatou Gómez
Project Duration:	February, 2023 - November, 2023
Faculty:	3ME, Delft
Department:	Process and Energy

TU Delft TNO

Preface

I was inspired to conduct this research because of the large uncertainties on how to tackle climate change in a way that is economic, quick and effective. I believe hydrogen will play a large role however affordability will always remain the main driver for large scale implementation. Therefore looking at low-carbon solutions that can already be cost-competitive in the short term with minimal carbon taxes or subsidy is very important. Comparative research like this shows the impact of certain conditions in future energy systems, giving both policy makers and investors more information to make more informed decisions. Moreover, I hope to create more awareness of the actual implications of certain operational conditions and economic decisions.

Predicting the future is a near impossible task therefore the results are subject to many specific boundary conditions and assumptions. In this research, these conditions can be easily manipulated to reflect the scenario that needs to be considered. Therefore even though this research runs only a few simulations to generate comparative outcomes, it offers a broader framework from which dozens of scenarios can be run with specific assumptions to properly compare different policy outcomes and investment risks.

I would like to give thanks to all the people who helped me throughout this thesis process. Firstly, I would like to thank my two supervisors: Asst. Prof. Dr. Ir. M. Ramdin from the TU Delft and Ir. J. Fatou Gónez from TNO. Both helped me tremendously during the process by asking critical questions and thinking along with me to solve the problems I encountered. I appreciated their dedicated involvement through frequent meetings and their large interest in the topic also increased my enthusiasm. I would also like to thank TNO for the opportunity to get to know the company and for offering me the means to pursue this research.

Lastly, I would also like to thank my family, friends and boyfriend for supporting me throughout the process especially when it got more difficult. Writing a thesis can be an overwhelming experience and therefore the support of family and the distraction of friends helps keep the process more balanced.

Nicole Eulderink
Delft, November 2023

Summary

Low-carbon hydrogen is expected to have a large role in future energy systems. Recent research shows the short-term financial feasibility of blue hydrogen is often higher than green hydrogen. Ammonia production is particularly carbon-intensive due to its hydrogen production routes. This research focuses on the physics-based modelling of blue hydrogen production for ammonia synthesis, examining the influences of varying input conditions and economic scenarios on process performance and economics. Future energy systems will rely on flexible integrated solutions, emphasizing the importance of understanding how system parameters respond to diverse input conditions.

The ammonia plant consists of a desulphurization unit, a pre-reformer, an ATR, two water gas shift reactors, a physical absorption tower for CCS, a PSA for H_2 purification and a Haber-Bosch ammonia synthesis reactor. Auxiliary components consist of heat exchangers, compressors and dehydration units. The modelling efforts focus on medium-fidelity models, reflecting the main thermodynamics and kinetics through first-order differentials assuming reactor simplifications. The plant simulations are based on plant operation in the Netherlands in 2030 under the following price assumptions: C_{NH_3}= 0.472 €/kg_{NH_3}, C_{elec}= 41.77 €/MWh, C_{NG}= 22.64 €/MWh, C_{CO_2-tax}= 0.135 €/$kg_{CO_{2_{(eq)}}}$, C_{CCS}= 0.05 €/kg_{CO_2}.

Each reactor model was separately validated through industrial data. Then the operational window was selected based on individual reactor limitations and the overall system chain performance: α=0.6, β=2.0, T_{in}=873.15K, P_{in}=2.8MPa. α and T_{in} are the most influential parameters from an economic and environmental perspective, showing the largest influence on levelized costs and emissions. Overall, under the simulated conditions, blue ammonia results in an 85% direct emission reduction compared to grey ammonia. The levelized costs of blue ammonia amount to 0.417€/kg and the NPV is 104 MEUR, the most influential economic parameters are the natural gas price and the ammonia selling price.

Three case studies were conducted in which specific economic and operational conditions were compared. Simulations of three IEA policy scenarios for 2030 show that the overall cost reduction in more sustainable scenarios is mainly driven by the lower natural gas price. Carbon taxes have a limited effect on the price of blue ammonia however do significantly increase the price of grey hydrogen compared to blue (a 0.11-0.17 €/kg difference). This results in a minimum 0.05 €/kg_{NH_3} margin for the capture process costs in the stated scenario (0.09 €/$kg_{CO_{2_{(eq)}}}$), the other scenarios give a larger margin.

Green ammonia gives a levelized cost of 0.457 €/kg NH_3 under the same economic assumptions. The NPV is -480 MEUR, which is most affected by the electricity price and ammonia price. This research yields a 9% LCOA increase for green ammonia when compared to blue. The evolution of electricity prices is paramount in the financial competitiveness of green ammonia, more so than the CAPEX evolution. The indirect emission intensity of green ammonia is lower than blue ammonia in the simulated conditions. However, this depends on the electricity source. Through carbon taxes blue and green ammonia can become cost-competitive to grey however this comes at a cost for the everyday consumer.

A simulation with dynamic operation yielded that inputting NG feed following seasonal natural gas pricing is not cost-effective when compared to steady-state production at the same seasonal pricing, even for +/-44% price fluctuations. The additional CAPEX costs for storage and larger process units are not sufficiently compensated by the lower variable OPEX costs. Further research should focus on shorter-term supply and demand matching.

Overall, it can be concluded that this model can sufficiently simulate a blue hydrogen chain and be used for further simulation cases, also with alternative economic and operational assumptions. The technical parameters that affect blue ammonia production most are α and T_{in}. Economically the ammonia and the natural gas price are most influential. In comparison with grey and green ammonia, under the simulated conditions, blue hydrogen is the most cost-effective. Finally, the economic incentives through the seasonality of natural gas prices do not justify a dynamic operation of the process plant.

Contents

List of Figures

List of Tables

Nomenclature

Abbreviations

Abbreviation	Definition
1D	One-dimensional
2D	Two-dimensional
3D	Three-dimensional
amp	Amplitude
ASU	Air Separation Unit
ATR	Autothermal reformer
CAGR	Compound Annual Growth Rate
CAPEX	Capital Expenditure
CCS	Carbon Capture and Storage
CCUS	Carbon Capture, Usage and Storage
CEPCI	Chemical Engineering Plant Cost Index
CFD	Computational Fluid Dynamics
Comp	Compressors
CPOx	Catalytic partial oxidation
DCFA	Discounted Cash Flow Analysis
GHG	Green House Gasses
HB	Haber-Bosch
HEX	Heat Exchanger
HTWGS	High Temperature Water Gas Shift
IEA	International Energy Agency
IPCC	Intergovernmental Panel on Climate Change
LC	Levelized Cost
LCOA	Levelized Cost of Ammonia
LCOH	Levelized Cost of Hydrogen
LHV	Lower Heating Value
LNG	Liquid Natural Gas
LTWGS	Low Temperature Water Gas Shift
LUMM	Lagrange Undefined Multiplier Method
MEUR	Million euros
MS	Marshall Swift
NG	Natural Gas
NPV	Net Present Value
NZE	Net-Zero Emission
O&M	Operation and Maintenance
OPEX	Operating Expenditure
PORTHOS	Port of Rotterdam CO2 Transport Hub and Offshore Storage
POx	Partial Oxidation
PPA	Power Purchasing Agreement
ppm	Parts per million
PSA	Pressure Swing Adsorption
R&D	Research and Development
RE	Renewable Energy
Replace	Replacements
SEA	Standardized Economic Assessment
SMR	Steam Methane Reformer

Abbreviation	Definition
Syn	Synthesis
TNO	Nederlandse organisatie voor toegepast-natuurwetenschappelijk onderzoek
TRL	Technology Readiness Level
USD	US Dollars
WGS	Water Gas Shift

Symbols

Symbol	Definition	Unit
Roman		
C	Cost	[MEUR]
c_{p}	Specific heat capacity	[J/K]
COP	Coefficient of performance	[-]
E_{a}	Activation energy	[J/mol]
f	Factor	[Variable unit]
H	Enthalpy	[kJ/mol]
H_{s}	Henry's law constant	[MPa]
K	Equilibirum constant	[Variable unit]
k	Kinetic rate constant	[Variable unit]
L	adsorbent loading	[mol/kg]
l	Power law exponent CO	[-]
LC	Levelized Cost	[€/kg]
$\dot{m}$	Mass flow rate	[kg/s]
M	Maximum adsorbent loading	[mol/kg]
m	Power law exponent H_2O	[-]
MW	Molecular weight	[mol/kg]
$\dot{n}$	Molar flow rate	[mol/s]
N	Counter	[Variable unit]
n	Power law exponent CO_2	[-]
NPV	Net Present Value	[MEUR]
o	Power law exponent H_2	[-]
P	Product revenue	[MEUR]
p	Partial pressure	[Pa]
P_{rev}	Revenue	[€]
q	Quantity	[kg]
Q	Capacity	[Variable unit]
R	Rate	[Variable unit]
r	Conversion rate	[-]
R_g	Gas constant	[J/mol/K]
S	Entropy	J/K
t	Time	[Variable unit]
T	Temperature	[K]
$\dot{V}$	volumetric flow rate	[m^3/s]
$\frac{V}{F}$	Vapour-feed ratio	[-]
x	Conversion	[-]
z	mass fraction in feed	[-]
Greek		
α	Oxygen-to-methane ratio	[-]
β	Steam-to-methane ratio	[-]
γ	heat capacity ratio	[-]

Symbol	Definition	Unit
Δ	Difference	[-]
ζ	Conversion factor	[-]
η	Efficiency	[-]
θ	Equilibrium convergence factor	[-]
ξ	Financial correction factor	[-]
ρ	Density	[kg/m^3]
χ	solubility	[mol/(kg $\cdot$ MPa)]
Ω	Adsorption factor	[-]
Subscript		
abs	absorption	
atm	Atmospheric	
aux	Auxiliary	
base	Base value	
capture	Carbon capture	
cat	Catalyst	
comb	combustion	
comp	Component	
compr	Compression	
d	Discount	
desorb	Desorption	
Elec	Electricity	
eq	equilibrium	
evap	evaporation	
FT	Flash tank	
furnace	Furance	
gas	Gas	
HEX	Heat exchanger	
i	Molecular component	
in	Input	
inert	Inert	
infl	Inflation	
initial	Initial	
liq	liquid	
max	maximum	
new	New value	
oxi	Oxidation	
out	output	
p	Pressure	
pump	pump	
reac	Reaction	
req	Required	
s	Scaling	
sol	solution	
solvent	solvent	
T	Temperature	
t	operating	
transfer	Transfer	
util	Utilization	
Molecules		
Al	Aluminium	
Ar	Argon	
CH_4	Methane	

Symbol	Definition	Unit
CO	Carbon monoxide	
CO_2	Carbon dioxide	
Cr	Chromium	
Cu	Copper	
ceFe	Iron	
H_2	Hydrogen	
H_2O	Water	
K	Potassium	
N_2	Nitrogen	
NH_3	Ammonia	
O_2	Oxygen	
Zn	Zinc	

1 Introduction

Compared to pre-industrial level, the global average temperature has risen by 1.08 °C, and is projected to rise up to 1.5 °C in the early 2030s. This rise has resulted in an increase in natural disasters which have led to many negative humanitarian consequences (IPCC Working Group II, 2022). In order to combat climate change, immediate carbon-reducing actions are necessary in all sectors. Many researchers believe hydrogen will play a key role in the energy transition; both in its current form as feedstock for industrial processes but also as a future large-scale energy carrier (e.g. IEA (2019c), Oshiro and Fujimori (2022)). Hydrogen and specifically low-carbon hydrogen have received more attention over the past few years both in the private (Hydrogen Council, 2022) and public sector (Fazioli & Pantaleone, 2021). Hydrogen is an attractive fuel source due to its favourable chemical properties: highly combustible, carbon-free, and largely available in different molecular forms. As an energy carrier it is also attractive due to its high energy content per weight (Møller et al., 2017). To reach the Net-zero emission (NZE) goals, IEA (2022a) predicts globally the absolute amount of low-carbon hydrogen that will need to be produced in 2050 is almost 6 fold the total hydrogen production in 2020 (accounting for 10% of the projected total energy consumption worldwide in 2050). In the Netherlands, the hydrogen demand will also most likely grow in the coming 30 years, past research has estimated a total growth varying from 100 PJ/yr up to 1700 PJ/yr by 2050, in which the distribution over the sectors is still highly debatable. However, all past research predicts growth in the industrial sector (Detz et al., 2020). The actual growth of the hydrogen markets in the different sectors is strongly dependent on the generation of affordable low-carbon hydrogen. Moreover, it is dependent on the large-scale integration of hydrogen into the entire value chain (Mac Dowell et al., 2021). To account for the intermittency and fluctuations of the future energy mix, integrating flexible multi-commodity energy systems is becoming more important.

1.1. Hydrogen

Hydrogen is currently mainly produced from fossil fuels. Grey hydrogen (from natural gas) accounts for approximately 76% of the international hydrogen production (IEA, 2019c), coal accounts for 23% (majority of coal-based production in China (Chai et al., 2021)) and the final 1% is produced through other routes like electrolysis and oil. This production mix resulted in approximately 900 Mt of CO_2 emissions in 2022 (IEA, 2023b). Therefore a growth in low-carbon hydrogen production is essential if hydrogen is going to play a role in the energy transition.

1.1.1. Low-carbon hydrogen

The two main low-carbon routes are green and blue hydrogen. Green hydrogen refers to the production through electrolysis powered by renewable energy. Blue hydrogen refers to the production in the traditional manner (through fossil fuels) however partially capturing the produced CO_2 and then storing it long-term to make sure it is not released into the atmosphere.

The large-scale implementation of green hydrogen and its environmental impact is very much dependent on the technological advancements in electrolyzers and the capacity of renewable energy.

Green hydrogen cannot be considered green if the electricity source used to produce it is taken from a carbon-intensive grid. Moreover, the TRL (Technology Readiness Level) of green solutions is relatively low (IEA, 2021). Due to its novelty, there are more uncertainties in the long-term performance and upscaling of the technology. Currently, green hydrogen is often not cost-competitive with grey or blue hydrogen without heavy subsidies. However, green hydrogen has no direct emissions and electrolyzers are much more flexible to fluctuating input conditions than large-scale reactors. Moreover, the feed for green hydrogen is water so it has no upstream emissions. Finally, the technological advancements in electrolyzers are large. Green hydrogen therefore has great potential in the longer term of affordably decarbonizing hydrogen production without large subsidies (Detz et al., 2019).

Blue hydrogen is the second promising decarbonizing option. This option is attractive due to its relatively simple retrofitting options for existing processes. In general, this process is less costly to implement and also reduces direct carbon emissions significantly compared to grey hydrogen. For countries with limited space and access to renewable energy, it is a good way to decarbonize. However, the sequestration of carbon dioxide is at medium TRL, which could result in technical difficulties. Large-scale CCS pilots are being rolled out worldwide. In the Netherlands, PORTHOS is planned to become operational in 2026 with a 37 Mt capacity for CO_2 storage (PORTHOS, 2023). The second downside of blue hydrogen versus grey is that the capture process requires extra energy and process steps, which also has a financial impact. Capture rates close to 100% have only been proven feasible in theory due to technical and economic bottlenecks (M. Lyons et al., 2021). Current large-scale deployments have capture rates of 60%-80% (M. Lyons et al., 2021). However, on a smaller scale, cost-effective pre-combustion CCS processes capture about 85% to 93% in commercial set-ups (Jansen et al., 2015). The current form of CCS always results in some direct CO_2-emission and the balance between economic and environmental implications will ultimately decide the capture rate. Moreover, upstream emissions from fossil fuels also contribute to the indirect emissions.

To make either of these technologies competitive with conventional hydrogen the cost gap should be compensated through subsidies for green initiatives or additional taxes for non-green processes (Mac Dowell et al., 2021). It is essential to find an optimum between the timeline, economics and environmental impact when investing in solutions. Past research has shown that the feasibility of low-carbon solutions in the shorter term is much higher for blue hydrogen than for green. These feasibility studies are based on both economic and technical factors, especially in areas with a limited capacity for renewable energy or very low natural gas prices (Mayer et al. (2023), Tetteh and Salehi (2023), Collodi et al. (2017)). However, in the long-term, both solutions will have to be applied simultaneously to reach the desired emission reduction (IEA, 2023b). The Dutch Ministry of Economics and Climate stated the expectation that, for the Dutch evolution of the energy mix, from 2035 onwards green hydrogen will become feasible. This suggests before 2035, alternatives like blue hydrogen are the preferable low-carbon path (EZK, 2023).

1.1.2. Hydrogen market

Globally, 95 Mt of hydrogen was produced in 2022, mainly for industrial applications and refineries (IEA, 2023b). The Netherlands currently follows a similar pattern to the global shares with 35.7 % of the produced H_2 going to refineries (approximately 0.54 Mt yearly) and 35.1 % to the production of ammonia (approximately 0.53 Mt), the remaining share is split over multiple industries (methanol, steel production etc.) (Detz et al., 2020). The hydrogen demand for refineries is likely to shrink due to the expected decrease in oil demand (IPCC Working Group II, 2022).

The ammonia market, on the other hand, is projected to have a global compound annual growth rate (CAGR) of 7.22% till 2030 (ChemAnalyst, 2023). This growth is mainly driven by population growth and the consequential agricultural demand growth, 70% of all ammonia produced currently is used to produce fertilizers. The environmental regulatory landscape restrains the increase due to the climate impact of ammonia and the possible health hazards (INDEXBOX, 2022).Klijn (2023) (Minister of Foreign Affairs) emphasizes the future role of ammonia as a hydrogen carrier in the Netherlands. Ammonia is easier and safer to transport than pure hydrogen and can be locally cracked to form hydrogen again. This would lead to an increase in global imports and exports of ammonia. IEA (2023b) also identified ammonia as the first mover in the large-scale hydrogen carrier sector, with multiple projects announced

for 2030. The Netherlands and Germany are the two main European ammonia exporters accounting for more than two-thirds of all European exports (INDEXBOX, 2022), however, the global export and import market is currently limited to 10% of all ammonia produced (IEA, 2023b). Ammonia as a hydrogen carrier could prove to have a large influence on how the ammonia market develops further and could overtake the conventional role of ammonia in the longer term.

Ammonia production

Ammonia is predominantly produced through Haber-Bosch (HB) synthesis. Hydrogen is mixed with nitrogen at high pressure and forms ammonia. Ammonia production is a very carbon-intensive process, it has almost two times more direct emission intensity than crude steel processing (Pagani et al., 2022). In 2020, the ammonia sector accounted for 1.3 % of anthropogenic global emissions, with approximately 450 Mt of direct emissions. These emissions are projected to double by 2030 if just the current stated policies are followed through (IEA, 2021). The majority of the emissions released during the ammonia production process are emitted during the production of hydrogen. Efforts in decarbonizing the hydrogen production process therefore also have a large impact on the net direct emission of ammonia. Therefore utilizing more sustainable low-carbon process routes to produce ammonia is paramount to limit its further effect on climate change, whilst still meeting the growing demand due to population growth.

All decarbonization efforts currently being pursued in the ammonia production business lead to an increase of costs of 10% to 100% (IEA, 2021). Therefore policymakers also have an essential role in the realization of a low-carbon future. The International Energy Agency (IEA) has made projections for three climate scenarios: the Stated Policies Scenario, the Pledged Policies Scenario and the Net-Zero Emission (NZE) Policy Scenario. The first follows the current trends and only officially implemented policies are taken into account for its projections. The second also includes the trends following from what policies countries have announced or pledged to implement however are not yet enforced. The third (NZE) is a scenario projecting a possible route to reach net-zero emissions by 2050 and the required policies for this specific route. They all reflect a large role for ammonia in the future energy system, however, the share and role of the different low-carbon production routes vary. This research will focus on the production of blue hydrogen from natural gas to produce ammonia.

1.2. Multi-commodity energy systems

The integration of energy systems is likely to become more important in future energy systems as no solution is expected to be fully suitable on its own. Ideally, energy systems are sustainable, affordable, reliable and flexible. To meet these demands at all time, most researchers agree that the solution is most likely an integration of multiple technologies in parallel. The intermittency of renewable energy and the large deviations in the supply and demand market call for more research on the effects of certain dynamic parameters on the operation of these integrated systems (Arent et al., 2021).

Financial, environmental and technical synergies can be reached by integrating energy systems and properly operating them (Garcia et al., 2013). Models that can flexibly predict the behaviour of integrated energy systems offer a possible acceleration route for the energy transition. In the long run, these models can adopt machine learning techniques to improve their asset management and operations even further (Manfren, 2012). All in all, future energy systems are likely to consist of more hybrid multi-commodity set-ups, in which proper modelling of the behaviour of these systems beforehand can have a significant environmental, economic and technical impact. Currently, there is a lack of models that can simulate the behaviour of flexible multi-commodity energy systems through a chain of physics-based models whilst taking in dynamic inputs and outputs and boundary conditions.

1.3. Research Questions

In this research, the multi-commodity chain that is focused on is the production of blue hydrogen to be used for ammonia synthesis. The focus is put on both the influence of operational conditions on sub-models and the chain as a whole. Moreover, the model can easily be manipulated to execute comparative studies for different operational and economic case studies. The main research question is:

What influence do operating conditions and financial scenarios have on a technical and economic level for a physically modelled, flexible multi-commodity system for blue hydrogen used to produce ammonia?

1.3.1. Sub-Questions

Some supporting sub-questions were formulated in support of answering the main research question and 3 case studies were generated:

- How do the different process units and the chain as a whole respond to variations in input conditions?
- What input parameters are most influential in the operation of a blue hydrogen process for the synthesis of ammonia?
- What is the economic and environmental performance of the system as a whole?
- What are the financial implications of the three IEA energy scenarios for this production chain?
- How does blue ammonia compare to green ammonia?
- Does a possible price seasonality warrant a system set-up with storage capacity?

1.3.2. Thesis outline

This chapter has presented the possible role of hydrogen in the future energy system, specifically for the production of ammonia. It has presented the relevance of decarbonizing this sector in the short term and the added value of dynamic multi-commodity energy system modelling to support future energy systems. After which the main research question and sub-questions have been presented. In chapter 2, a literature review is given in which the process flow diagram is motivated and the past research on the topic is shortly summarized, focusing on past modelling efforts. In chapter 3, the research method is explained, then the basis for all models and their assumptions are presented and finally the method for generating results. In chapter 4, the results are presented in graphical and tabular format and the outcomes and their implications are discussed. Chapter 5 discusses the limitations of the research and their consequences for the outcome. Lastly, chapter 6 summarizes the entire research and gives the key conclusions in light of the research question. Thereafter some recommendations are formulated for further research directions.

2

Literature review

In this chapter, a literary review will be presented discussing the process flow diagram design. After which, past process modelling efforts per sub-component will be presented and their typical operational windows. Finally, past process integration and evaluations on both performance and economic levels will be summarized.

2.1. Conceptual Process Design

Following the basics of design, first, a description of the boundary conditions of the design is established. After which, a simplified block scheme is given to summarize the inputs, outputs and boundary conditions. Then per unit of operation, the options are compared and the most suitable is selected. This will result in a more extensive process flow diagram.

2.1.1. Design conditions

The design process was based on the hierarchical design method by Douglas (1985). This design method focuses on the choice of the main components first and then iteratively adds other components whilst optimizing the outcome based on boundary conditions. Boundary conditions are necessary to limit the options per step. Four initial boundary conditions are set in this process design: the plant is built in the Netherlands and planned for 2030; the inlet feed consists of natural gas and auxiliary input, often an oxidant: water and/or air; the final product is ammonia and the carbon must be captured and treated to meet storage and further transport requirements.

Location and time

The plant design and simulations are run based on the assumption that the location is the Port of Rotterdam. This choice was made because it is a pre-existing large industrial cluster, therefore the option for retrofitting existing plants and possibly generating synergies with other industrial parties is possible. Moreover, the pressure for processes to become more sustainable could prove to be a driver for the reinvestment of industrial ground into more sustainable processes.

Secondly, the port of Rotterdam has easy access to import and export routes. Therefore the uncertainty in the market evolution of natural gas and the ammonia market offers more flexible access to LNG imports and possible ammonia export. Moreover, the Port of Rotterdam is planned to have easy access to PORTHOS, one of the large-scale CCS projects in the Netherlands. Therefore limiting possible CO_2-transport costs and offering the advantage of a combined CO_2 purity with other processes to meet the PORTHOS CO_2 specifications (appendix A).

The realization of the project is simulated to be completed in 2030. Firstly due to logistical reasons, the actualization of such a large-scale project requires time, therefore earlier timeline is not realistic. Moreover, most literature makes projections for emission regulations, feed prices and technology development by 2030. This makes the comparison to other literature and the price assumptions easier. Furthermore, climate change requires swift action so research into short-term solutions for 2030 is

important for both private and public sectors. It is believed that to meet emission goals by 2050, blue hydrogen is necessary by 2030 to bridge the gap for affordable green hydrogen (Dickel, 2020). By 2050, green hydrogen is projected to be a lot less expensive if the hydrogen market takes off (IEA, 2022c). Finally, as the projection is extended further into the future, the margin of error in our assumptions regarding the technology and price developments tends to increase.

Inlet feed

Natural gas (NG) was selected as inlet feed. As previously mentioned, with a 72%- share, the majority of the ammonia produced worldwide in 2021 was produced from natural gas (IEA, 2021). Implementing blue ammonia solutions from natural gas therefore has more potential impact than from other fossil fuels. Moreover, this offers organizations the option to retrofit current set-ups without completely changing their production strategy. Finally, because this is a relatively less polluting feed stream than other fossil fuels used to produce hydrogen, it is therefore also least likely to be phased out soon (EIA, 2023).

Many different theories on how the NG market will develop have arisen over the years. The Ukraine war and earthquakes in Groningen for example, have shown the (geo)political influences on the market (Ministry van Economic Affairs and Climate Policy, 2022). Moreover, the growing ease of import and export due to the development of liquid natural gas (LNG) storage and transport (IEA, 2023a) and the large-scale electrification of many industries (Nandakumar & Annaswamy, 2017) show the technical influence on market development. Finally, the environmental concerns around natural gas also influence the market development. This leads to large uncertainties in the projections of the natural gas market for 2030. In this research, the IEA pledged energy scenario for Europe is taken as a base case for the market assumptions for NG, which will be touched upon further in chapter 3.

Product: Ammonia

There are multiple production routes for ammonia synthesis, however, the Haber-Bosch process is predominantly applied (>96%) (C. Smith et al., 2020). The Haber-Bosch process offers both economic and technical benefits because it is a very mature process. Ammonia is synthesized by mixing nitrogen and hydrogen with the right composition under the right conditions (pressure and temperature). The chemical reaction is given by reaction 2.1. The simplified reaction flow sheet is given in figure 2.1.

$$N_2 + 3\,H_2 \rightleftharpoons 2\,NH_3; \qquad \Delta H_{298K} = \text{-}92.4\text{kJ/mol} \tag{2.1}$$

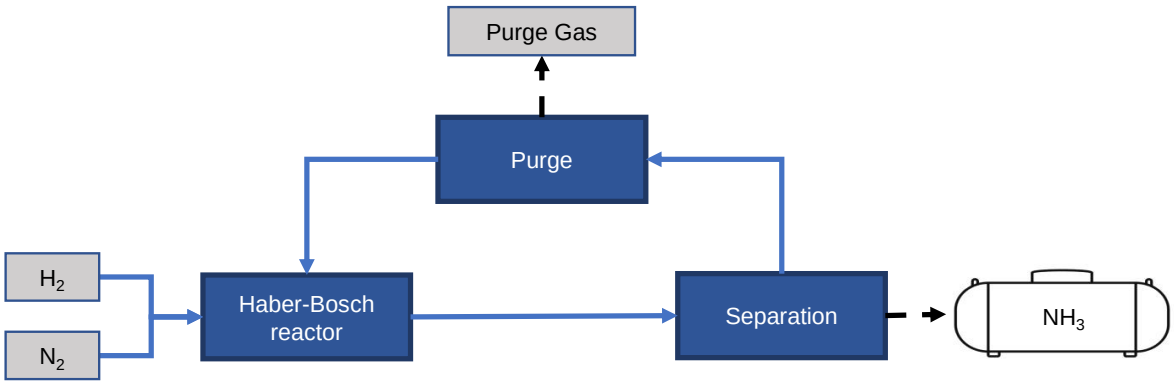

Figure 2.1: Standard process flow sheet for ammonia synthesis through the Haber-Bosch process

Operating Conditions

The Haber-Bosch process operates at a 400 - 450 °C temperature, with a pressure of 150 - 250 bar and the reactor often contains an iron-based catalyst on K_2O promoter for chemical and thermal stability (Rouwenhorst et al., 2021). The conversion yield is relatively low per round: approximately 15% (C. Smith et al., 2020). This is due to the 'Le Chatelier's principle' (Le Chatelier, 1884); a higher conversion is expected at lower temperatures and higher pressure. However, lowering the temperature

results in much slower reaction kinetics. Therefore, a compromise in the operating conditions is always made. Moreover, the pressure increase yields a shift towards ammonia also enhancing the reaction thermodynamics but compression requires a large amount of energy and increases the CAPEX of all process equipment due to the necessary pressure resistance, thus also requiring compromise. The Haber-Bosch process has a total shut-down and start-up time of several days (Morgan et al., 2017).

The catalyst enhances the reaction rate however is very sensitive to degradation, for this reason, the level of impurities must be low. Catalyst poisoning occurs in the presence of oxygen, water, carbon monoxide or carbon dioxide, this results in quick deactivation, leading to higher maintenance and replacement costs and slower reaction kinetics. After about 15% has been converted, the outlet feed is cooled to a temperature below -20 to -30 °C, so that ammonia condenses and is easily separated (Rouwenhorst et al., 2021). After this, the unreacted gas is partially purged and the majority is recycled back into the reactor after being reheated (C. Smith et al., 2020), this leads to an eventual conversion yield of about 99% (Cha et al., 2021).

The process leads to the following boundary conditions: the composition of H_2:N_2 that is fed to the reactor is 2:1 (Amhamed et al., 2022) or 3:1 (stoichiometric) (C. Smith et al., 2020) dependent on the flow velocity. Impurity levels should be very low, a maximum of 2 vol% of methane is allowed in the reactor and the total amount of carbon oxides should be below 50 ppm to protect the catalyst. The amount of inert gases can vary from 0 - 15 mol%. The more impurities, the larger the purge stream will be, which is not advantageous for yield nor environmental impact (Cheema & Krewer, 2018). Past research on process optimization has shown that the operation of the synthesis loop at approximately 200 bar with a 3:1 ratio, a high feed flow rate and low levels of impurities is advantageous. These inputs form boundary conditions for the output of the hydrogen production process.

Carbon capture usage and storage

To produce blue hydrogen, the integration of a carbon capture method in the process is necessary. Carbon capture, usage and storage (CCUS) consist of three main steps: capture, transport and storage/usage. CCUS aims to limit the amount of CO_2 released into the atmosphere. The capture step tends to be the most cost-intensive part of the process, the higher the partial pressure of the CO_2 in the mixture entering the capture unit, the easier it is to reach higher capture rates or make the process less cost-intensive. After capture, the CO_2 is purified and compressed for transport. Transportation is done by pipelines, ships and railroads depending on the location of the emissions and the final storage destination. Next, it is stored in multiple possible sites, of which geological storage and 'beneficial usage' are the two most mature options. A summary of the CCUS process and alternative technologies is given in figure 2.2 copied from Muradov (2014), the bold options are the technically more mature options.

It is important to mention that although these technologies claim to be mature, not many large-scale CCUS projects have been executed to date. Storage in depleted gas fields, for example, still has many challenges to overcome politically, technically and financially (Raza et al., 2019). Moreover, CO_2 beneficial usage seems like a good alternative, however, the scale and the long-term CO_2 reduction are limited. The amount of CO_2 that was reused in 2018 was 230 Mt globally (IEA, 2019b), and the amount emitted was 33.1 Gt (IEA, 2019a), indicating the scale of the gap. Furthermore, the reuse of CO_2 can be argued to be a delay of emissions as they are still often released in a later stage (IEA, 2019b), therefore not offering a long-term solution. CO_2 usage results in an average of 13% emission reduction compared to the reductions from storage (Malischek & McCulloch, 2021). These issues are considered outside the scope of this research. It is assumed by 2030 large-scale storage in depleted gas fields will be technically possible and financially affordable.

Operating Conditions

The scope of this research is bounded by the product conditions that must be met for CO_2 transportation to a larger central compression station by pipeline. The conditions for transport are based on scientific literature and the commercial information available for the PORTHOS project. PORTHOS is the largest CCS initiative in the Netherlands, in which they plan to transport carbon offshore and store it in depleted

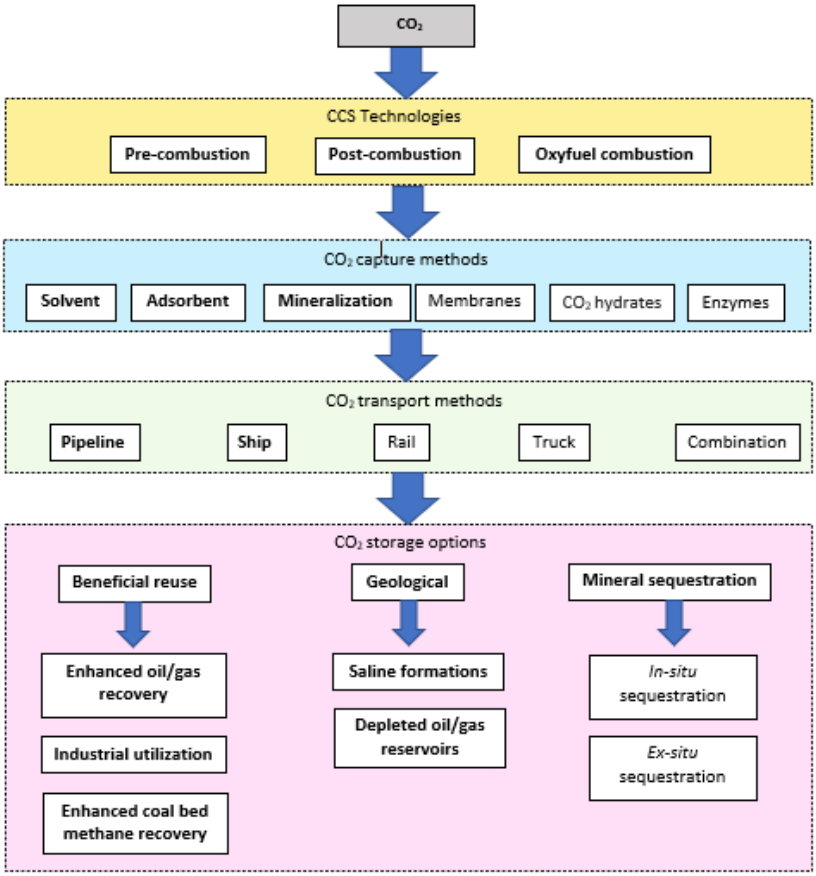

Figure 2.2: CCS process steps and technical options copied from Muradov (2014), bold represent mature technologies, less mature storage options were not considered in this research.

gas fields under the North Sea. CO_2 that is captured from a gaseous mixture is often transported in a compressed form, at a pressure of 100-135 bar to the storage location (Muradov, 2017). Impurities like water and sulphur must be removed before transport, as these form corrosion risks for pipeline transport, especially under high pressure.

In the PORTHOS project, a central compression station is situated in the Port of Rotterdam. After capture, the CO_2 must be compressed to 35 bar to be transported to the central compression station. The client must comply with certain purity conditions before being able to enter the central transport to the compression central: The stream must consist of at least 95 mol% CO_2 and a maximum combined impurity of 4 mol% of H_2, N_2, Ar, CH_4, CO and O_2. Specific impurity conditions for PORTHOS are presented in appendix A. The most important is that the water content should be below 70 ppm and the H_2 content should be below 0.75 mol% (PORTHOS, 2020). The transport and storage are estimated to cost €0.05 per kg of CO_2 in total (Fuller & Spence, 2020).

Block-flow diagram

The summarized block-flow diagram is given in figure 2.3, with the mentioned boundary conditions summarized in the figure.

2.1.2. Selection of unit operations

In this section, a summary is given on what units of operation were selected per process step and why.

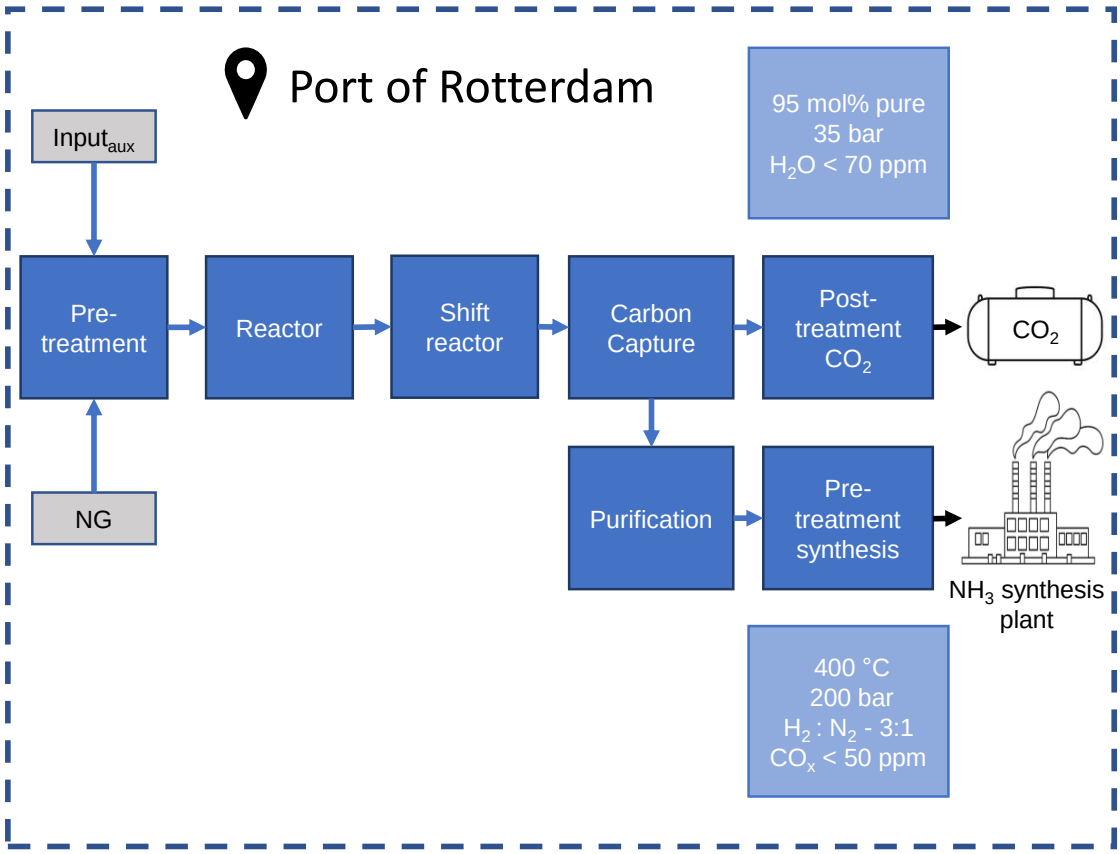

Figure 2.3: Process block diagram (darker blue) with imposed boundary conditions (lighter blue).

Main reactor

According to the Douglas (1985) method, the main reactor is the first to be selected. Three main reactor options are mature and applicable at a large scale for the production of blue hydrogen from methane with CCS. These three main process reactors are: the steam methane reformer (SMR), the partial oxidation reactor (POx) and the autothermal reformer (ATR) (Ersoz et al., 2006).

SMR

Steam methane reforming is the most conventional and widely applied reforming process for the production of hydrogen (Bahadori & Kashiwao, 2019). The reactor takes in water and methane as feed and this is converted into hydrogen, carbon monoxide and carbon dioxide. The main reaction is given in formula 2.2, due to its endothermic nature, the reactor is dependent on an external heat source to power the main reaction. Traditionally this heat is supplied through the burning of flue gas and natural gas, generating more CO_2 emissions (Palma et al., 2017). Besides the main steam methane reforming equilibrium reaction, a secondary slightly exothermic reaction namely the water gas shift reaction also takes place simultaneously (formula 2.3). Depending on the reactor conditions, the product ratios move towards a certain equilibrium condition (Fahim et al., 2010).

$$\text{SMR:} \quad CH_4 + H_2O \rightleftharpoons CO + 3\,H_2; \qquad \Delta H_{298K} = 206.1 \text{ kJ/mol} \tag{2.2}$$

$$\text{WGS:} \quad CO + H_2O \rightleftharpoons CO_2 + H_2; \qquad \Delta H_{298K} = \text{-}41.15 \text{ kJ/mol} \tag{2.3}$$

A large amount of research has been done in the field of optimization of the operating conditions for an SMR plant. Overall, standard conditions for this reaction is a temperature range of 700-900 °C (Carapellucci & Giordano, 2020) at a pressure of 5-40 bar (Parkinson et al., 2019). With higher pressure, a higher temperature is required but the reaction kinetics are enhanced (Palma et al., 2017). Industrially a nickel catalyst is the most used, Meloni et al. (2020) have reviewed the recent advances in the Ni catalyst performance in reformers. The steam-to-methane molar ratio is between 2.5 and 5. By maintaining a H_2O:CH_4 ratio above 2.5 the coke formation is suppressed (Fahim et al., 2010), coke formation leads to catalyst deactivation which in turn leads to slower reaction rates (D. Chen et al., 2001).

SMR has a hydrogen-to-carbon outlet ratio of approximately 3, this is seen as one of the main advantages of the SMR process (Meloni et al., 2020). Other advantages include relatively low operating temperature and extensive industrial experience (Ma et al., 2019). However, SMR also has disadvantages. The reactor needs to be brought to a high temperature very gradually, resulting in a start-up time of the order of days to reach a steady state operational condition (Rostrup-Nielsen & Christiansen, 2011), this decreases the flexibility of the system. Maintaining this high temperature and preheating the large volume of steam makes SMR an energy-intensive process. Moreover, the reactor size is relatively large due to the temperature control and steam presence (Meloni et al., 2020). Lastly, a large disadvantage is that the CO_2-emission takes place at two locations. To reach capture rates of 90% two capture sites are necessary and the capture of low partial pressure CO_2 is necessary, which is expensive and technically challenging.

POx

The second hydrogen production process considered is partial oxidation. This process can be run with or without a catalyst. The reactor takes in methane and oxygen as feed, the reaction is exothermic, therefore no external heat source is necessary for the reactor. Previous research has shown increased interest in catalytic partial oxidation (CPOx) due to the lower temperature regime in the reactor (Carapellucci & Giordano, 2020). The main reaction that takes place in the reactor is presented in reaction 2.4.

$$\text{POx:} \quad CH_4 + 0.5\,O_2 \longrightarrow CO + 2\,H_2, \qquad \Delta H_{298K} = \text{-35.7 kJ/mol} \tag{2.4}$$

In a non-catalytic reactor, the reaction temperature varies from 1100 - 1500 °C at high pressures: 50-70 bar (York et al., 2003). For catalytic partial oxidation process, the temperature is lower: 600 °C (Carapellucci & Giordano, 2020) - 1000 °C (Palma et al., 2017), which is a significant decrease. The reaction is more favourable at low pressures when a catalyst is present: atmospheric pressure (1 bar) and an oxygen-to-carbon ratio of 0.6 is maintained (M. W. Smith & Shekhawat, 2011). Amirshaghaghi et al. (2010) found the significant impact of the oxygen-to-carbon ratio: with a decrease in the O_2:CH_4 ratio, the H_2:CO ratio increases significantly. However, with ratios lower than 0.5 coke formation is stimulated (Ávila-Neto et al., 2009). The increase of pressure results in lower catalytic conversion and selectivity (Christian Enger et al., 2008), (York et al., 2003). Multiple reviews on the suitability of catalysts have been performed over the years (e.g.Christian Enger et al. (2008), Ma et al. (2019), Siang et al. (2022)). Meloni et al. (2020) claim that Nickel-based catalysts are the best choice for POx, in this having the right operational conditions is essential (York et al., 2003). However other researchers claim there is no clear superior choice (Ma et al., 2019). POx yields a Hydrogen-to-carbon ratio of 2 (York et al., 2003). M. W. Smith and Shekhawat (2011) have identified the ideal reaction conditions for CPOx, based on hydrogen yield, methane conversion and limited coke formation, to be above 800 °C.

The high temperature of the reaction is a major drawback for non-catalytic partial oxidation, this makes controlling the system complex. Moreover, the non-uniform temperature distribution creates hot spots and can trigger unwanted side reactions (Palma et al., 2017). For catalytic partial oxidation, the temperature is lower so hydrocarbon cracking does not occur. However, hot spot formation still creates problems on the catalytic surface, resulting in coke formation and catalyst deactivation (Carapellucci &

Giordano, 2020). Industrial implementation of catalysts is still limited due to selectivity, catalyst preservation and costs. In the application of ammonia synthesis, reactors that operate at a high pressure offer an advantage, therefore CPOx is less suitable (Bharadwaj & Schmidt, 1995). The advantage of the (C)POx process is that the reaction tends to be very quick (less than 1 second) resulting in more flexibility and shorter start-up time. However, due to this highly exothermic nature, safety issues are also a concern (Ma et al., 2019). At high temperatures the reaction occurs with an almost stoichiometric feed ratio which is another advantage (Vernon et al., 1990), this is easier to obtain for CPOx than POx (Ma et al., 2019). Moreover, the partial oxidation reactor is small (Bharadwaj & Schmidt, 1995); heat recovery from the system is, on the other hand, more complex (Palma et al., 2017). The final disadvantage of POx, specifically for ammonia production is the low hydrogen-to-carbon ratio and the costs of the pure oxygen feed (Ma et al., 2019). POx is generally applied more in the absence of a pre-reformer or when the input consists of higher hydrocarbons (Muradov, 2017).

ATR

ATR (autothermal reforming) is the third reactor that is considered. The type of ATR is dependent on the oxidant used: H_2O or CO_2. ATR is a process that reforms hydrocarbons by combining the steam methane reforming and partial oxidation (POx) process or CO_2 methane reforming and POx in one reactor. Hydrocarbons are injected into the reactor with oxygen and the second oxidant. First, the oxygen combusts with a share of the hydrocarbons generating hydrogen and a lot of heat due to the exothermic nature of the reaction. This heat is then used to power the endothermic reformer reaction in the catalytic bed, generating more hydrogen from the leftover methane (Palma et al., 2017). In the first part of the reactor, non-catalytic partial oxidation takes place: reaction 2.4. In the second part, a catalytic bed stimulates the reforming reaction. For the steam ATR, reactions 2.2 and 2.3 occur (similar to the SMR). For the CO_2-ATR, first partial oxidation takes place and then reaction 2.5 in the reformer section.

$$\text{CO}_2\text{- ATR:} \quad \text{CH}_4 + \text{CO}_2 \rightleftharpoons 2\,\text{CO} + 2\,\text{H}_2, \qquad \Delta H_{298\text{K}} = 247 \text{ kJ/mol} \tag{2.5}$$

The H_2:CO ratio for CO_2 ATR is 1:1 whereas for steam ATR the ratio is approximately 2.5:1 (Speight, 2023). Moreover, a comparative study by Li et al. (2008) showed that coke formation in a carbon-ATR is much higher and this can only be prevented through temperature increase. Besides the previously mentioned drawbacks, Ma et al. (2019) also pointed out the larger energy intensity of the endothermic reaction for CO_2 reforming as a major disadvantage. York et al. (2003) found that for producing ammonia, CO_2-ATR is not the optimal choice because additional H_2 would need to be added to reach the right ratios. Therefore, only the steam ATR is further considered in this research.

In general, the operational conditions of an ATR reactor are a temperature of 800-1150 °C and a pressure of 1-80 bar (Voldsund et al., 2016). The steam-to-methane ratio is between 1 - 3 (Li et al., 2008), dependent on the other conditions a low steam-to-methane ratio can lead to coke formation. The oxygen-to-carbon ratio must also be at least 0.5 to prevent coke formation (Ávila-Neto et al., 2009), (Rabenstein & Hacker, 2008). Lower ratios lead to higher hydrogen-to-carbon monoxide ratios. However, the amount of oxygen also controls the amount of heat generated, this amount should be high enough that the reactor is thermally neutral or exothermic. The process yields a hydrogen-to-carbon ratio of 2-3.5 (Carapellucci & Giordano, 2020). The combustion zone where the POx reaction mainly takes place must be thermally equipped to handle the temperature, however, the presence of steam stimulates a more uniform and quick temperature distribution, limiting the hot spot formation. The catalytic zone is heated by the exothermic POx reaction which can then trigger the endothermic SMR reaction. This reaction takes place in the presence of a nickel catalyst, due to its industrial suitability (low-cost and effective).

ATR offers multiple advantages over SMR. Firstly, the process is thermally neutral: the heat generated by POx is used to power SMR. Secondly, the reactor is smaller and easier to control. Thirdly the start-up and shutdown time is shorter and the operating pressure is lower (Bukkholm et al., 2021). Finally, the H_2:CO ratio is easy to vary and control, so in the case of specific ratio requirements for

chemical processes, this method can be preferential (Speight, 2023). A disadvantage is the necessity of an air separation unit (ASU) to generate pure oxygen if the outlet stream cannot be diluted by nitrogen. An ASU is expensive both regarding capital expenditures (CAPEX) and operating expenditures (OPEX), it also requires additional electricity which also forms indirect emissions (Nakaten et al., 2014). Another disadvantage of ATR compared to SMR is the lower maximum H_2:CO ratio it achieves and due to its relative novelty, it has not been implemented as much as SMR therefore lagging regarding research on retrofitting possibilities and technical optimization.

Air vs. Oxygen

All three processes involve a combustion reaction. In the SMR the combustion heat is used to heat the reformer externally to generate heat for the endothermic reaction. The combusted products have no direct contact with the reactants. Using air for this process results in a more expensive SMR system, a lower flame temperature and the combustion efficiency is decreased. However, air can be taken straight from the atmosphere, therefore being significantly less expensive than combusting with pure oxygen. Often in this process, the combustion is executed with air. In the POx and ATR, the combustion occurs within the reactor. Air contains approximately 21 Vol% oxygen therefore the other 79% act as diluents that hinder the reaction efficiency and heat transfer similarly to the SMR. However, in the ATR and POx, the large volume increase results in higher CAPEX costs for each component because the feed stream is larger in every step due to the presence of inert nitrogen. On the other hand, pure oxygen is very expensive to produce, it requires an ASU which has been estimated to increase the energy consumption of the system by 188% (Noelker & Johanning, 2010). Some research has looked at the influence of enriched air to come to an economic compromise. For the production of ammonia nitrogen is part of the end product anyway, therefore using air instead of oxygen can prove to be advantageous. Oxygen-enriched air results in a compromise offering a bit more temperature and component ratio control than combustion with normal air, and less costs than pure oxygen-blown processes because a smaller amount of additional pure oxygen needs to be generated. This research focuses on air-blown reactors, as the nitrogen is used in later steps of the process and an ASU is a large cost item in the process. However, using enriched air could form an interesting future use-case to reach the ideal product ratio for ammonia synthesis.

Reactor comparison

All three reactors have been compared over the past decades based on kinetics, thermodynamics, economics, safety, application suitability etc. (e.g. (Ma et al., 2019), (Ersoz et al., 2006), (Ávila-Neto et al., 2009), (Dincer & Acar, 2014)). The increased interest in CCS has triggered a reevaluation of the advantages and disadvantages of each process, taking into account this extra process step. This has triggered a second wave of more recent comparisons (e.g. (Oni et al., 2022), (Voldsund et al., 2016), (Khojasteh Salkuyeh et al., 2017)). Figure 2.4 summarizes the main advantages and disadvantages of each reactor.

The autothermal reformer was chosen as superior for this process and specifically, the boundary conditions presented earlier. The ATR offers high capture rates at reasonable pricing. Moreover, the ATR is thermally neutral therefore no external energy is necessary to power the reactor. The operation of the ATR is more flexible than the SMR due to the lower temperature at which the oxidation reaction can be executed safely. In the future energy system, processes that can be operated dynamically are favourable. Furthermore, due to the presence of steam, it is easier to control the heat distribution in the reactor and thereby the safety hazards are reduced. The hydrogen yield in an ATR is moderate compared to the SMR however, this yield can be enhanced in later process steps. One of the largest drawbacks to oxygen-blown ATR is the need for a large ASU unit, therefore in the case of ammonia production, an air-blown ATR offers possible economic advantages and therefore this was opted for in this research.

Water Gas Shift

The following process step is the water gas shift. The gaseous mixture is lowered in temperature and the unreacted carbon monoxide and steam react to carbon dioxide and hydrogen (reaction 2.3). This increases the hydrogen yield and generates a higher partial pressure of CO_2. The process usually consists of two shift reactors that differ in temperature and catalyst to shift thermodynamic equilibrium

Reactor	Type	Advantages and disadvantages
SMR	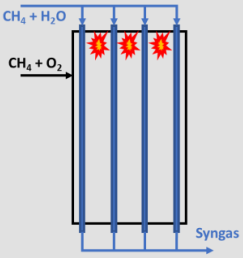	+ High H:C ratio + Highly mature technology + Relatively low operating temperature - Long start-up time (less flexible operation) - Endothermic: High energy intensity - Large reactor - Two emission locations
POx	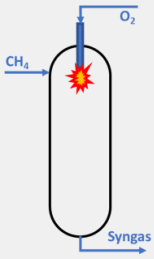	+ Exothermic reaction: lower energy intensity + Fast kinetics and more operating flexibility + High CCS rate possible - Low H:C ratio - Difficult to control: risk of safety hazard - Possible need for pure oxygen - High operating temperature
ATR	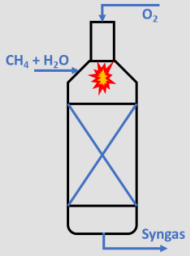	+ Thermally neutral + Easy to control + Smaller reactor than SMR + Moderately flexible + High CCS rate possible - Moderate H:C ratio - Possible need for pure oxygen

Figure 2.4: Main reactor comparison - including simple reactor schematic and the advantages (+) and disadvantages (-) per reactor

and improve the reaction kinetics. First, the high-temperature shift takes place at an inlet temperature between 320 °C (Mendes et al., 2010) - 450 °C (Smith R J et al., 2010). However, the exit temperature can rise to 550 °C due to the exothermic nature of the water gas shift reaction. Usually, this shift is aided by a Fe-Cr oxide catalyst (Maroño et al., 2009) and is performed in an adiabatic or isothermal reactor. The latter of which has been found to require less catalyst (Rosner et al., 2020). After the high-temperature shift, a concentration of 1% - 5% of the CO is expected in the outlet (Mendes et al., 2010). This shift reactor is called the: High-Temperature Water Gas Shift (HTWGS) reactor.

To shift the reaction even further, a second shift is implemented at a lower temperature. This reactor works on the same principles however has a temperature of 180 °C - 220 °C on a Cu-Zn catalyst (Maroño et al., 2009). This process yields a CO concentration of 0.1% - 0.3% (Phan et al., 2022). This process step is called the Low-Temperature Water Gas Shift (LTWGS). After the second shift, the gaseous mixture is cooled down further and dehydrated. This is necessary because steam has negative effects on the capture and purification step.

CO_2 capture

For the capture of CO_2 there are multiple methods: adsorption, absorption, membrane separation and cryogenic separation. Membrane separation is generally not applied in pre-combustion capture, the developments in this field are still at low TRL (Madejski et al., 2022). Moreover, membranes present limitations in the selectivity and purity of the product and retentate (Voldsund et al., 2016). Cryogenic separation is a very costly process due to the extreme conditions under which it takes place and is often opted for in post-combustion applications where the partial pressure of CO_2 is low. For pre-combustion high-pressure scenarios, adsorption and absorption form the most feasible options technically and financially. Both methods have high selectivity to CO_2 and high purity outputs. Adsorption is an order

of magnitude 3 more rate-limiting than absorption due to its slower diffusion rate of CO_2 into the pores (Yu et al., 2012). Therefore at higher concentrations or larger scale absorption is preferable as they yield similar purity and selectivity. Another advantage to absorption is the output gas mix is still at high pressure after the process. The drawback to absorption is the energy intensity of the regeneration process and the limited effectiveness at lower concentrations. In this process the CO_2-concentration is high and the pressure of the product after CO_2-removal is also preferably high, therefore absorption was opted for. Within absorption both chemical and physical absorption are possible. Physical absorption has a less energy-intensive regeneration process (Tennyson & Schaaf, 1977) and is more suitable at high partial pressures (Jansen et al., 2015). However, physical absorption does require larger columns to reach the same purity and yield. In general, at high partial pressures with moderate purity demands physical absorption outperforms chemical absorption on a financial and technical level, therefore physical absorption was selected as the capture method.

Purification

To meet the purity demands of the Haber-Bosch synthesis reactor, the gaseous mixture must be purified after CO_2-removal. In industry pressure swing adsorption (PSA) or methanation are used for this purpose. Other options are too expensive, energy-intensive or do not reach the purity levels necessary (Luberti & Ahn, 2022). At this point, the gaseous mixture should contain minimal amounts of CO, CO_2 and CH_4 and bulk amounts of N_2 and H_2. For the production of ammonia, a small concentration of methane in the feed stream is not hazardous. However, the larger this percentage, the larger the purge stream will be, resulting in downstream product loss and emissions through methane purging. Methanation is the process of letting hydrogen react with carbon monoxide and dioxide to form methane. It is therefore the opposite reaction of that used in the steam reformer. Methanation eliminates the carbon oxides that act as catalyst poison in the ammonia synthesis reactor (Schaaf et al., 2014). Methanation reduces the final yield of H_2 and the excess N_2 is inert and therefore is not removed, which is not advantageous for the 3:1 ratio that is required for ammonia synthesis.

PSA works by adsorption and saturation. Multiple layers of adsorbents are packed into a column under a certain pressure, the impurities in the gas are adsorbed one by one dependent on component and adsorbent properties. Then they are desorbed at lower pressure, depressurization and repressurization power each other resulting in low operational costs and energy demands (Luberti & Ahn, 2022). Moreover, by proper design and operation, the ratio of nitrogen and hydrogen in the output can be controlled to meet the ammonia synthesis preferred ratio and purity needs (Sircar, 2007). However, to regenerate the adsorption bed, 5%-20% of the product is used to form the counter-current flow which decreases the final ammonia yield because this blow-down gas is the purified product which would otherwise be synthesized.

In summary, for methanation the components that cause catalyst deactivation are turned into methane, however, the methane is not removed. Therefore, a larger fraction of impurities enter the synthesis step in the form of methane. These impurities are purged and vented, which results in extra emissions. The PSA can be designed and operated to control the nitrogen-to-hydrogen ratio. With low fractions of impurities, the PSA does not have to be extremely large and the blow-down stream can be relatively small as well reducing the disadvantages of the PSA. Therefore in this case the PSA seemed the more appropriate choice.

Auxiliary units

In order to integrate all units additional auxiliary units are necessary. These are summarized under feed pre-treatment, heat integration, compressors and dehydration. Pre-treatment consists of a desulphurization plant and a pre-reformer. The presence of sulphur can cause accelerated catalyst degradation, severely compromising reactor performance. The pre-reforming step is to break down the higher hydrocarbons in the natural gas feed to methane, which can consequently be fed to the main reactor to generate syngas (Dybkjaer, 1995).

Ideally, a system is brought to its highest pressure in the first step and then per step the pressure is reduced due to losses. This way the process flow will never have a flow back which is hazardous for operation. In this process, the feed is brought to pressure with multi-stage reciprocating compressors

with intercoolers in between. This compressor type reaches higher efficiencies for lower molecular weight (Darazz & Al-Obaidan, 2013). Further on in the process, the compression of CO_2 is also necessary to be transported to the central compression station and the compression of H_2 and N_2 to meet the synthesis conditions is important. For these processes, multi-stage reciprocating compressors with intercoolers were also selected.

For heat integration, the choice was made to work with shell and tube heat exchangers (HEXs) because the conditions are quite extreme: high pressure, high mass flow rate and high temperatures (Towler & Sinnott, 2013). Through compression the product temperature is increased, this is used as partial preheating. The other heating comes from heat recovery in the system due to the exothermic reactions in the ATR and the WGS reactors. Finally, the flue gas that would otherwise be purged is burnt in a furnace to generate additional heat for the pre-heating process. This is the only direct carbon emission the hydrogen production process has.

Dehydration is the final auxiliary process step. This is used to remove all water from the mixture. The presence of water makes the solvent requirement much higher due to the high solubility of water. Moreover, the CO_2 storage has strict conditions regarding water impurities. Lastly, the PSA also has unfavourable performance in the presence of water or steam. The water is adsorbed in the adsorption cavities that should go to the other impurities that need to be removed. Therefore dehydrating before these steps but after the water gas shift is the easiest and best option as a significant temperature reduction is necessary for the physical absorption step anyway.

2.1.3. Process flow sheet

The above evaluation of alternative process units leads to the process flow sheet shown in figure 2.5.

In summary, first, all feed streams are pressurized with reciprocating compressors and then preheated with the shell and tube heat exchangers and the furnace. The steam and natural gas enter the pre-reformer, in which the higher hydrocarbons in natural gas are converted to methane. The methane steam mixture is then preheated further to the input temperature of the ATR. At the top of the ATR, the pre-heated air is injected and mixed with the steam methane mixture coming from the pre-reformer. This causes the combustion to take place, after which more methane is reformed in the reformer section.

Next, the gaseous mixture is cooled and enters the water gas shift reactors in which the equilibrium is pushed towards the hydrogen and carbon dioxide side. This increases the partial pressure of CO_2 for the capture step and generates a larger hydrogen yield. The high-temperature shift covers the bulk conversion with quicker kinetics. The mixture is then cooled even further and the small amount of CO left is also converted in the low-temperature shift with a better thermodynamic equilibrium.

Subsequently, the mixture is cooled and simultaneously dehydrated. The temperature is brought back down to room temperature, therefore the steam takes on a liquid form which is easy to separate. The final trace amounts of water are removed through the dehydration process. This is important because the following process steps are more effective with no H_2O presence.

Then the dehydrated stream enters the absorption column and most of the CO_2 is absorbed along with some trace amounts of the other gasses. Then they enter the flash tank that operates at a certain pressure to maintain a good balance between power consumption for regeneration, CO_2 purity and recovery. The desorbed gas stream is recycled to the absorption column to reenter the process, whereas the rest of the stream is led back to the stripper or final flash tank. There, the bulk CO_2 is released and the solvent and trace amounts still dissolved are repressurized and led back to the absorption column. The gas that is not absorbed moves on to the PSA purification step still at high pressure.

To meet the boundary conditions for purity and of the H_2 and N_2 mixture, the stream needs to be further purified to remove the last trace amounts of impurities. The PSA tackles the CH_4, CO and CO_2-impurities and also adsorbs significantly more N_2 than H_2, therefore resulting in the right ammonia synthesis ratio through proper dimensioning and operating. The impurities and the blow-down gas are used as combustion fuel for the furnace therefore accounting for the final system's direct emission. The

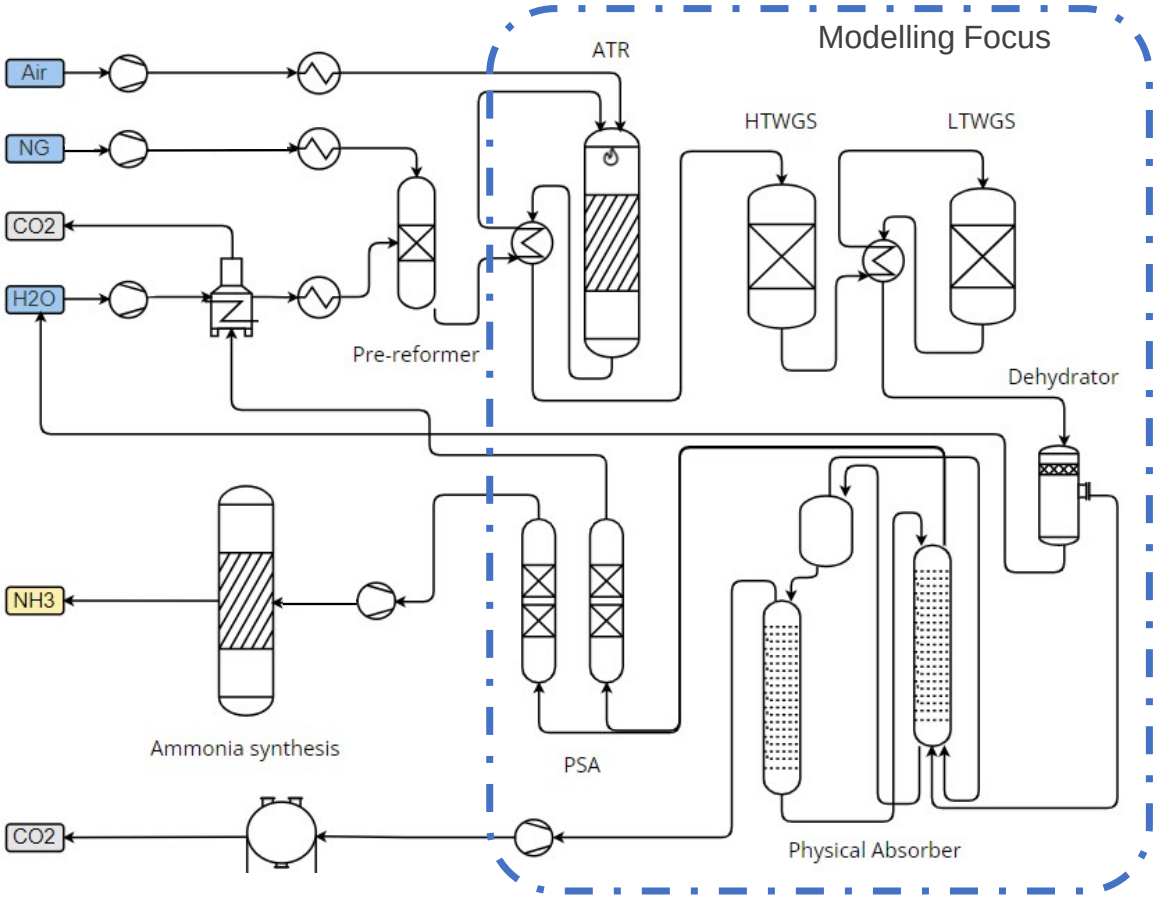

Figure 2.5: Final process flow sheet, the blue area indicates the blue hydrogen production on which the modelling is mainly focused.

remaining mixture of H_2 and N_2 is compressed to 200 bar and enters the Haber-Bosch synthesis.

2.2. Past modelling efforts

Past models of similar systems have focused on either one sub-reactor or the system chain as a whole but using auxiliary programs that limit the dynamic operation and simulation applicability. The past research can be summarized in three categories by their fidelity level.

2.2.1. Fidelity levels

High fidelity refers to highly detailed models of reactor thermodynamics and particle-level kinetic evaluation accounting for several side reactions. Medium fidelity focuses on physical relations within one process step but assumes certain micro-level kinetics and thermodynamics to be negligible. Whereas low fidelity looks at the integrated system and assumes certain efficiency factors per step to calculate the outcomes, to generate a global idea of the process performance. An example of how these physical laws are combined to give a high fidelity, medium fidelity or low fidelity outcome is presented in figure 2.6.

This figure shows that at high fidelity, a CFD is made based on a turbulence model in combination with the continuity equation and conservation of momentum, energy and species. The computational time of this model is quite high as it takes into account quite complicated intra-particle relations and considers 336 reforming reactors, 96 burners and 8 flue gas tunnels. It gives a clear 2D thermal output model, this modelling level is only necessary for final design purposes, in which more detailed analyses and designs are necessary. High-fidelity models tend to be very accurate and therefore can simulate

Interactions modelled	Mathematical modelling example	Results
High Fidelity - CFD • Radiative heat transfer (3D mesh) • Finite rate/eddy dissipation model • k-ε turbulence model for consumption and formation rates Tran et al. (2017)	$\frac{\partial}{\partial t}(\rho_{comb}\vec{v}_{comb}) + \nabla\cdot(\rho_{comb}\vec{v}_{comb}\vec{v}_{comb}) = -\nabla P_{comb} + \nabla\cdot\bar{\bar{\tau}}_{comb} + \rho_{comb}\vec{g}$ $\frac{\partial}{\partial t}(\rho_{comb}E_{comb}) + \nabla\cdot(\vec{v}_{comb}(\rho_{comb}E_{comb} + P_{comb})) = \nabla\cdot\left[k^{eff}_{comb}\nabla T_{comb} - \left(\sum_i h^i_{comb}\vec{J}^i_{comb}\right) + \left(\bar{\bar{\tau}}_{comb}\cdot\vec{v}_{comb}\right)\right] + S^{h,rxn}_{comb} + \nabla\cdot\vec{q}_{rad}$ $\frac{\partial}{\partial t}(\rho_{comb}Y^i_{comb}) + \nabla\cdot(\rho_{comb}\vec{v}_{comb}Y^i_{comb}) = -\nabla\cdot(\vec{J}^i_{comb}) + R^i_{comb}$ $\frac{\partial}{\partial t}(\rho_{comb}\epsilon_{comb}) + \nabla\cdot(\rho_{comb}\epsilon_{comb}\vec{v}_{comb}) = \nabla\cdot\left[\left(\mu_{comb} + \frac{\mu^t_{comb}}{\sigma_\epsilon}\right)\nabla\epsilon_{comb}\right] + C_{1\epsilon}\frac{\epsilon_{comb}}{k_{comb}}G^k_{comb} - C_{2\epsilon}\rho_{comb}\frac{\epsilon^2_{comb}}{k_{comb}}$	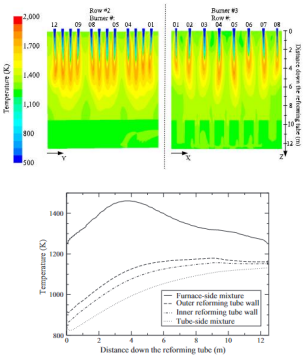
Medium Fidelity – Parameter study • Langrange undetermined multipliers method for thermodynamics • Virial equation of state • Langmuir-Hinshelwood model for kinetics Avila-Neto et al. (2009)	$\Delta G_{fi} + RT\ln\left(\hat{f}_i/f^o_i\right) + \sum_k \lambda_k a_{ik} = 0 \;;\; (i = 1,2,\ldots,N-1)$ $\sum_i n_i a_{ik} = M_k \;;\; (k = 1,2,\ldots,w)$ $\ln\hat{\phi}_i = \frac{P}{RT}\left[B_{ii} + \frac{1}{2}\sum_k\sum_j y_k y_j\left(2\delta_{ki} - \delta_{kj}\right)\right]$ $\Delta G^o_{f,C_{(S)}} + \lambda_{C_{(S)}} = 0$ $k_j = k^o_j \exp(-E_j/RT)$ $K^{ad}_i = K^{ad,o}_i \exp(-\Delta H_i/RT)$	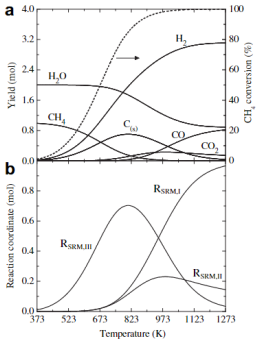
Low Fidelity – Techno-economic comparison • Aspen HYSYS simulations • Process-design • Economic comparisons • Levelized costs • Static models Oni et al. (2022)	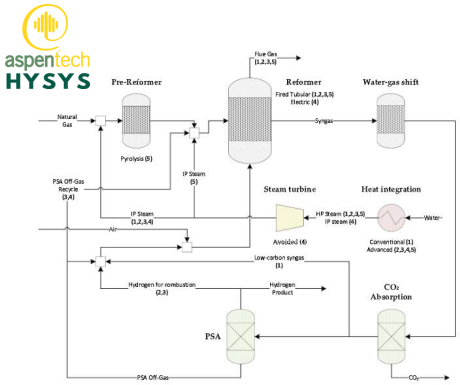	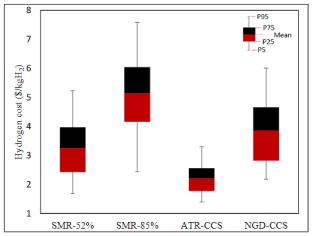 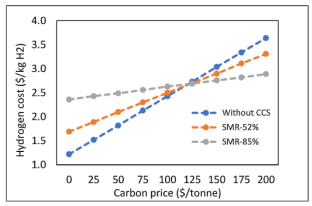

Figure 2.6: Fidelity level examples for methane reactors based on (Tran et al., 2017), (Ávila-Neto et al., 2009) and (Oni et al., 2022)

a specific situation over a short time frame quite well, however, the high level of complexity in these models; the large number of inputs and the long computational time are major drawbacks for purposes like process design and overall operational simulations over longer time periods.

At medium fidelity, the influence of different operating parameters is considered in a more general way. Often the reactor behaviour is simplified through multiple assumptions which yields a 1D thermodynamic or kinetic model. The molecular conservation of mass combined with the Gibbs free energy minimization is used to find the chemical equilibrium. The non-ideal behaviour of the gas is compen-

sated by equations of state and the models like the Langmuir-Hinshelwood model are used to describe the 1D kinetics. Medium-fidelity models yield moderately accurate mathematical models of the influence of input parameters and reaction conditions, these are often focused on a single reactor. These models are used to evaluate the operational window of a reactor.

At low fidelity, the analysis is performed using programs like Aspen HYSYS or compared to previous literature using scaling factors. These models usually give a more generalized comparison of costs in a steady-state simulation. Therefore giving less insight into the reactors' internal behaviour. Low-fidelity models often give techno-economic analysis and often compare different design options. Some of the past research at each fidelity level is shortly summarized in table 2.1.

Table 2.1: Past Reactor modelling research per fidelity level

Fidelity Level	Outcome	Reference
High fidelity	Multi-reaction non-linear models	Zahedi nezhad et al. (2009)
	Computational Fluid Dynamics models	Rowshanzamir et al. (2012) Shi et al. (2009) Kim et al. (2013)
Medium fidelity	Thermodynamic 1D model	Biesheuvel and Kramer (2003) De Souza et al. (2014) Yan et al. (2018)
	Kinetic 1D model	Halabi et al. (2008) Piña and Borio (2006)
	Operational window analysis	Li et al. (2008) Simeone et al. (2008)
Low fidelity	Auxiliary programs (Aspen, UNISIM)	Khojasteh Salkuyeh et al. (2017) Cloete et al. (2022) Bodhankar et al. (2021)
	Conversion rate models	Voldsund et al. (2016)
	Economic comparison based on literature	Oni et al. (2022) Kumar et al. (2020)

Latham et al. (2011) has summarized the past research on reactor modelling and identified that though many mathematical models were established for single reactors, entire process simulations using these models were limited. This research addresses this gap. The goal is to create a mathematical model that operates between medium and low fidelity, on the one hand offering more insights into the key internal behaviour of each process step and the option to customize kinetic relations to match the specific scenario. On the other hand, simplifying certain relations in order to run dynamic simulations over the entire process chain without large computational time even if the simulation is over a multi-year period. Therefore it is able to link technical operational conditions to financial outcomes and easily run more dynamic operating simulations without using external software.

2.3. Economic analyses

Process economics was also thoroughly considered in past research. Multiple techno-economic analyses have been performed on the different hydrogen production processes and a few have also compared them. Oni et al. (2022) compared SMR, ATR with CCS using Aspen HYSYS (flow based) and the DCFA (Discounted Cash Flow Analysis) to work out the economics. Khojasteh Salkuyeh et al. (2017) also compared ATR and SMR using Aspen Plus (process-oriented). The financial analysis was based on values found in the literature for both the CAPEX and OPEX. Aspen Capital Cost Estimator was used for the units not found in the literature. Collodi et al. (2017) performed a techno-economic com-

parative analysis on SMR with different locations and CCS processes, the cost estimations were based on in-house data, vendor quotes and the operational costs were defined as a percentage of the total plant costs. Cloete et al. (2022) also compare SMR and SMR with CCS on a techno-economic level using Unisim and they use the standardized economic assessment (SEA) tool to evaluate the economic feasibility of the different hydrogen pathways. The tool calculates costs based on benchmark values from literature (Arnaiz del Pozo et al., 2021).

Equation 2.6 shows how past CAPEX values can be used to calculate the current CAPEX. The base cost (C_{base}) and base capacity (Q_{base}) are taken from existing literature, and the scaling factor (f_{s}) is an indication of the economies of scale for this technology. The inflation rate is denoted by R_{infl}, this factor is used to compensate for the inflation difference between the base year and the moment of construction, special factors can be used to compensate for this base year difference. The Chemical Engineering Plant Cost Index (CEPCI) and the Marshall & Swift Equipment Cost Index (MS Index) are two indexes that account for the inflation of chemical engineering equipment. Finally, ζ gives any other conversion factor to match units or other conditions. This factor includes installation factors, financial conversion rates and other process-specific factors.

$$C_{\text{new}} = \zeta \cdot (1 + R_{\text{infl}}) \cdot C_{\text{base}} \cdot \left(\frac{Q_{\text{new}}}{Q_{\text{base}}} \right)^{f_{\text{s}}}. \tag{2.6}$$

In order to properly compare different systems, the levelized costs can be calculated in which the OPEX, CAPEX and the production of the useful product are compared to generate a price per kg of product. For hydrogen production processes this is usually expressed in the levelized cost of hydrogen (LCOH). This same comparison can be made for the levelized cost of ammonia (LCOA). Equation 2.7 shows how the levelized cost (LC) for product i is calculated. This method of calculating costs serves as a good comparative measure between different hydrogen and ammonia production processes. The C_{initial} represents the initial investment for the production of the plant. N represents the expected lifetime of the plant or the period over which the levelized costs should be calculated. The t is the counter for the number of years over which the levelized costs must be calculated. $C(t)$ is the operating cost of the project over that year and R_{d} is the discount rate as a percentage. Finally, Q_{i} is the quantity of product i produced over that time period (in this case i is ammonia). In these calculations, future tax and subsidy scenarios and technology progression can also be accounted for to give a more accurate representation of the financial viability.

$$\text{LC}_{\text{i}} = \frac{C_{\text{initial}} + \sum_{t=1}^{N} \frac{C(t)}{(1+R_{\text{d}})^t}}{\sum_{t=1}^{N} \frac{q_{\text{i}}}{(1+R_{\text{d}})^t}}. \tag{2.7}$$

Most financial comparisons use discounted cash flow analysis to calculate the net present value (NPV). This value gives an indication of whether an investment is financially worthwhile. A positive NPV indicates under those conditions it is expected that profit is made, preferably the NPV is higher than the cumulative interest rate of the bank or a low-risk investment. The more uncertainty the cost estimations have the higher the NPV should be to justify the investment. The calculation for NPV is given in equation 2.8. In some cases, investments with a lower NPV are still justifiable because they offer intangible benefits. The difference between the levelized cost calculation and NPV is that the revenue ($P(t)$) is taken into account in the NPV whereas in the levelized costs, only costs are accounted for. It is important to note that in both cases all estimations of future costs are subject to uncertainty therefore this is an initial indication of the profitability of the project.

$$\text{NPV} = \sum_{t=1}^{N} \left(\frac{P_{\text{rev}}(t) - C(t)}{(1 + R_{\text{d}})^t} \right) - C_{\text{initial}}. \tag{2.8}$$

3

Methodology

In this chapter the overall research methodology is summarized, followed by a more extended explanation per step. This extension includes the presentation of each selected sub-component model with their respective assumptions. Next, the integration and simulation methodology to join the sub-components is further explained and the simulation parameters are discussed. Then the methods for economic evaluation are explained and finally, a summary of the desired research outcomes is given.

3.1. Research methodology

In figure 3.1 the method is depicted schematically. The first step in the model is reactor modelling. In this step per sub-component thermodynamic and kinetic models were assessed and compared. The most suitable model was selected, trading off physically accurate modelling with computational time, to reach the appropriate level of fidelity. Thereafter, the models were validated by comparing the outputs to other published values and ideal values. After which, the economics of each sub-component was added and the sub-models were integrated into a joint chain. The outputs of the chain were once again validated through comparison with published values in other research papers. Next, a sensitivity analysis for the main input parameters was conducted on each sub-model and the chain as a whole was run to identify the optimal operational window and identify which parameters were more influential. These values were used as inputs for the financial performance evaluation of the chain: overall CAPEX, OPEX, levelized costs and the net present value calculations. Finally, a few case study simulations were run to reach results that could further answer the main research questions and sub-questions posed in chapter 1.

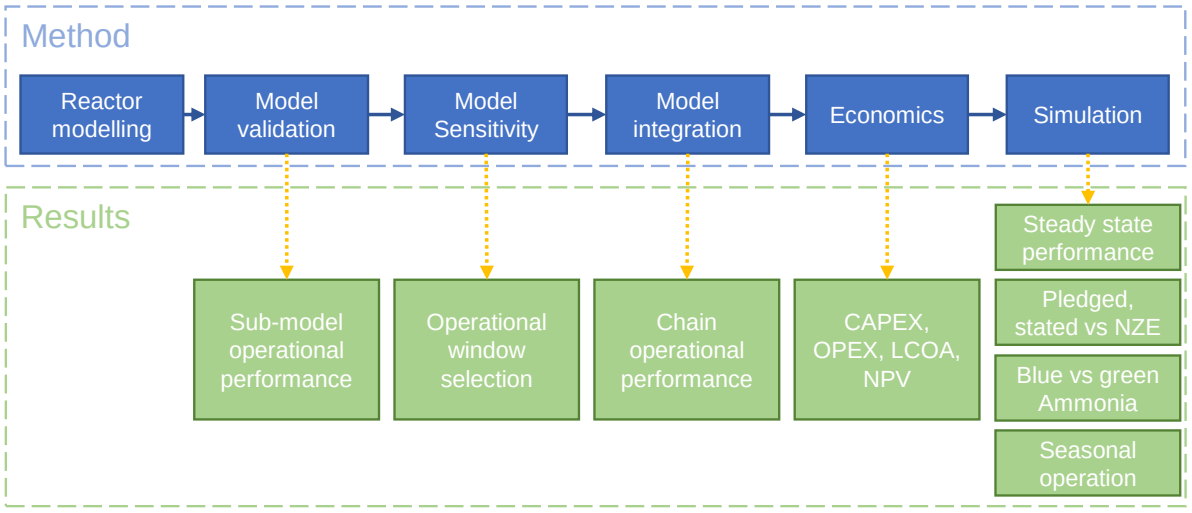

Figure 3.1: Schematic representation of the methodology and results that follow from each step

3.2. Sub-component models

First, each selected sub-model will be discussed on thermodynamic and kinetic levels. Moreover, the assumptions and boundary conditions for the application of the model will be given. For each model, the purpose of conceptual design and preliminary process evaluations medium fidelity models sufficed. The large advantage of this approach is the implementation of simple thermodynamic and kinetic relations therefore respecting the physics of the system without taking unnecessary levels of detail into account that increase the computing time.

3.2.1. ATR

The choice was made to combine two kinetic and thermodynamic models to simulate the autothermal reformer (ATR). The first and most important assumption made in this model is that the autothermal reformer can be modelled as two separate sections. The first is the oxidation section in which all the oxygen is used to convert methane into syngas primarily. It is assumed this composition is not influenced by the second reformer section. That section consists of a catalytic reformer bed often modelled as a packed bed. The four main chemical reactions presented in equations 3.1, 3.2, 3.3 and 3.4 were considered in this process.

$$\text{POx:}\quad CH_4 + 0.5\,O_2 \longrightarrow CO + 2\,H_2; \qquad \Delta H_{298K} = \text{-35.7 kJ/mol}, \tag{3.1}$$

$$\text{SMR 1:}\quad CH_4 + H_2O \rightleftharpoons CO + 3\,H_2; \qquad \Delta H_{298K} = 206.1 \text{ kJ/mol}, \tag{3.2}$$

$$\text{SMR 2:}\quad CH_4 + 2\,H_2O \rightleftharpoons CO_2 + 4\,H_2; \qquad \Delta H_{298K} = 164.9 \text{ kJ/mol}, \tag{3.3}$$

$$\text{WGS:}\quad CO + H_2O \rightleftharpoons CO_2 + H_2; \qquad \Delta H_{298K} = \text{-41.15 kJ/mol}. \tag{3.4}$$

The oxidation section of the reactor is based on the relation published by Biesheuvel and Kramer (2003). The reformer section was based on the kinetic relations presented by Halabi et al. (2008). It is assumed the reforming reaction is rate limiting and that the oxidation reaction is extremely quick and therefore takes place before the reforming reaction (Rice & Mann, 2007) and requires a negligible reactor length (Biesheuvel & Kramer, 2003).

The oxidation section

In the first section pre-heated air enters the bed simultaneously with the steam and methane which results in a combustion reaction generating heat which is uniformly spread due to the presence of steam. Biesheuvel and Kramer (2003) published an empirical relation for the fuel utilization ratio (x_{util}) of methane during air-blown combustion in an autothermal reformer, in short the conversion of methane in the oxidation zone. This correlation is presented in equation 3.5.

$$x_{\text{util}_{CH_4}} = -1.6492 \cdot \alpha^2 + 2.664 \cdot \alpha - 0.2348 - 0.033 \cdot \beta. \tag{3.5}$$

In this relation, α represents the oxygen-to-methane ratio and β the steam-to-methane ratio. A higher steam ratio results in less methane combustion so a lower temperature in the reactor. A higher oxygen ratio can lead to hot spots or an excess of oxygen which can cause issues in later process steps. From this empirical relation, it is possible to calculate the amount of CH_4 that has combusted after the oxidation section. The enthalpy balance is presented in 3.6, stating that the sum of the reacants' enthalpy should be equal to the sum of the products' enthalpy. It is assumed that the reactor is fully

adiabatic so no heat is lost to the external environment and all heat is transferred to the second section of the reactor: the catalytic bed. The conservation of mass in the form of an atomic balance of carbon, hydrogen, oxygen and nitrogen is given by equations 3.7, 3.8, 3.9, 3.10 respectively; throughout the ATR the nitrogen is assumed to be inert. The model assumes the water gas shift always reaches equilibrium, therefore equation 3.11 should always hold. The seven equations were simultaneously solved to reach the composition and temperature at which the gasses enter the reformer section.

$$\sum \left(H_{\mathrm{i}_{(\mathrm{T_{in}})}} \cdot \dot{n}_{\mathrm{i_{in}}} \right) = \sum \left(H_{\mathrm{i}_{(\mathrm{T_{oxi}})}} \cdot \dot{n}_{\mathrm{i_{oxi}}} \right). \tag{3.6}$$

C-atoms: $$\dot{n}_{\mathrm{in}_{(\mathrm{CH_4})}} = \dot{n}_{\mathrm{oxi}_{(\mathrm{CH_4})}} + \dot{n}_{\mathrm{oxi}_{(\mathrm{CO})}} + \dot{n}_{\mathrm{oxi}_{(\mathrm{CO_2})}}, \tag{3.7}$$

H-atoms: $$\dot{n}_{\mathrm{in}_{(\mathrm{CH_4})}} \cdot (4 + 2 \cdot \beta) = 4 \cdot \dot{n}_{\mathrm{oxi}_{(\mathrm{CH_4})}} + 2 \cdot (\dot{n}_{\mathrm{oxi}_{(\mathrm{H_2})}} + \dot{n}_{\mathrm{oxi}_{(\mathrm{H_2O})}}), \tag{3.8}$$

O-atoms: $$\dot{n}_{\mathrm{in}_{(\mathrm{CH_4})}} \cdot (2 \cdot \alpha + \beta) = \dot{n}_{\mathrm{oxi}_{(\mathrm{CO})}} + 2 \cdot \dot{n}_{\mathrm{oxi}_{(\mathrm{CO_2})}} + \dot{n}_{\mathrm{oxi}_{(\mathrm{H_2O})}}, \tag{3.9}$$

N-atoms: $$\dot{n}_{\mathrm{in}_{(\mathrm{N_2})}} = \dot{n}_{\mathrm{oxi}_{(\mathrm{N_2})}}. \tag{3.10}$$

$$\begin{aligned} K_{\mathrm{WGS}} &= \exp\left(-\frac{1}{R_g * T} ((H_{H_2} + H_{CO_2} - H_{CO} - H_{H_2O}) - T \cdot (S_{H_2} + S_{CO_2} - S_{CO} - S_{H_2O}) \right) \\ &= \frac{\dot{n}_{H_2} \cdot \dot{n}_{CO_2}}{\dot{n}_{H_2O} \cdot \dot{n}_{CO}}. \end{aligned} \tag{3.11}$$

The reformer section

The reformer section was based on the kinetic relations presented by Halabi et al. (2008) which were partially based on the earlier published kinetics by Xu and Froment (1989). The reactor is modelled as a one-dimensional plug flow reactor; thermal and mass dispersion in the radial direction are neglected. The gasses are at a high temperature and therefore assuming they can be modelled as ideal gasses is acceptable. The catalyst size, porosity and activity are assumed to also be uniform over the entire reformer bed. The Halabi et al. (2008) model considers all reactions to take place at the same time: oxidation, reforming and the water gas shift. Here the oxidation reaction and its rate respectively are neglected as the reaction is assumed to be fully completed in the oxidation section. Other side reactions were assumed to take place at much lower rates and were therefore also neglected. The ATR model takes into account reactions 3.2, 3.3, 3.4 for the reforming section. These three reactions are all equilibrium reactions and, therefore have equilibrium constants, which are presented in equations 3.12, 3.13, 3.14.

$$K_{\mathrm{SMR_1}} = \exp\left(\frac{-26830}{T_{\mathrm{cat}}} + 30.114 \right) \qquad [\mathrm{bar}^2]. \tag{3.12}$$

$$K_{\mathrm{SMR_2}} = K_{\mathrm{SMR_1}} \cdot K_{\mathrm{WGS}} \qquad [\mathrm{bar}^2]. \tag{3.13}$$

$$K_{\text{WGS}} = \exp\left(\frac{4400}{T_{\text{cat}}} - 4.036\right) \qquad \text{[-]}. \tag{3.14}$$

The reactor and gas temperature are assumed to be identical over the reactor length therefore T_{cat} (the catalyst temperature) is assumed to be the same as the gas temperature. The missing values of constants are expressed in the auxiliary equations 3.15, 3.16 for which the parameters are given in table 3.1. The subscript 'reac' refers to that specific reaction and the subscript 'comp' refers to that specific component.

$$K_{\text{comp}} = K_{0_{\text{comp}}} \cdot \exp\left(\frac{-\Delta H_{\text{comp}}}{R_{\text{g}} \cdot T}\right). \tag{3.15}$$

$$k_{\text{reac}} = k_{0_{\text{reac}}} \cdot \exp\left(\frac{-E_{\text{a}_{\text{reac}}}}{R_{\text{g}} \cdot T}\right). \tag{3.16}$$

Table 3.1: Constants used in kinetic equations for ATR model taken from Halabi et al. (2008)

Reaction or component	Symbol	Value	Unit
SMR_1	k_0	1.17E15	$bar^{0.5}$
	E_{a}	240100	J/mol
	η	0.07	[-]
SMR_2	k_0	2.83E14	$bar^{0.5}$
	E_{a}	243900	J/mol
	η	0.06	[-]
WGS	k_0	5.43E5	bar^{-1}
	E_{a}	67130	J/mol
	η	0.7	[-]
CH_4	K_0	6.65E-4	bar^{-1}
	ΔH	-38280	J/mol
CO	K_0	8.23E-5	bar^{-1}
	ΔH	-70650	J/mol
H_2	K_0	6.12E-9	bar^{-1}
	ΔH	-82900	J/mol
H_2O	K_0	1.77E5	[-]
	ΔH	88680	J/mol

Each reaction has its respective reaction rate, presented in equations 3.17, 3.18, 3.19, with auxiliary function for the Ω value in equation 3.20. The Ω describes the adsorption behaviour of each species on the catalyst and its relative effect on the reaction rate.

$$R_{\mathrm{SMR_1}} = \frac{k_{\mathrm{SMR_1}}}{p_{\mathrm{H_2}}^{2.5}} \cdot \left(p_{\mathrm{CH_4}} \cdot p_{\mathrm{H_2O}} - \frac{p_{\mathrm{H_2}}^{3} \cdot p_{\mathrm{CO}}}{K_{\mathrm{SMR_1}}} \right) \cdot \frac{1}{\Omega^2}. \tag{3.17}$$

$$R_{\mathrm{SMR_2}} = \frac{k_{\mathrm{SMR_2}}}{p_{\mathrm{H_2}}^{3.5}} \cdot \left(p_{\mathrm{CH_4}} \cdot p_{\mathrm{H_2O}}^{2} - \frac{p_{\mathrm{H_2}}^{4} \cdot p_{\mathrm{CO_2}}}{K_{\mathrm{SMR_2}}} \right) \cdot \frac{1}{\Omega^2}. \tag{3.18}$$

$$R_{\mathrm{WGS}} = \frac{k_{\mathrm{WGS}}}{p_{\mathrm{H_2}}} \cdot \left(p_{\mathrm{CO}} \cdot p_{\mathrm{H_2O}} - \frac{p_{\mathrm{H_2}} \cdot p_{\mathrm{CO_2}}}{K_{\mathrm{WGS}}} \right) \cdot \frac{1}{\Omega^2}. \tag{3.19}$$

$$\Omega = 1 + K_{\mathrm{CO}} \cdot p_{\mathrm{CO}} + K_{\mathrm{H_2}} \cdot p_{\mathrm{H_2}} + K_{\mathrm{CH_4}} \cdot p_{\mathrm{CH_4}} + \frac{K_{\mathrm{H_2O}} \cdot p_{\mathrm{H_2O}}}{p_{\mathrm{H_2}}}. \tag{3.20}$$

Finally, to find the rate of conversion for each species, the reaction rates were added and an efficiency factor was used to represent the relative effectiveness taken from De Groote and Froment (1996) to account for intra-particle transport limitations.

$$r_{\mathrm{CH_4}} = -\eta_{\mathrm{SMR_1}} \cdot R_{\mathrm{SMR_1}} - \eta_{\mathrm{SMR_2}} \cdot R_{\mathrm{SMR_2}}. \tag{3.21}$$

$$r_{\mathrm{CO}} = \eta_{\mathrm{SMR_1}} \cdot R_{\mathrm{SMR_1}} - \eta_{\mathrm{WGS}} \cdot R_{\mathrm{WGS}}. \tag{3.22}$$

$$r_{\mathrm{CO_2}} = \eta_{\mathrm{SMR_2}} \cdot R_{\mathrm{SMR_2}} + \eta_{\mathrm{WGS}} \cdot R_{\mathrm{WGS}}. \tag{3.23}$$

$$r_{\mathrm{H_2O}} = -\eta_{\mathrm{SMR_1}} \cdot R_{\mathrm{SMR_1}} - 2 \cdot \eta_{\mathrm{SMR_2}} \cdot R_{\mathrm{SMR_2}} - \cdot \eta_{\mathrm{WGS}} \cdot R_{\mathrm{WGS}}. \tag{3.24}$$

$$r_{\mathrm{H_2}} = 3 \cdot \eta_{\mathrm{SMR_1}} \cdot R_{\mathrm{SMR_1}} + 4 \cdot \eta_{\mathrm{SMR_2}} \cdot R_{\mathrm{SMR_2}} + \cdot \eta_{\mathrm{WGS}} \cdot R_{\mathrm{WGS}}. \tag{3.25}$$

The conversion over the reformer length is calculated using these reaction rates, therefore depending on the length of the reactor and the input stream, a certain component composition is the output. This model also gives an insight into the kinetics inside the reactor. The model is applicable above 830 K and for oxygen to methane ratios of 0.3 - 5 (De Smet et al., 2001), normal operational conditions fall within these limits.

Summarized assumptions

- The ATR can be split into two separate sections: the oxidation and reformer section
- All oxygen reacts in the oxidation section
- The empirical utilization formula is representative of the actual conversion
- Chemical equilibrium of the water gas shift is reached in the oxidation section
- All heat from the oxidation is transferred to the reformer bed
- The reactor is completely adiabatic and well-insulated

- The temperature is assumed to be uniform in the radial direction
- Radial dispersion is neglected
- The catalyst is uniform
- The nitrogen in the reactor is an inert
- No carbon formation or sintering occurs
- The gasses are modelled as ideal
- Only the main reactions are accounted for
- Gas temperature is equal to the catalyst temperature
- There is no catalyst degradation over time
- The reaction effectiveness factors properly account for intra-particle diffusion limitations

3.2.2. WGS

After the ATR the product is led to the first water gas shift reactor which is operated at a lower temperature than the ATR. The WGS reaction also takes place in the ATR, its chemical reaction is repeated in equation 3.26, it has an exothermic nature, therefore the reactor temperature rises during the reaction. The water gas shift is split over two reactors to enhance the H_2 yield: one high-temperature water gas shift (HTWGS) reactor and one low-temperature water gas shift (LTWGS) reactor. The thermodynamics of the reaction are similar in both reactors however the high-temperature shift is used for the bulk conversion of carbon monoxide and water whereas the low-temperature shift is used to further convert the smaller portion of carbon monoxide still left in the gaseous mixture. This reaction often takes place with an excess of steam to push the equilibrium towards the hydrogen side.

$$\text{WGS:} \quad CO + H_2O \longrightarrow CO_2 + H_2; \qquad \Delta H_{298K} = \text{-41.15 kJ/mol.} \tag{3.26}$$

The reaction kinetics of the two reactors are different due to the different operating temperatures and catalysts. The kinetics of the HTWGS are quicker than the LTWGS, however, LTWGS has a more favourable output component composition with the equilibrium shifted more towards the hydrogen and carbon-dioxide side of the reaction. For this reason, the bulk conversion is done at a higher temperature and the final conversion step at a lower temperature. Both reaction kinetics are given in the form of the power law presented in which the Arrhenius parameters and the power exponents are empirical values from fitting real-life data. The general form of the power law is given in equation 3.27, due to the lack of sulfide in the system, the power law is deemed sufficient to reflect the kinetics of the reactions (Boon et al., 2009). The exponents l, m, n, o per reactor are discussed later and presented in table 3.2.

$$r = k \cdot p_{CO}^{l} \cdot p_{H_2O}^{m} \cdot p_{CO_2}^{n} \cdot p_{H_2}^{o} \cdot (1 - \theta) \cdot f_p. \tag{3.27}$$

The rate constant k follows from the Arrhenius parameters through the relation shown in equation 3.28, in which k_0 represents the pre-exponential factor and E_a represents the activation energy of the reaction. The partial pressure of component i is denoted by p_i. The θ-term (equation 3.29) makes sure the rate converges to the equilibrium. The total pressure only influences the reaction speed, not the composition. According to Adams and Barton (2009) this can be modelled by including a pressure factor presented in equation 3.30, where P_{atm} refers to atmospheric pressure, this relation is valid up to 55 atm.

$$k = k_0 \cdot \exp\left(\frac{-E_a}{R \cdot T}\right). \tag{3.28}$$

$$\theta = \frac{p_{CO_2} \cdot p_{H_2}}{K_{eq} \cdot p_{CO} \cdot p_{H_2O}}. \tag{3.29}$$

$$f_p = \left(\frac{P_{in}}{P_{atm}}\right)^{\left(0.5 - \frac{P_{in}}{500 \cdot P_{atm}}\right)}. \tag{3.30}$$

The equilibrium constant (K_{eq}) that is used to calculate θ is related to temperature. Moe (1962) published a widely accepted relation for the equilibrium constant, given in equation 3.31. This relation is used for both the high- and low-temperature shifts as it is applicable in both temperature ranges, 423.15-823.15 K (200-550 °C).

$$K_{eq_{(WGS)}} = \exp\left(\frac{4577.8}{T} - 4.33\right). \tag{3.31}$$

For the high-temperature water gas shift the indexes were taken from Hla et al. (2009) which is an empirical correlation based on the usage $Fe_2O_3/Cr_2O_3/CuO$ catalyst. For the low-temperature water gas shift the indexes were based on the empirical correlation by Choi and Stenger (2003) and take place over a $Cu/ZnO/Al_2O_3$ catalyst. Table 3.2 shows the parameters for both the high- and low-temperature water gas shift reaction. K_0 is the pre-exponential value, its unit and thereby size depends on the exponents per component. E_a is the activation energy for the reaction to take place and the exponents give an indication of the relative influence each partial pressure has on the reaction rate.

Table 3.2: Constants used in the kinetic equations for the WGS model, taken from Hla et al. (2009) for the HTWGS and Choi and Stenger (2003) for the LTWGS

Reaction	K_0 [$\frac{mol \cdot Pa^{(l+m+n+o)}}{kg_{cat} \cdot h}$]	E_a [kJ/mol]	*l* [-]	*m* [-]	*n* [-]	*o* [-]
HTWGS	56.4E6	111	1	0	-0.36	-0.09
LTWGS	103.8	47.4	1	1	0	0

The reaction kinetics were used to size the reactor to make sure the reaction reached its plateau. At the plateau the kinetics slow down because it is approaching equilibrium. This model assumes the reactor is ideal so there are no mass transfer limitations, transport phenomena or local variations in the operating conditions and so full equilibrium can be reached.

Assumptions

- The reactors are adiabatic and ideal
- The catalyst is uniform
- The temperature in the radial direction is distributed uniformly
- Diffusion is neglected
- The gas can be approached as ideal gas
- The power law relations give an accurate interpretation of the actual industrial conditions
- No catalyst degradation

3.2.3. Physical absorption

Physical absorption usually consists of a large absorption tank, one or multiple flash tanks and a desorption tank. The solvent enters the top of the absorption column with a certain rate and the gas enters the column at the bottom. In this case, the CO_2 is almost fully absorbed and the rest of the gaseous

mixture is partially absorbed. The absorption is estimated using the Henry coefficient therefore the absorption and desorption profiles are linear compared to the amount of solvent. In order to maintain a physically more realistic model it was assumed that if the solvent flow rate is higher than necessary for a 95% absorption rate of CO_2, no more CO_2 is absorbed, therefore a minimum of 5% CO_2 will always be led to the next process step. This boundary condition was selected based on the Selexol modelling efforts by Adams et al. (2014) which shows the linearity of absorption and thereby capture percentage decreases at higher capture percentages and stagnates around 95.5% independent of how much solvent is added or the flow rate is increased. In order to calculate the respective amount of gas absorbed in the Selexol a relative solubility factor per gaseous species was used. It is assumed that these relative solubilities properly reflect the competition between the species. For the absorption column the relations for solubility are given by Henry's law presented in equation 3.32, the relative solubilities were taken from Kapetaki et al. (2015) and are given in table 3.3. Henry's law states there is a linear relationship between the partial pressure of a gas and the amount of that gas that is dissolved in the solvent. H_{i} refers to the Henry constant per component, p_{i} the partial pressure of that component and n_{i} and n_{solvent} is the molar flow rate of the component and the solvent respectively.

$$\frac{\dot{n}_{\text{i}}}{\dot{n}_{\text{solvent}}} = \frac{p_{\text{i}}}{H_{\text{s(i)}}}. \tag{3.32}$$

Table 3.3: Relative solubility compared to CO_2 and the Henry coefficient for each component in Selexol

Component	**Relative solubility** [-]	**Henry's constant H_{i}** [MPa]
CO_2	1.0	3.16
CH_4	0.067	47.2
CO	0.028	113
H_2	0.013	243
N_2	0.020	158

The Selexol and absorbed gasses are then led to the first flash tank in which the largest amount of impurities are desorbed and recycled back to the main absorption column and the absorbed components continue on to the next tank. A lower flash tank pressure leads to a higher CO_2-purity. However, it also leads to a lower total recovery and a higher energy consumption to re-pressurise the recycle feed. Therefore picking the right solvent flow rate and flash tank pressure to meet both purity and recovery demands at the lowest cost is important, the optimum for this trade-off is very project and condition-specific. To calculate the amount of gas per species that remains absorbed and what part is desorbed in the flash tank, the mass balance and the Rachford and Rice (1952) flash equation were used. The latter is shown in equation 3.33.

$$\sum \frac{z_{\text{i}} \cdot (\frac{H_{\text{i}}}{P_{\text{FT}}} - 1)}{1 + \frac{V}{F} \cdot (\frac{H_{\text{s(i)}}}{P_{\text{FT}}} - 1)} = 0. \tag{3.33}$$

The Rachford-Rice equation is used again to calculate the desorption behaviour of the system, for all consecutive flash tanks and the final desorption tank. z_{i} refers to the mass fraction of each component in the input feed, H_{i} is the earlier mentioned Henry's constant per component, this is divided by the flash tank pressure (P_{FT}), $\frac{V}{F}$ refers to the vapour-feed ratio. In this research, one flash tank and one final desorption step were considered. In practice this amount is often higher than one, resulting

in less energy consumption for the recycle and purer CO_2 extraction. For modelling ease, this was not considered here. The right purity and recovery are already reached with this model, the difference in power consumption for the recycle stream compressor is negligible compared to the total power consumption of the system (Padurean et al., 2012).

To evaluate the operation of the absorption system the amount of solvent and its flow rate needs to be established. A high flow rate results in higher costs for regeneration, a larger tower requirement and an increase in the absorption of impurities in the first absorption step. The maximum amount of CO_2 that can be absorbed surpasses its linear maximum, the other impurities can still be absorbed which is not favourable. A low flow rate results in a larger amount of CO_2 not being absorbed therefore resulting in higher emissions. The first indication of the amount of solvent necessary was given by the relation presented in equation 3.34 from the paper by Guo et al. (2012).

$$\dot{m}_{\text{Selexol}} = \frac{\dot{n}_{CO_2} \cdot \eta_{\text{capture}} \cdot H_{CO_2} \cdot \text{MW}_{\text{Selexol}}}{P_{\text{abs}} \cdot \chi_{CO_2} - f_{\text{eq}} * P_{\text{desorb}}}. \tag{3.34}$$

In equation 3.34 the mass flow rate of Selexol ($\dot{m}_{\text{Selexol}}$) is calculated based on a desired capture efficiency (η_{capture}), in this case 95%, and a correction factor f_{eq} is introduced to compensate for the fact that absolute equilibrium is not reached in the absorption column so additional Selexol is necessary. H_{CO_2} is the Henry constant for CO_2, M_{Selexol} is the molecular weight of Selexol and P_{abs} and P_{desorb} are the absorption and desorption pressure respectively. Finally $\dot{n}_{CO_2}$ is the input flow rate of CO_2, whereas χ_{CO_2} is the solubility of CO_2. The preliminary amount of Selexol was calculated based on this rate. Iterating on this value, the system was further optimized to reach the desired absorption and desorption behaviour with the right recycle stream. The Selexol flow rate was also used to calculate the power consumption of the pump. The total power for the physical absorption unit was calculated based on relations presented by Guo et al. (2012) shown in equation 3.35. The first term describes the pump and compression power for Selexol and trace gas circulation, the second term refers to the refrigeration power in which the ΔT_{sol} was taken from literature. Finally, the third term describes the compression power for the recycle stream and is calculated similarly to the other compressors, which will be explained in section 3.2.6.

$$Q_{\text{Elec}_{\text{abs}}} = \frac{\dot{V}_{\text{Selexol}} \cdot \Delta P_{\text{abs}}}{\eta_{\text{pump}}} + \frac{\Delta H_{\text{abs}_{(CO_2)}} \cdot \dot{n}_{\text{abs}_{(CO_2)}} + c_{p_{\text{Selexol}}} \cdot \dot{m}_{\text{Selexol}} \cdot \Delta T_{\text{sol}}}{\text{COP}} + Q_{\text{compr}} \tag{3.35}$$

Assumptions

- No water enters the system
- The co-competition can be properly modelled through the relative solubilities.
- Full equilibrium is not reached, therefore a correction factor is added
- No inter- or intra-molecular interactions between the gas species
- The shares of CO, H2, CH4 and N2 are so low that they can be neglected in the pump power consumption
- No flooding takes place in the trays
- Full equilibrium is reached in the flash tanks
- Henry's law accurately depicts the absorption behaviour

3.2.4. PSA

The pressure swing adsorption system was modelled using an auxiliary python model: pyIAST published by Simon et al. (2016). This model fits pure adsorption loading data per component over different pressure variations to the Langmuir isotherm. The format of the fit is given in equation 3.36. This isotherm is often used because it respects both the linear behaviour described by Henry's law for dilute

gasses as well as non-linear behaviour at higher concentrations.

$$L_{\mathrm{i}}^{0}(P) = M_{\mathrm{ads}} \cdot \frac{K_{\mathrm{ads}} \cdot P}{1 + K_{\mathrm{ads}} \cdot P}. \tag{3.36}$$

This gives the adsorption loading (L_{i}^{0}) of the pure component on the adsorbent per mass unit. In which M_{ads} represents the maximum loading and K_{ads}, the adsorption equilibrium constant. These values are often found through fitting experimental data. These correlations combined are used to calculate the competitive Langmuir adsorption (3.37). In the competitive Langmuir isotherm, partial pressure is used. This method is often used to give an initial indication of the competitive behaviour between gasses in a gaseous mixture. It compensates for the fact that in competition the sum of the total adsorbed amount of gas is not the sum of the pure gasses adsorbed.

$$L_{\mathrm{i}}(p_{\mathrm{i}}) = M_{\mathrm{i_{(ads)}}} \cdot \frac{K_{\mathrm{i_{(ads)}}} \cdot p_{\mathrm{i}}}{1 + \sum_{i=1}^{N} \left(K_{\mathrm{i_{(ads)}}} \cdot p_{\mathrm{i}}\right)}. \tag{3.37}$$

There are only trace amounts of all impurities when entering the PSA step therefore it is assumed a bed with two different adsorbents is acceptable to remove all necessary impurities and reach the right hydrogen-to-nitrogen ratio for ammonia synthesis. Depending on the required purity and ratio, the necessary adsorbent volume is sized theoretically. Pressure swing adsorption models are very complex, therefore for a more detailed process-plant design, the set-up should be thoroughly discussed with industry experts and more comprehensive models should be implemented. The power consumption of the PSA was calculated as a linear function of the molar flow rate of hydrogen taken from Song et al. (2015), presented in equation 3.38. This is a very rough assumption however the power consumption of the PSA is relatively low so large variations from this power consumption will have a limited effect on the total power consumption.

$$Q_{\mathrm{Elec_{PSA}}} = 9710 \cdot \dot{n}_{H_2}. \tag{3.38}$$

In this research, the two selected adsorbents are activated carbon and zeolite X13. The first layer will remove all the remaining CO_2 and most of the CO, and the zeolite will adsorb the remaining trace of CO and all CH_4. Both adsorbents adsorb the N_2 partially. The sizing of the zeolite layer mainly dictates the H_2:N_2 ratio. A nine-bed PSA system with 10% blow-down was recommended by an industry expert. It was assumed this design would suffice for this purpose. The relatively low blow-down percentage is due to the low amount of impurities in the gas and the nine-bed system is to maintain continuous operation. The repressurization of one column is powered by the depressurization of a parallel column, therefore limited additional energy consumption is necessary. The loading data for H_2, CH_4 and CO_2 was taken from Rother and Fieback (2013). The missing data for CO is taken from Y. Park et al. (2014) that looked at similar adsorbents. The constants for the Langmuir isotherms per component for these two adsorbents are given in table 3.4.

Assumptions

- Ideal adsorption theory is applicable
- Equilibrium state is reached
- Adsorbed molecules do not interact

- Ideal mixture
- All molecules have the same surface access
- Changes in the thermodynamics of the adsorbent are negligible compared to adsorbate
- The selected Langmuir isotherms accurately reflect the single adsorption isotherms
- The relative loading of the components is accurately represented by the competitive Langmuir adsorption

Table 3.4: Pure Langmuir isotherm parameters from pyIAST (Simon et al., 2016)

Component	$M_{i_{(ads)}}$ [mol/kg$_{(ads)}$]	$K_{i_{(ads)}}$ [MPa^{-1}]
CO_2	12.407	1.767
CH_4	7.327	1.394
CO	3.517	1.746
H_2	2.835	0.321
N_2	5.435	0.619

3.2.5. Ammonia synthesis

For the ammonia synthesis, a TNO in-house model was used. This model is based on the Haber-Bosch process. The operation was assumed to reach 99% hydrogen conversion when the recycle loop is operated properly (Cha et al., 2021). The PSA limits the number of impurities to a ppm level, therefore the losses are minimal. The process occurs at a pressure of 200 bar and in an adiabatic reactor. It is assumed no side reactions take place therefore the stoichiometric ratio is used to describe the conversion with the earlier mentioned efficiency factor (η_{NH_3}). Equation 3.39 shows how the conversion was calculated. The heater, cooler, compressor and separator are accounted for within the CAPEX and fixed OPEX price and the additional electricity demand was extrapolated from data by Nosherwani and Neto (2021) and Morgan et al. (2017) shown in equation 3.40.

$$\dot{m}_{NH_3} = \eta_{NH_3} \cdot \frac{2}{3} \cdot \dot{m}_{H_2} \cdot \frac{MW_{NH_3}}{MW_{H_2}}, \tag{3.39}$$

$$Q_{Elec_{NH_3}} = 2.356 \cdot 10^6 \cdot \dot{m}_{NH_3}. \tag{3.40}$$

Assumptions

- Ideal operation of the reactor
- No reactor degradation over time
- Constant reaction rate
- Temperature gradients in the reactor do not influence the outcome
- A 99% conversion is assumed
- No side reactions
- A perfect stoichiometric reaction occurs.

3.2.6. Other

Some auxiliary models were used to generate the right conditions for the reactions to take place. These conditions mainly refer to temperature, pressure and feed composition per reactor. These models are based on very simple relations or are assumed to be properly reflected in the literature from which conversion factors were taken.

Compressors

The first auxiliary process is compression, all feed streams need to be compressed and intercooled to meet the necessary input conditions. The intercooling of a compressor is necessary to prevent overheating and the literature states a maximum output temperature of 200 °C (Klotsche et al., 2019). This temperature rise is the boundary condition that dictates the number of necessary stages to reach the required pressure and indirectly the compression ratio. The compression process is modelled as isentropic compression in a reciprocating compressor with an efficiency factor of 0.75 to compensate for the thermal and mechanical losses. The relations are shown in equations 3.41 and 3.42.

$$\frac{P_{\text{in}}}{P_{\text{out}}} = \frac{T_{\text{max}}}{T_{\text{in}}}^{\left(\frac{\gamma_{\text{gas}}}{\gamma_{\text{gas}}-1}\right)}. \tag{3.41}$$

$$Q_{\text{compr}} = \frac{1}{\eta} \cdot \frac{N \cdot \gamma_{\text{gas}}}{\gamma_{\text{gas}} - 1} \cdot R_{\text{g}} \cdot T_{\text{in}} \cdot \dot{n}_{\text{tot}} \cdot \left(\left(\frac{P_{\text{out}}}{P_{\text{in}}}^{\left(\frac{\gamma_{\text{gas}}-1}{N \cdot \gamma_{\text{gas}}}\right)} \right) - 1 \right). \tag{3.42}$$

The γ_{gas} refers to the heat capacity ratio, T_{max} is the maximum temperature that the compressor may reach and T_{in} is the temperature at which the gas enters the compression stage, often room temperature. The pressure ratio is used as an inverse power to the final pressure to calculate the amount of compression stages necessary (N). This is then used to calculate the power consumption (Q_{compr}). The η is the efficiency factor, $\dot{n}_{\text{tot}}$ is the molar flow rate of the gas and finally P_{in} and P_{out} are the input and final output pressures respectively.

With this modelling method, the gas is assumed ideal which is less accurate at higher pressures. The compression of real gas at higher pressure is easier than ideal gas. This leads to a possible overestimation of the power consumption of the compressor and therefore the compressor might be over-dimensioned and costs could be lower in actuality. However, a perfectly adiabatic system does not exist so some heat loss in the compression steps is likely to occur in reality and some pressure loss over the compressor is also inevitable. All compressor stages are rounded up and therefore should be able to compensate for these possible losses. All in all, it is assumed the losses and the over-estimations partially compensate each other, therefore this model sufficiently represents reality.

Heat exchangers

For heat integration, a furnace burning the PSA-off gas is used to partially pre-heat components. The process design is based on the fact that the autothermal reactor is thermally neutral, after which the following reactors have exothermic reactions and absorption and adsorption take place at room temperature. Because the heat demand is lower in each process step heat exchangers are used to cool the product to the feed conditions for the next reactor. The recovered heat is then used to preheat the original feed. The necessary pre-heat required per input feedstock ($Q_{\text{i}_{\text{req}}}$) to reach the right temperature was calculated using equation 3.43.

$$Q_{\text{i}_{\text{req}}} = \sum_{i=1} \left(c_{p_{\text{i(liq)}}} \cdot \dot{m}_{\text{i}} \cdot \Delta T_{\text{i(liq)}} + \Delta H_{\text{evap}} \cdot \dot{n}_{\text{i}} + c_{p_{\text{i(gas)}}} \cdot \dot{m}_{\text{i}} \cdot \Delta T_{\text{i(gas)}} \right). \tag{3.43}$$

c_p refers to the heat capacity per component or mixture in that particular phase. The $\dot{m}$ is the mass flow rate whereas the $\dot{n}$ is the molar flow rate. The ΔT refers to the temperature difference in liquid and gaseous phase and the heat of evaporation is denoted by ΔH_{evap}. For steam, the heat required is the sum of the heat to reach the boiling point, the heat to evaporate the entire body of water and the heat to further heat the steam to the required temperature. The other components are in the gaseous

phase at 25 °C and therefore only require the final part of the summation. This gives the entire amount of required heat. The available heat for transfer by the intercooling between processes (Q_{HEX}) was calculated through equation 3.44.

$$Q_{\text{HEX}} = \eta_{\text{HEX}} \cdot \dot{m} \cdot c_p \cdot \Delta T. \tag{3.44}$$

The heat exchangers were assumed to have a 20% loss of heat during transfer, resulting in a heat exchanger efficiency (η_{HEX}) of 0.8 (Mehanovic et al., 2023). The available heat generated by the furnace (Q_{furnace})was calculated using the equation 3.45.

$$Q_{\text{furnace}} = \eta_{\text{transfer}} \cdot \eta_{\text{inert}} \cdot \sum_{i=1} \left(\dot{n}_{\text{i}} \cdot \Delta H_{\text{comb}}\right). \tag{3.45}$$

In equation 3.45, two efficiency factors are used. The first refers to the efficiency of heat transfer in a furnace which was set to 0.92 based on the value published by Guthrie (1969). CO_2 and N_2 were considered to be inert in the furnace, therefore limiting the heat transfer for which another efficiency factor was introduced. Its value is dependent on the process because it is taken as the percentage of combustibles in the PSA off-gas, in this case, that amount is about 35%, therefore seriously impairing the heat transfer.

A full heat integration analysis falls outside of the scope of this research. Therefore the above-mentioned efficiency factors were used to compensate for heat loss through heat exchangers. No pinch-point analysis was conducted. However due to the relatively low input temperature compared to the output temperature of the ATR it is assumed the heat transfer through heat exchangers and the furnace is sufficient to reach the required temperature without cross-overs. Instead, the final heat integration was done through the summation of all required heat minus the sum of all generated heat including the transfer efficiencies. The sum of the heat generated was higher than the sum of the heat required therefore no additional pre-heaters were necessary. Other processes sell excess heat or steam to generate extra revenue, in this research, this aspect is not considered.

Composition treatment

Composition treatment refers to the pre-treatment of the feed through desulfurization and pre-reforming but also to the dehydration step before absorption. These processes were included in the model with conversion factors taken from previous literature.

It is assumed the sulphur is at ppm-level after desulphurization and can therefore be neglected throughout the process. It is also assumed the original composition of the mixture excluding the sulphur remains unchanged. For pre-reforming data was taken from Rovere (2019) and a conversion factor was established of 1.04 in which the assumption is made that all higher hydrocarbons are converted to methane. A second assumption is made that, due to the lower temperature in the pre-reformer, the methane does not yet react to make hydrogen. Therefore the pre-reformer only outputs methane and steam. For the dehydration step, it is assumed all water is removed to the ppm level whereas the rest of the composition is not affected. By lowering the temperature to 25 ° C, most of the steam has condensed and is easy to separate already. The dehydrator therefore needs to remove mainly the trace amounts of steam left in the gas.

3.2.7. Validation

All models were first validated by comparing outcomes to previous literature. Then some essential operational parameters were set based on the model's performance and the limitations of the reactors internally. After this, it was investigated what the influence of varying the input conditions was for each sub-model.

3.3. Integration and simulation

Next all models were integrated and multiple simulations were run to test technical and economic parameters. The integration and the simulations were run in an auxiliary framework developed by TNO named PyDOLPHIN. The framework aims to integrate physics-based models in order to help parties such as industrial partners and policy-makers in the optimization of the design and operation of their systems. Ultimately PyDOLPHIN aspires to combine the physics-based models, domain knowledge and data to contribute to digital models, shadows and twins of energy systems (Fatou Gómez et al., 2022). Through integration into this framework, comparisons can be made to existing multi-commodity systems like green hydrogen for the production of ammonia. Furthermore, the implementation of the above-mentioned components can also be used in future research, in a different system composition or operational window to improve the system design, operation or maintenance.

3.3.1. Model integration

In the model integration step, the models were joined together using the three main operational parameters: component composition, temperature and pressure. Through this integration, a better insight was gained into how the system works individually but also as a chain. Moreover, it gave the technical inputs for the economic evaluation. The model was further integrated into the existing framework, where other processes could be linked to the models. Here the electricity and natural gas market were connected as inputs and the ammonia synthesis process and market was linked to the output of the chain. From this integration step, simulations could be run with different scenarios. Figure 3.2 summarizes how the models are implemented and integrated to run simulations. The figure also shows some of the main physical relations used in the sub-models.

3.3.2. Simulation parameters

In order to reach meaningful results a sensitivity analysis was run on the entire system altering the 4 input parameters: oxygen-to-methane ratio (α), the steam-to-methane ratio (β), the input pressure (P_{in}) and the input temperature (T_{in}). For each iteration, each model was post-processed individually to see what happens within that process step with these different input conditions. Based on the technical and physical limits of the systems, some critical operational conditions were identified.

Finally, the impact on the output of the entire system: power consumption, ammonia yield and carbon emissions were investigated. The performance of the models and some critical boundary conditions mentioned in chapter 2 formed the foundation for the technical perspective on the ideal operating window.

3.4. Economics

The economics of the process also play a large role in the evaluation of the merit of the process. The economics can be quantified through multiple methods. First, the focus was put on quantifying the capital costs of each sub-component individually including installation costs. After this the yearly fixed OPEX per sub-component was established, to account for maintenance and other standard yearly costs. Then the variable OPEX was computed for the entire system chain and the sub-components when applicable. To evaluate the final financial performance of the system the Levelized Costs of Ammonia (LCOA); the Net Present Value (NPV) and the cumulative cashflows were calculated.

3.4.1. CAPEX calculation

All CAPEX calculations were based on the costing method presented in chapter 2. The parameterization of all components with the benchmark year 2023 in million euros (€) is given in table 3.5. All process steps are mature, therefore it is assumed the price will not reduce as a result of new developments or a learning curve like in other newer processes, the CAPEX is assumed to increase by an average of 2% per year, in line with inflation. The factor ζ differs per unit because some CAPEX base cases already included installation factors, whereas others did not, and due to the currency differences and other process step-specific factors.

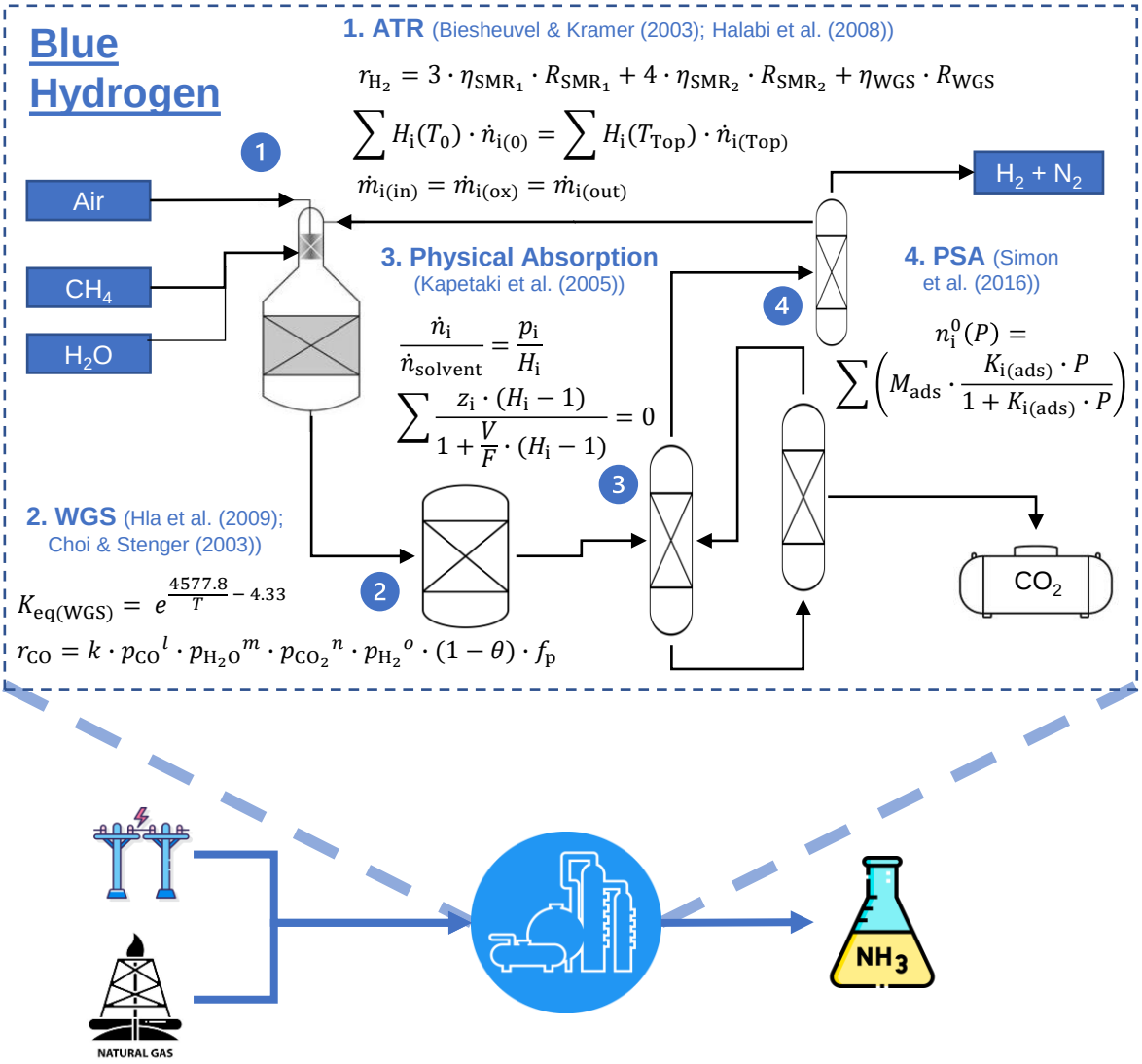

Figure 3.2: Summary of main equations per model and their integration into the larger framework. Step 1: the ATR, step 2: WGS, step 3: physical absorption in Selexol and step 4: PSA, are joined connected and then integrated into one blue hydrogen model that is then connected to the inputs NG and electricity and the output is used to produce ammonia.

3.4.2. Fixed OPEX - O&M

The fixed OPEX mainly refers to the yearly fixed operation and maintenance (O&M) costs of each sub-component. Table 3.6 gives the percentages of the total CAPEX assumed for the fixed OPEX (O&M) and the reference from which the value was taken. All main equipment is assumed to last the entire lifetime of the plant due to proper maintenance.

Some processes are more prone to failure and therefore require more and better maintenance, leading to higher fixed OPEX costs. Relatively, the highest maintenance costs go to the compressors because they have many moving parts. Certain operating units require internal replacements of parts every few years, these were considered separately. They are presented in table 3.7. The table does not include Selexol replacement because this is replenished yearly and accounted for in an additional OPEX calculation assuming a 10% refill necessity at €3.68 per litre (C. Chen, 2005).

Table 3.5: Base case CAPEX values and their base reference, from which the CAPEX per unit is calculated

Component	C_{base} [MEUR]	Q_{base}	f_s	t_{base}	ζ	Reference
Pre-reformer	24.8	1800 J	0.75	2022	0.92	Katebah et al. (2022)
De-sulphurization	12.4	10.3 kg/s	0.72	2018	0.69	Mohajerani et al. (2018)
ATR	4.70	386.11 mol/s	0.6	2002	2.12	Hamelinck and Faaij (2002)
WGS	12.2	2450 mol/s[1]	0.65	2002	1.81	Hamelinck and Faaij (2002)
Absorber	180	2547 mol/s[2]	0.79	2020	1	Rosner et al. (2020)
PSA	10.7	1 $kmol/s$	0.81	2018	0.69	Mohajerani et al. (2018)
Compressor	0.658	1 MW	0.82	2018	$1.94 \cdot f_{med}$[3]	Luyben (2018)
HEX	1.80	57.2 MW	0.9	2014	$2.29 \cdot f_{mat}$[4]	Campanari et al. (2014)
Furnace	1.44E-2	1 MW	0.85	1988	2.76	Douglas (1988)
Dehydrator	3.5E-2	0.33 m^3/s	0.7	2006	1.61	Sjardin et al. (2006)
NH_3-synthesis	39.8	3.47 kg/s	0.64	2021	1.09	Nosherwani and Neto (2021)

[1] mol CO + H_2
[2] mol CO_2
[3] f_{med} is the medium correction factor
[4] f_{mat} is the material correction factor

3.4.3. Variable OPEX

The calculations of the variable OPEX only consider the main contributors: natural gas (NG) feed, power consumption, CO_2-equivalent emission costs and CCS costs for transport and storage. These costs depend on the running hours of the plant and the possible dynamic pricing of the markets. Table 3.8 gives the default price assumptions, followed by an explanation of why these values were assumed.

NG

The natural gas market development contains many uncertainties, in this study, a few case scenarios were considered to see the influence of these uncertainties. IEA has generated price projections for both natural gas prices as CO_2-taxes based on three scenarios. The first is the stated scenario in which only the stated policies to counteract climate change are taken into account. The second scenario is the pledged scenario in which additionally the pledged policies are taken into account. Finally the net-zero emission (NZE) scenario is given, which is based on the policies that need to be implemented to reach NZE by 2050 for one of many projected NZE energy mixes. In this research, the base case was taken as the pledged scenario price indication. However comparative studies were conducted to show the financial outcome of the other two scenarios as well, varying the natural gas prices to the values in

Table 3.6: Yearly fixed OPEX percentages (O&M costs)

Component	Fixed OPEX [%]	Lifetime [years]	Reference
Pre-reformer	4	>25	Katebah et al. (2022)
Desulphurization	4	>25	Mohajerani et al. (2018)
ATR	5	25	Khojasteh Salkuyeh et al. (2017)
WGS	4	>25	Rosner et al. (2020)
Absorber	4	>25	Ashkanani et al. (2020)
PSA	3	>25	Yousefi et al. (2023)
Compressor	8	>25	Yousefi et al. (2023)
HEX	4	>25	Aromada et al. (2020)
Furnace	2	>25	S. Lyons et al. (2018)
Dehydrator	4	>25	Sjardin et al. (2006)
NH_3-synthesis	6	>25	Nosherwani and Neto (2021)

Table 3.7: Component internal replacements

Replacement	Lifetime [years]	Price [€/kg]	Reference
ATR Catalyst	3	20.00	Spath and Dayton (2003)
HTWGS Catalyst	4	16.56	Ratnasamy and Wagner (2009)
LTWGS Catalyst	3	18.40	Sakurai et al. (1997)
Activated Carbon Adsorbent	5	0.60	Burgers et al. (2022)
Zeolite Adsorbent	5	1.30	Burgers et al. (2022)

Table 3.8: Variable OPEX default price values used in base case

Variable OPEX	Price	Unit
Natural gas (NG)	22.64	€/MWh
CO_2-tax	0.135	€/$kg_{CO_{2(eq)}}$
Electricity	41.77	€/MWh
CCS price	0.05	€/kg_{CO_2}

table 3.9.

Besides a fixed price profile for natural gas a seasonal profile was also considered as the renewable energy mix might result in seasonality in other commodities as well. Moreover, whether the natural gas market already has some seasonality in its pricing due to the larger demand in the winter than in the summer is debatable. Fladmark and Grimstad (2013) and S. H. Chen et al. (2022) found a correlation between natural gas prices and seasonality, whereas industry experts have not found significant evidence for this seasonality due to the large available storage capacity for NG. In this research, it is assumed seasonality can occur to warrant a simulation case with more dynamic operation. The data for

Table 3.9: IEA (2022c) price projections for natural gas and carbon taxes for three climate scenarios, the base case assumptions are bold.

Scenario	**NG-price** [$\frac{€}{MWh}$]	**CO_2-taxes** [$\frac{€}{kg}$]
Stated	24.36	0.09
Pledged	**22.64**	**0.135**
NZE	13.80	0.14

2017 natural gas prices did show seasonality as is shown in figure 3.3. From this, a simple sinusoidal function was extrapolated. This was transposed to the 2030 pricing scenario in which the pledged natural gas price was taken as the average and larger extremes were considered through variation of the amplitude. The degree of seasonality to justify non-steady-state operation throughout the year is researched with this seasonality pattern.

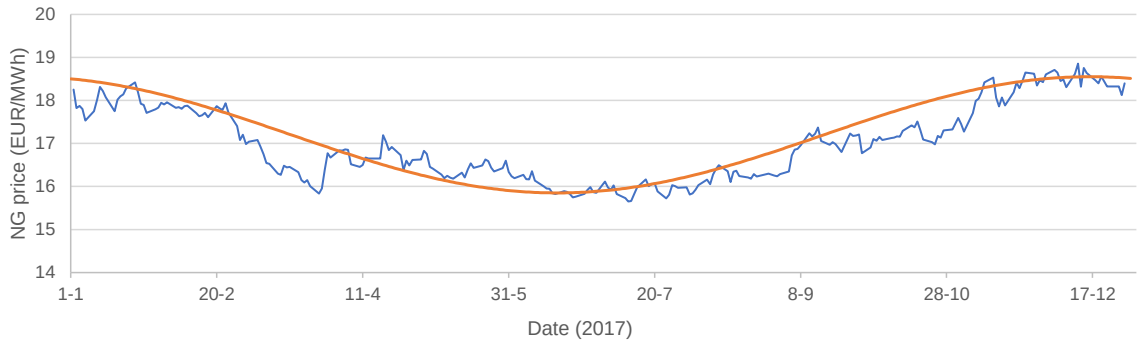

Figure 3.3: Natural gas price seasonality in the Netherlands in 2017, used to extrapolate a seasonality pattern for NG prices to test feasibility of dynamic operation

CO_2-taxes and CCS costs

The CO_2-taxes are also considered in the variable OPEX. Emissions can be divided into scopes one, two and three. Scope one emissions refer to the direct emissions the process produces. Scope two emissions are the indirect emissions from feedstock and other auxiliary processes. So in this, case scope two emissions are the upstream methane emissions and the carbon intensity of the electricity used. Finally, scope three emissions are all indirect emissions not accounted for in scope one and two emissions. This includes a range of emissions: e.g. downstream product emissions, employee commute emissions and emissions for the production of the necessary materials for plant fabrication. Scope three emissions were not considered in this research, however, it should be acknowledged that higher carbon taxes could have an influence on the CAPEX of the plant because of the rise in production costs of materials.

The scope one and two emission types were calculated to generate a complete picture of the direct emissions of the process and the additional indirect emissions (grid-intensity and upstream emissions). This gives a better indication of the actual environmental impact of blue and green ammonia versus grey. However for the calculation of carbon taxes only scope one emissions need to be considered. The values for the carbon taxes are also taken from the IEA price projections for 2030 (IEA, 2022c) and are given in table 3.9. The base case uses the price assumptions from the pledged scenario: 0.135 €/kg CO_2.

Besides CO_2-taxes the costs of using the PORTHOS infrastructure to transport and store CO_2 are also accounted for. The previously mentioned expected tariff of 0.05 €/kg_{CO_2} published by Fuller and

Spence (2020) is assumed. These costs include transport to the storage location and the storage itself. Due to the assumed proximity to the PORTHOS compression station, no additional costs are considered for transport to the station (they are assumed negligible).

Electricity

The third contribution to the variable OPEX is the electricity market. In 2030 it is assumed a larger share of the electricity generated will come from renewable sources compared to now. However, the electricity demand is also likely to rise. This introduction of more renewables is likely to result in even more variability in electricity pricing. An in-house TNO projection for the energy mix of 2030 resulted in an estimation for electricity pricing and an average CO_2 grid intensity. The average price of electricity is 41.77 €/MWh over the year, with a standard deviation of 30.02 €/MWh. The grid intensity throughout the year is 75 kg/MWh on average. In reality, the power in the grid comes from multiple sources and the grid intensity fluctuates throughout the day depending on the renewable energy production, here these fluctuations are ignored and a year-round steady grid intensity is assumed.

In the future, Power Purchase Agreements (PPA) are most likely going to play a larger role in European markets. This entails that a company enters a long-term contract with a renewable energy supplier guaranteeing a certain amount of the generated green power goes directly to them for a standard price. This contract form offers more security to both the consumer and the supplier, therefore partially eliminating the financial risk for both parties. It also reduces the indirect emissions of the process by reducing the electricity emissions in the process. Recently PexaPark (2023) published some figures on the current PPA contract prices over Europe. The published PPA value for the Netherlands is currently 56.7 €/MWh. De Jong (2020) projected the 2030 PPA price in the Netherlands to be around 45.0 €/MWh. This indicates that in the case of a PPA, the assumption might be a bit optimistic that the day-ahead market price for electricity is similar to PPA market prices. Therefore, the costs might be higher in the case of a PPA but a PPA also guarantees a long-term predictable tariff. In this research, the day-ahead market projections by TNO are used for the electricity pricing in all scenarios.

3.4.4. LCOA and NPV

For the calculation of the levelized costs and NPV a lifetime of 25 years was selected as this is the industry standard (Oni et al., 2022), however, research has found that in Europe plants last 40 years on average (IEA, 2021), potentially increasing possible profits. The discount rate was set to 10%, which is considered a reasonable maybe even high value as all process steps are mature and the regulatory environment is likely to promote sustainable initiatives in the future lowering some of the risks. Other researchers use similar discount rates, therefore it is assumed to be a valid rate (e.g. Arnaiz del Pozo et al. (2021), S. Park et al. (2023)). Lastly, it is assumed the plant is 90% operational throughout the year, resulting in approximately 7890 hours per year, this same assumption is made by IEAGHG (2017) and other research often assumes 8000 hours, again confirming the validity of this assumption. The standard yearly costs were built up out of fixed OPEX costs; variable OPEX costs and replacements of adsorbents and catalysts. The revenue for the NPV calculation is based only on ammonia sales. The selling price of ammonia is assumed to be €0.472 per kg. This price is the current selling price of blue ammonia in the Netherlands of €0.419 per kg compensated by inflation for 2030. The initial investment is defined as the investment made in year 0 to build the plant.

3.5. Results

After validating the sub-models and looking at the influence of each input parameter on each unit and the entire chain, an operational window is selected. The blue ammonia chain is then evaluated as a whole on a technical and financial level in that operating window. Firstly, the composition per sub-component; the system's efficiency for steady-state production and the carbon emissions will be presented. Then, the CAPEX distribution is given and the LCOA, cumulative cashflows, and NPV are discussed for the base case, using pledged scenario pricing. Finally, three comparative simulations will be presented.

In the first simulation, the comparison is made between the three 2030 IEA emission scenarios. These have different CO_2 and natural gas prices. Showing the influence of pricing and policy. Secondly, blue ammonia production will be compared to green ammonia production in 2030. Finally, a dynamic

seasonal operation will be considered. In some cases the outcome is compared to ammonia produced from grey hydrogen, which is assumed to have a levelized cost of €0.317 per kg of ceNH3 without CO_2-taxes (Arnaiz del Pozo et al., 2021) which amounts to €0.357 per kg ceNH3 in 2030 due to inflation. A direct carbon emission intensity of 1.40 kg CO_2 per kg NH_3 is assumed for grey ammonia taken from the analysis by Lee et al. (2022).

3.5.1. Case assumptions

Case 1 - IEA comparison

For the first case, the three IEA pricing scenarios are taken as the main variables. This then shows the financial implications of the different routes and the relative influence of carbon taxes. To make this comparison, it is assumed that natural gas prices and carbon taxes are steady all year round at the values presented by the IEA. It also assumes the electricity is taken from the grid with a carbon intensity of 75 kg/MWh. This is based on an internal energy mix projection for 2030 and does not vary per IEA scenario. This comparison is made between the three scenarios mentioned earlier: stated, pledged and NZE. The influence of each scenario on the electricity price, grid intensity and CAPEX is not considered in this research however could prove to shift the financial and environmental outcomes.

Case 2 - Blue ammonia vs green ammonia

For this case study the blue base case is compared to the green route, from a financial and emissions perspective. Certain assumptions were made for the green ammonia production to match the blue case. First, the basis of the green ammonia model is explained after which the case-specific assumptions are given.

Green ammonia is synthesized from hydrogen produced by a 1.4GW alkaline electrolyzer which is connected to a 1.51GW wind farm. The wind farm's total capacity matches the electrolyzer and ammonia synthesis power requirements for this scale. The wind profile connected yields a capacity factor of 58% yearly. Alkaline electrolyzer stacks were selected for the comparison because they have the highest TRL and therefore are most likely to be implemented in 2030 (C. Smith et al., 2020). The hydrogen, generated through electrolysis, is mixed with nitrogen and synthesized through the Haber-Bosch process, similar to the blue ammonia path. The electrolyzers operate at 1 MPa pressure. The electrolyzer model is a pre-existing model by TNO, mainly based on the previous modelling efforts of de Groot et al. (2022). The anode and cathode pressure were assumed to be balanced. The CAPEX assumptions were made based on the correlation by (Reksten et al., 2022), in which a learning and development factor is accounted for to reflect the costs in 2030. The stack exchange data was based on the work by Krishnan et al. (2023) and assumed to need replacement every seven years. The performance is assumed not to degrade over time and the scale of production is assumed to not give any issues.

For the financial performance, the assumption is made that variable grid pricing reflects the power consumption costs. In reality, this is more likely to be a PPA (Power Purchase Agreement) with a standard price, which is likely higher than the average price of the volatile market, however, it guarantees green electricity when it is available making the hydrogen greener. For emissions, the wind profile was used to calculate the power generation at each time step. The necessary power for steady-state production is taken from wind energy in the first instance therefore resulting in no emissions and when the power generated through the wind farm cannot meet the demand (58% capacity factor), it is supplemented by grid power, therefore also associated with grid emissions. Electrolysis and an ASU give very pure hydrogen and nitrogen so the 99% assumption for ammonia synthesis also holds for this set-up. It is important to note that the costs of nitrogen or ASU were not considered in the price evaluation for green hydrogen.

Case 3 - Dynamic operation

Finally, a dynamic seasonal operation will be considered under the assumption that next to variability in electricity, there is also seasonality in natural gas prices. This case will compare a new process chain including the CAPEX and OPEX costs of ammonia storage and compare it to the base case with steady-state production. Over a year time, the two cases produce the same amount of ammonia.

Large-scale systems are often not very flexible to different loads and have relatively long transient periods from one operating point to the next. An ATR has been considered to be relatively flexible in operation however a Haber-Bosch reactor has a start-up and shutdown time of multiple days (Morgan et al., 2017). For both reactors, the transient behaviour was not considered in this research, however, it was found that the Haber-Bosch reactor can have a safe load shift of 20% of its capacity within one hour (Armijo & Philibert, 2020), surpassing this limit can be detrimental to the catalyst due to the exothermicity of the reaction. Research shows a load capacity flexibility of 50% is possible (Verleysen et al., 2021), however below 70% the efficiency of the process deteriorates quickly (Bonnet-Cantalloube et al., 2023). Therefore, in this research, only longer-term operational changes were considered to respect the physical boundaries of the system and maintain a safe operation. The operation of the plant will be varied from approximately 75% to 100% (1200-1600 mol/s). In the winter when the prices are higher, 75% production is run, whereas in the peak of summer, 100% capacity will be generated. The total yearly ammonia yield was kept constant; the reactors were resized to meet the new peak load so that the final total yield of the variable case was the same as the base case. The surplus of ammonia generated in the summer is stored in storage tanks to be depleted in the winter when the excess is sold.

The NG supply is given a monthly discrete value that follows a sinusoidal curve that is in the opposite phase of the sinusoidal curve for the price relation. Multiple price variations were considered by increasing the amplitude of the sinusoidal function. The function still has an average value equal to the IEA NG pledged price of €22.64 to make a fair comparison. The hours it takes to change from one operational point to the next were summed and then deducted from the operational hours, therefore the production in transient periods is disregarded. The demand remains at a steady state, like in the base case. This case should yield a comparison in levelized costs of ammonia year-round for the variable operation versus the base case. It should also give an insight into the effect of running at a lower capacity on process efficiency. Furthermore, it should show whether there are scenarios in which variable operation is financially preferential over steady-state operation when the demand and price are fixed. Finally, it should give a first indication of which factors impact the feasibility of dynamic operation.

4

Results and discussion

4.1. Model validation

The important results of each sub-model will be presented graphically and then compared to existing literature to validate the outcome. For the three reactors, the temperature, molar flow rates and conversion will be regarded as the major outputs. For the separation steps the overall physical outcomes and profiles will be validated. All model simulation outcomes are presented in appendix B.

4.1.1. ATR

In order to validate ATR the model, firstly the temperature and molar compositions and conversions were simulated in the base-case conditions to confirm that the expected profiles emerged. Then other operating points were inputted to compare the simulation to existing literature and industrial data. Figure 4.1 shows the temperature profile over the reactor length for the base case and compared to a reference case under the same conditions. Figure 4.2 gives the compositions per component over the reactor length and the percentual conversion of methane is shown in figure 4.2. These outcomes are based on the thermodynamic and kinetic model presented in chapter 3.

Figure 4.1a represents the temperature profile after combustion over the reformer bed. A peak temperature is visible in the temperature profile at 1314.5 K (1041.3 $^\circ$ C), it is assumed this peak is reached straight after combustion and that both the catalyst and the gas are at this temperature. After which, the temperature profile converges to a steady state of 1170.9 K (897.7 $^\circ$C). This behaviour is expected as the endothermic steam methane reforming reaction consumes this heat. This temperature profile has also been experimentally established by Piña and Borio (2006).

To further validate the outcome a simulation was run based on industrial conditions (α = 0.51, β = 1.7, P_{in}=3.0 MPa, T_{in} = 850 $^\circ$ C) and the model's temperature profile showed similar values. The industrial top temperature was measured at 1202 $^\circ$ C and the output temperature at 936 $^\circ$ C (Mirghani, 2007). This model gives 1188 $^\circ$ C (1.2% deviation) and 941 $^\circ$ C (0.5% deviation). The comparison is also visible in figure 4.1b. This is considered sufficient validation for the temperature profile.

The component outputs shown in figure 4.2a were also validated. The general trend of the molar flow rate development over the reactor length matches the expected behaviour also reflected in past research. To check the actual values, three simulations were run using input data compatible with a pilot plant and two industrial plants taken from Aasberg-Petersen et al. (2001). When the model is operated under the same conditions as the pilot plant the H_2 + CO yield is 95.9 dry mol%, in the pilot case this is 93.1% (a 2.8% difference). The same was done for data from two industrial reactors, in which the deviations were larger: 5.1% and 6.0% respectively. These offsets are most likely due to the assumptions and simplifications made in the model.

On the other hand, the H_2:CO ratio was found to be significantly higher in the simulation than in the industrial data. From this comparison it can be concluded that the simulation tends to overestimate the

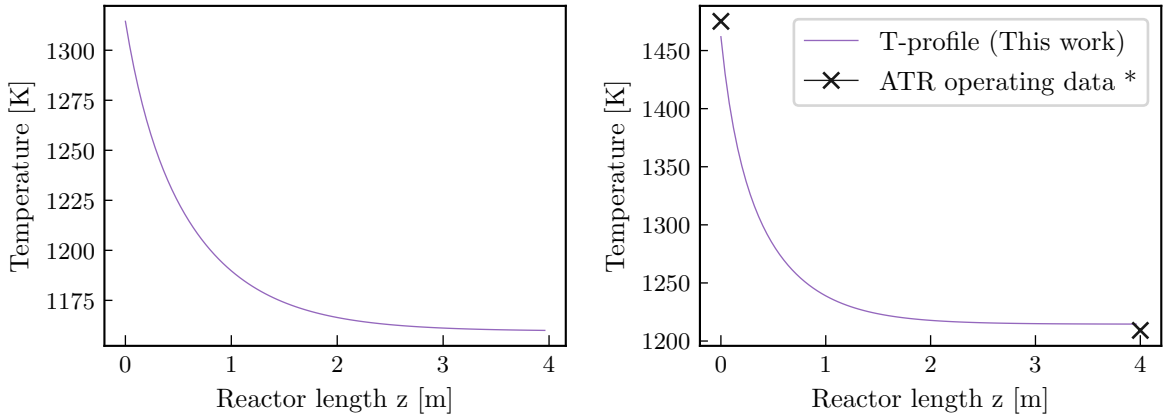

(a) Temperature profile for the base case conditions: $\alpha = 0.6$, $\beta = 2.0$, $P_{\text{in}} = 2.8$ MPa, $T_{\text{in}} = 873.15$ K

(b) Temperature profile compared to industrial data from *Mirghani (2007) ($\alpha = 0.51$, $\beta = 1.7$, $P_{\text{in}} = 3.0$ MPa, $T_{\text{in}} = 1123.15$ K)

Figure 4.1: ATR temperature profile validation over reactor length (instant oxidation assumed)

syngas yield and ratio and underestimate the CO_2 + CH_4 dry yield. However, Rice and Mann (2007) found the H_2:CO ratio should be between 1.7 and 5 (Rice & Mann, 2007), the simulation gives a value of 4.9, indicating it is indeed quite high however not unrealistically high. Moreover, a higher or lower H_2:CO ratio will be compensated in the water gas shift reactor, therefore it is more important the total yield matches the data closely. Finally, the lower estimation of CH_4 and CO_2 yield can be attributed to the assumptions made in the simulation model. More residual CH_4 in reality can be attributed to the fact that it is assumed all O_2 combusts with CH_4, that there are no heat losses in the reactor, that the catalyst is uniform and does not degrade and finally that equilibrium is reached in the reactor.

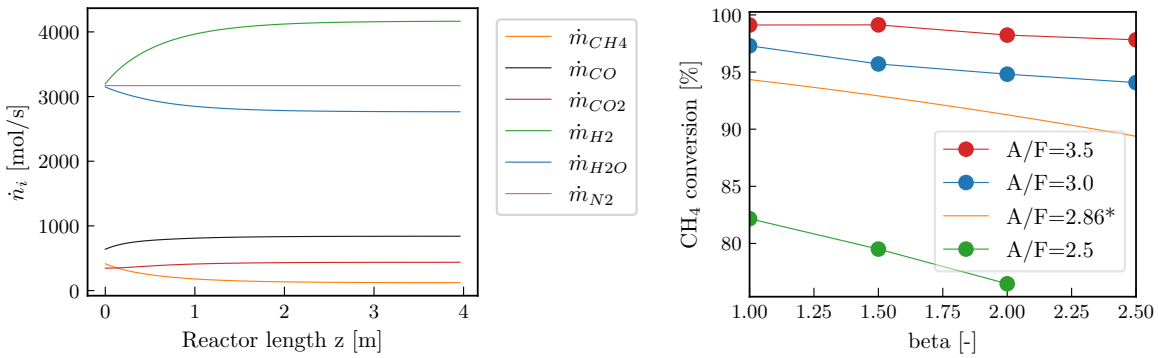

(a) Molar flow rate per component over the reformer length of the ATR with α=0.6, β=2.0, P_{in}=2.8 MPa, T_{in}=873.15 K.

(b) Methane conversion as a function of water-to-carbon (β) ratio and air-to-fuel (A/F) ratio, compared to experimental data by Hoang et al. (2006), * Simulation results from this work.

Figure 4.2: ATR composition and conversion data in base-case scenario and compared to other experimental data.

Figure 4.2b shows the experimental outcomes by Hoang et al. (2006) compared to the outcomes of this model. Hoang et al. (2006) experimentally established the methane conversion for air-blown ATRs over different conditions. A methane conversion of 95% is reached for a 3:1 air-to-methane ratio and a conversion 78% conversion is reached with a 2.5 ratio when the steam ratio is 2. For this model, the chosen operating window is 2.86:1 air-to-methane ratio and a 2:1 steam ratio, this gives a conversion of 89.8%. When the experimental data is interpolated this conversion seems to match the behaviour as can be deduced from figure 4.2b. Rice and Mann (2007) found an approximate 75% methane conversion during oxidation, the model used in this research results in 79% for similar conditions. The slight difference can be explained by the assumption all oxygen reacts and no heat loss occurs. The final total ATR conversion (including the Halabi et al. (2008) reformer bed model) is also in line with the

overall conversion values published by Biesheuvel and Kramer (2003).

Overall, both the profiles and the values for the temperature and the component composition align with the limited available data. Therefore for preliminary process design and evaluation, it is assumed this model represents the the actual conditions sufficiently. The temperature profile in the final operating conditions remains above 860 ° C, therefore it is assumed no coke formation is apparent (Li et al., 2008) and therefore no catalyst deactivation occurs due to coke.

4.1.2. WGS

For the water gas shift model, again the temperature profile and component conversion over the length of the reactor are depicted. However due to the lower temperature, only one dominant reaction takes place with a 1:1 stoichiometric ratio, therefore the conversion of one component describes the conversion of all components.

HTWGS

Figure 4.3a and 4.3b show the respective temperature and conversion profile for the high-temperature water gas shift.

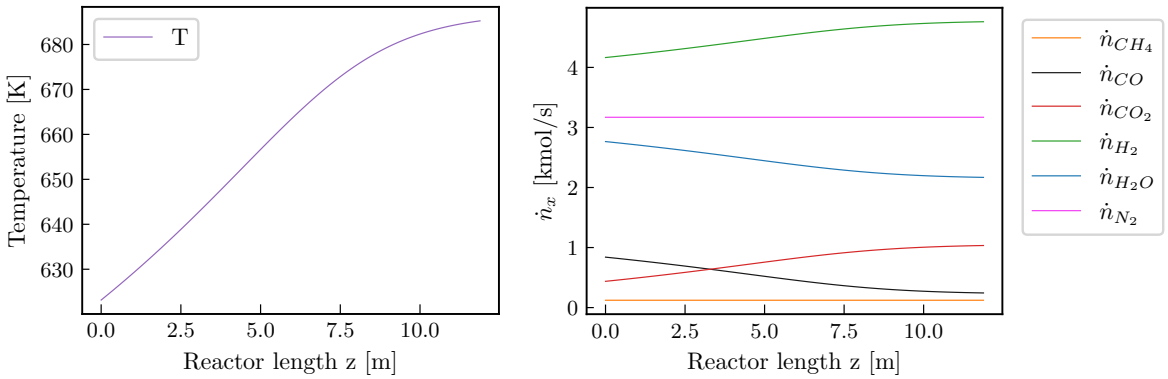

(a) Temperature profile over the reformer length of the HTWGS for $T_{\text{in}} = 873.15$ K

(b) Molar flow rate per component over the reformer length of the HTWGS $T_{\text{in}} = 873.15$ K

Figure 4.3: HTWGS validation

Figure 4.3a shows the temperature profile over the reactor length, the profile matches the expected behaviour. The temperature increases as the reaction occurs as the water gas shift is exothermic. Each temperature corresponds to a certain equilibrium state, which the components move towards. Depending on the partial pressure of each component the reaction moves towards a certain equilibrium state but also an equilibrium temperature. The plateau in the temperature and conversion is an indication the equilibrium is reached and the reactor sizing is sufficient, in appendix B the simulation is given over a larger length showing this is indeed the plateau. Devkota (2019) published an industrial model with an input temperature of 627.2 K (354 °C) and a final temperature of 695.2 K (422 °C). In this simulation, a final temperature of 698.8 K (425.6 °C) is reached under the same input conditions. The small difference can be attributed to heat loss because the reactor is not fully adiabatic.

Devkota (2019) also found a CO conversion of approximately 78%. This simulation yields a conversion of 78.2%. Finally, Reddy and Smirniotis (2015) indicates that after the HTWGS the molar percentage of CO should be around 2 mol% - 3 mol% CO. This simulation gives an output of 2.1 mol% CO, which falls within the limits. In reality, this value might be higher due to the idealized assumptions and model configuration that equilibrium is reached. The relative errors for conversion and temperature loss are 0.2% and 0.52% respectively, indicating the model can accurately simulate industrial conditions. Moreover, the power-law model selected was based on industrial catalyst data, therefore should

yield valid outcomes within its operational scope.

LTWGS
Figure 4.4 shows both the temperature and conversion over the length of the LTWGS reactor for the base case operational inputs. Similar patterns can be found in the LTWGS as in the HTWGS regarding temperature and conversion. In this case, the amount of CO that is converted is significantly lower, so the temperature rise is also limited. The exit temperature of 494.7 K (221.6 ° C) and the conversion is at 88.3 % resulting in a final yield of 0.2 mol% of CO in the mixture.

Amadeo and Laborde (1995) published data on the operation of an industrial LTWGS reactor, this was used to validate the outcomes of the model. A CO conversion of 86.6% is reached in the industrial reactor leaving 0.43 dry mol% CO. The temperature rises from 480 K to 505 K. In this work, for the same conditions, the conversion is 92%, leaving 0.247 dry mol% and the final temperature is 502.0 K. Therefore the 4% conversion difference translates to only a 0.18 dry mol% difference in the final product. This higher conversion can be explained by the assumption absolute equilibrium is reached. The industrial data also shows that the 1:1 stoichiometric assumption is not fulfilled in reality as other compositions (like methane) also change slightly. The lower temperature might be due to possible side reactions that are not accounted for in the simulation, this could also account for the difference in conversion and composition. The model does not perfectly reflect an industrial reactor, however it does suffice for the simulation purposes of this research.

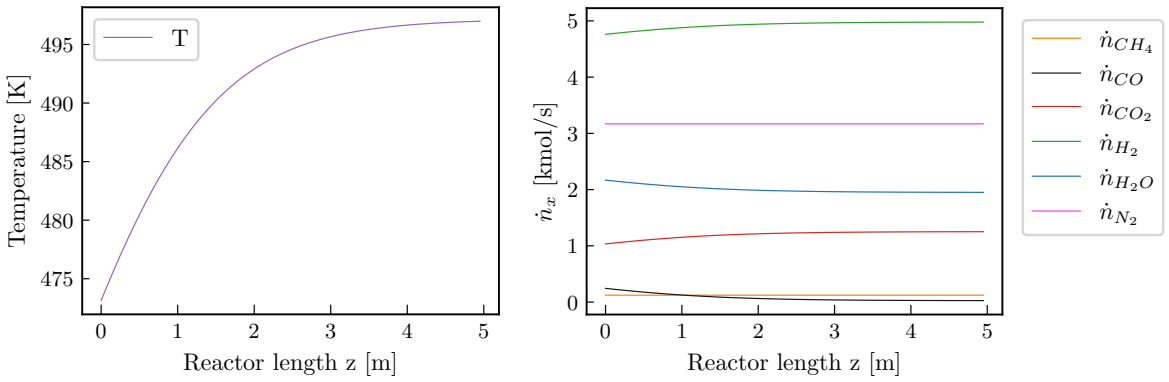

(a) Temperature profile over the reformer length of the LTWGS for $T_{\text{in}} = 873.15$ K

(b) Molar flow rate per component over the reformer length of the LTWGS $T_{\text{in}} = 873.15$ K

Figure 4.4: LTWGS validation

In the HTWGS, bulk conversion takes place and therefore it is subject to more temperature increase due to the exothermic reaction. Moreover, there is a slight s-curve noticeable in the temperature profile in the HTWGS, indicating the reaction rate increases slightly along the reactor before plateauing. In the LTWGS reactor, the temperature profile shows a clear decrease in reaction frequency over the length. The reactor length was based on the temperature and conversion profiles. When the temperature reaches the plateau, it indicates the net reaction rate is approaching zero and therefore further extension of the reactor does not yield extra conversion however does carry extra costs.

4.1.3. Absorption and stripping

For the absorption column and stripper, both purity and recovery should be maximized for the best performance. Therefore there is an optimum pressure for the flash tank and Selexol flow rate to reach these two demands. The Selexol flow rate was selected so that the recycle is perfectly compensated in steady-state operation. For this amount, the purity and recovery were plotted against the flash pressure to prove the correct physical behaviour is being implemented in the model. The result is given in figure 4.5.

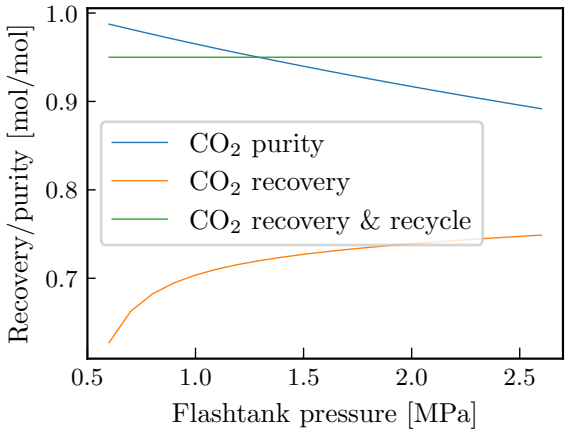

Figure 4.5: Physical absorption flash tank pressure versus the purity and recovery of CO_2

Figure 4.5 shows the expected behaviour for a physical absorption system. With a higher flash tank pressure, the purity of the product decreases, however the amount of CO_2 that is captured and released is increased. Literature mentions the usage of flash tanks that vary from 6 bar (Guo et al., 2012) to 19.5 bar (Kapetaki et al., 2015) for similar operational windows. In the latter, the purity of CO_2 is 97.6 %, confirming 95% capture with <95% purity is possible. It is important to note that an integrated solvent cycle might be necessary to reach the 95% purity conditions due to the possible pinch point formation at the top of the column because of the high solvent flow rate (Ahn et al., 2014). In this research, it is assumed the 95% capture rate can be obtained through proper operation, column sizing and flash tank pressure. This model assumes large simplifications like the applicability of Henry's law over the entire column length and neglects the competition between the solubility of the gasses. This might result in inaccuracies in the absolute values the model gives however, the system has been tested and proven to work for similar purposes, yielding the right purity and recovery. All in all, the behaviour of the model reflects the expected physical phenomena and suffices for this research purpose.

4.1.4. PSA

The pressure swing adsorption process was modelled as two layers of adsorbent in series. The competitive equilibrium is reflected by the Langmuir isothermal relations. For both adsorbents, the pure isotherms and their competitive loading are plotted versus their partial pressure. Figure 4.6 gives the results for the activated carbon layer that removes all CO_2 and the other components partially, then the second layer is zeolite X13 which removes the other impurities. All components have a low loading, but the amount of impurities at this point in the process is very limited, therefore this loading is still sufficient to remove all impurities. A PSA is used industrially for purifying hydrogen to extreme levels (Ruthven et al., 1996), therefore it is assumed the PSA is physically able to reach the required ratio and purity. Through this short-cut model a simplistic approach is taken to still include some physics in the model, the adsorbent mass is based on the outcomes of the model.

4.1.5. Reactor-specific conditions

Suitable operating conditions for the reactors were based on the performance that followed from the reactor models. For the HTWGS there is a peak in the conversion at input temperature around 350 ° C, this is also confirmed by (Callaghan, 2006). Therefore the input temperature for the water gas shift reactor is chosen to be 350 ° C. The same analysis was performed for the LTWGS, which showed a peak at 200 ° C, again in line with expectations and literature (Ruettinger et al., 2003). The absolute influence of the WGS input temperature is much more significant for the HTWGS due to the bulk conversion. These conclusions were drawn from the figures presented in appendix B, showing the CO-conversion, the absolute flow rates per component, the molar fraction per component and the temperature over the reactor length and finally the conversion over input temperatures.

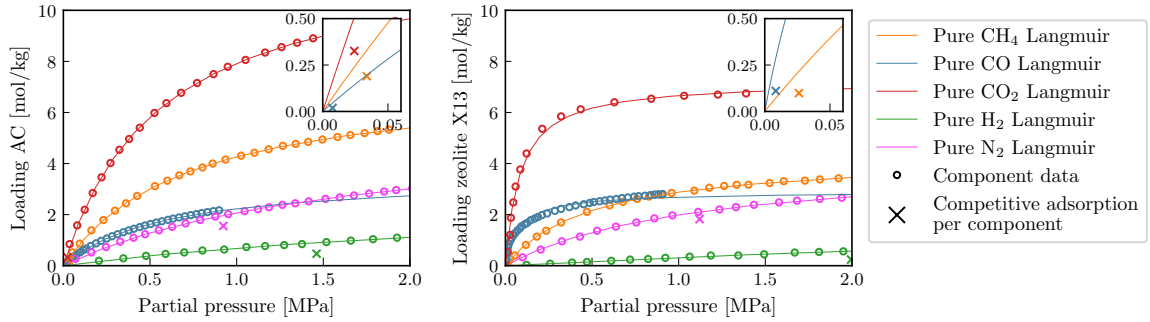

(a) Loading on activated carbon

(b) Loading on zeolite X13

Figure 4.6: PSA loading per adsorbent

For the separation processes the earlier mentioned flash tank pressure and Selexol flow rate were selected to meet both purity and yield demands. This resulted in a flash tank pressure of 1.25 MPa which was deduced from figure 4.5. The absorption model was physically limited by the 5% of the CO_2 that was assumed to never be absorbed. The Selexol flow rate and flash tank pressure were set to match the incoming flow rate and the recycle stream perfectly. For the PSA the adsorbent mass was selected based on two criteria: ppm level impurities and the right ratio between hydrogen and nitrogen. For the first layer of activated carbon, all CO_2 needs to be adsorbed, so the mass and volume were scaled to do so. After which the zeolite layer should adsorb the other impurities: CO and CH_4 and then finally absorb some of the remaining N_2 to meet the right ratio (3:1), ideally whilst losing as little H_2 as possible.

4.1.6. Model validation conclusions

The model performances have been compared to several values found in past research to validate their applicability. All reactor models showed the expected thermodynamic and kinetic behaviour. The data for certain industrial applications for the models was limited however did match the operational outcomes of the models to a satisfactory level. The separation and purification processes had a less extensive internal model. The purity and operational conditions were checked with industrial applications, therefore, they are assumed to be realistic, however, these models contain more uncertainty. Based on these validations, it is assumed these models accurately represented the industrial reality for process design purposes and initial comparative studies and simulations.

4.2. Operational window per reactor

4.2.1. Overall model performance

The entire chain performance was evaluated per input condition. The performance criteria are levelized cost of ammonia (LCOA), CO_2-intensity. The outcomes are graphically presented in figure 4.7. The absolute ammonia yield and the power consumption were also evaluated, these graphs can be found in appendix C. The results combined with possible physical restraints within reactors will decide the operating window. It is important to note that in each scenario the heat generated by the process (including efficiency factors to account for losses) surpassed the heat requirements however, this residual heat was not accounted for financially through direct sale or power generation. The base values for the sensitivity were set as the eventual selected operational set point: α=0.6, β=2.0, T_{in}=873.15 K and P_{in}=2.8 MPa. The choice for these conditions specifically is further explained in the coming section based on both the overall financial impact and the internal physical reactor limits.

LCOA

The results for the influence of each input parameter on the levelized costs are shown in figure 4.7a. The graph shows that the input pressure has a limited influence on the levelized costs. This is because theoretically reactor kinetics are improved by higher pressures, however the reactor was sized so that near equilibrium could be reached in all considered pressure conditions. Moreover, the pressure varies from 2.1-3.5 MPa because of physical constraints in the separation steps, therefore the compression

ratio is not changed significantly. The pressure variation has a limited effect on the component outcomes and even though the variable OPEX is influenced, it still does not significantly contribute to the LCOA. This graph shows a lower input pressure is financially more attractive. The relative influence of β (steam-to-methane ratio) is also not extremely significant, the variation shown in the graph is from 1.4 to 2.6, and the impact of the variation from 1-3 is also visible in appendix C. When varied over that window, the financial impact becomes larger, with a total variation of 0.05 €/kg. Figure 4.7a shows a higher β-value results in lower levelized costs. However, the increase in steam also results in a higher CAPEX for reactors, larger compression power and less possibility for heat recovery as a secondary revenue stream due to lower temperature regimes.

The influence of α, the oxygen-to-methane ratio (varied from 0.48 to 0.72), and input temperature (varied from 350 - 850 °C) is quite significant. At a higher reaction temperature more methane is converted. The temperature is decided by the input temperature and the level of combustion, therefore directly linked to α. With a higher input temperature, the levelized costs are brought down significantly with more than a 0.10 €/kg difference over the window span. However, again extra revenue due to excess heat or possible co-generation is not considered therefore these effects could change the financial forecast. For α, a higher value results in higher methane conversion and therefore lower levelized costs. The variation over the operational window amounts to a difference of about 0.08 €/kg. It is also visible that going beyond 0.7 no longer has the desired effect and the levelized costs start to plateau. Moreover, it is important not to have an excess of O_2 as this can cause problems down the line. Lastly, a higher α-value also results in more nitrogen again driving the CAPEX up. The main parameter that influences the levelized costs is the ammonia yield. The impact of each condition on the ammonia yield is close to the inverse of what is shown in the levelized costs. A higher α, β and T_{in} and a lower P_{in} leads to a higher ammonia yield. The values are not 1:1 transferable because the influence of each factor on power consumption and partially on the CAPEX also plays a role. The influence of these operational conditions on the power consumption and ammonia yield is visible in appendix C.

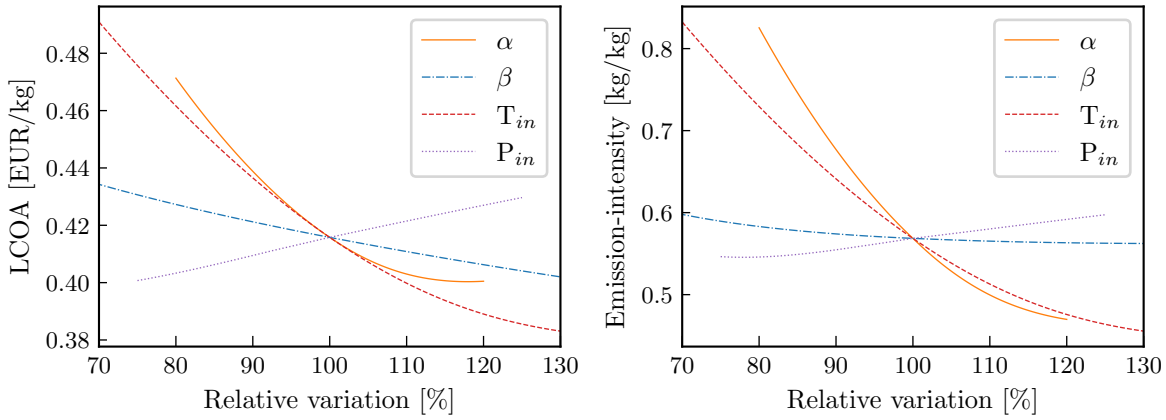

(a) Levelized cost sensitivity to input conditions

(b) Total CO_2-emission sensitivity to input conditions

Figure 4.7: Influence of operating conditions on the overall performance of the multi-commodity system. Base values: α_{base}=0.6, β_{base}=2.0, $T_{\text{in}_{\text{base}}}$=873.15 K, $P_{\text{in}_{\text{base}}}$=2.8 MPa. Definitions: α = O_2:CH_4 ratio, β = H_2O:CH_4 ratio.

CO_2-intensity

A second factor to consider, besides the financial performance of the system, is the amount of CO_2-emission that is released. Figure 4.7b shows the sensitivity of the total (direct and indirect) emission per produced kg of ammonia compared to the different input conditions. The graph shows the emission intensity follows the same trend as the levelized costs. Emission intensity is defined over the total amount of ammonia produced, so for a higher ammonia yield, this value is lower. However, it is visible that the values are not fully linearly correlated. The impact of β and pressure variations is limited as can be deduced from the gradient. The impact of the input temperature and α is more extreme. These parameters are directly correlated to the methane conversion rate: a lower conversion leads to more direct emissions because it is assumed the trace amounts of methane are inert after the ATR and

contribute the total direct emissions and a lower conversion leads to a lower yield. All in all, both the levelized costs and the emission intensity indicate a lower pressure value and higher α, β and T_{in} is preferential.

4.2.2. Sub-model sensitivity

To select the operating window, not just the environmental and financial impact need to be assessed but also the internal reactor limitations. Therefore based on the model sensitivity outcomes and the physical limitations of each reactor published in the literature the conditions were further inspected. All graphs are presented in appendix C, only the more noteworthy graphs will be discussed here.

α-sensitivity

The addition of air to the system will result in more methane combustion and therefore higher temperatures in the system. However, with higher temperatures, control and safety become more of an issue. The temperature after oxidation and after the reformer bed are presented as a function of α in figure 4.8a. The top temperature in the reactor is reached just after the oxidation reaction and is denoted by T_{oxi} and the output temperature after the reformer section is denoted by T_{ref}.

Higher temperatures in the ATR lead to hot spot formation which causes catalyst sintering and deactivation. To prevent this phenomenon, the maximum temperature should not exceed 1323.15 K (1050 °C) for the oxidation (Asaro & Smith, 2013), which corresponds to a 0.6 α-value. A high α-value can also result in incomplete combustion of the oxygen which can also lead to catalyst deactivation through nickel oxidation. Furthermore, a high α-value results in more inert N_2 entering the system which drives the CAPEX up and dilutes the partial pressure of other components impacting reaction efficiencies, this could also prove to be an issue for the separation steps.

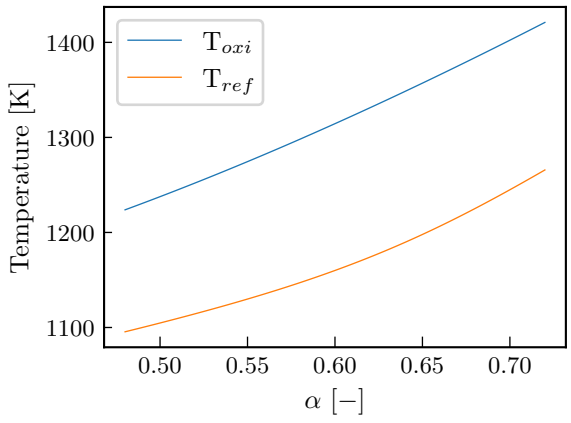

(a) Influence of α on the oxidation and reformer output temperature of the ATR

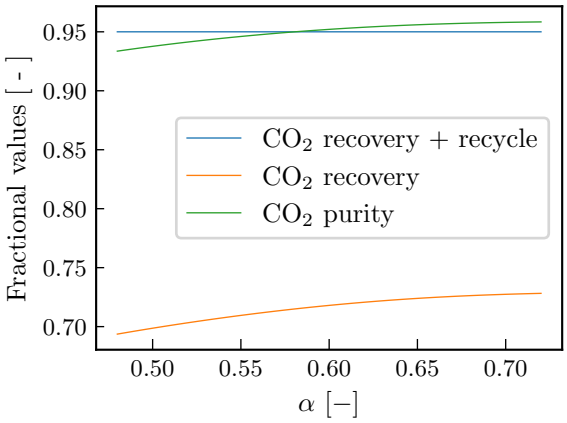

(b) Influence of α on the CO_2-purity in absorption process

Figure 4.8: Influence of α-value on reactor performance

However, the output reformer temperature cannot be too low because the temperature limit for coke formation is higher at high pressure, risking catalyst deactivation (Pashchenko & Gnutikova, 2021). Moreover to reach the right CO_2 purity in the absorption process, an α-value of at least 0.57 is necessary as is shown in figure 4.8b. Combining these technical bottlenecks and the overall system performance results in an α-value of 0.6 to minimize catalyst deactivation, the levelized costs and the carbon emissions. Further influence per reactor on conversion and temperature profiles are given in appendix C.

β-sensitivity

The increase of β influences the autothermal reactor by limiting the temperature profile in the reactor. The relative influence on the peak oxidation temperature is higher than the influence on the reformer output temperature. This results in fewer hot spots near the oxidation zone and a limited risk of coke formation in the reformer zone. It also ensures a less steep temperature gradient over the reactor length. However, the reactor must remain thermally neutral even if the thermal losses, in reality, are larger, therefore the β-value should also not become too high. The composition of each component in the ATR is visible in figure 4.9a. A higher β-value leads to less CH_4 conversion, and more H_2 yield after the ATR but less CO. The reduction in methane conversion is a limiting factor in the increase of the β-value. However, a higher β-value also results in higher CO-conversion in both shift reactors and lower output temperatures which is advantageous for the thermodynamic properties of the exothermic water gas shift reaction. Further research should quantify the effect of adding extra steam after the ATR for the water gas shift.

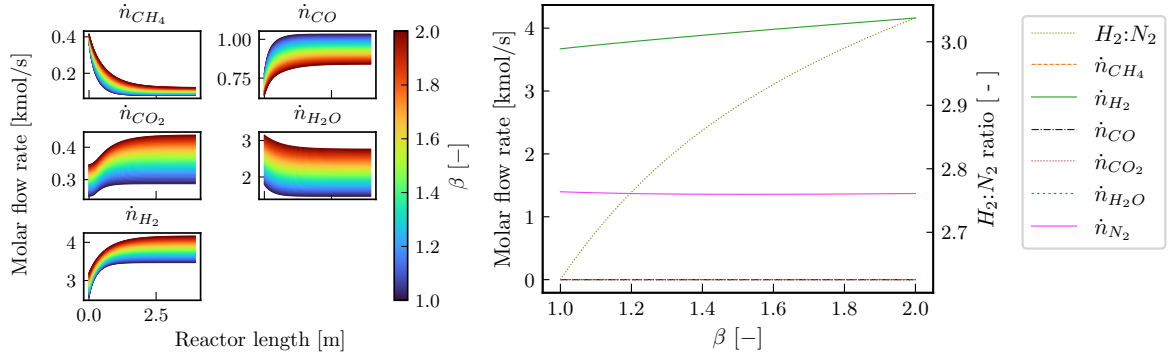

(a) Molar flow rates over the length of the ATR for different β-values represented by the rainbow from 1.0-3.0

(b) Molar flow rates and H_2:N_2-ratio in the PSA, the CH_4, CO, CO_2 and H_2O are removed to ppm level so all have a molar flow rate of 0 kmol/s

Figure 4.9: Influence of β-value on reactor performance

A higher β-value per definition requires the generation of more steam. This requires more heat, more compression power and larger reactors which is another downside. The effect of β on the PSA is indirect because the stream is dehydrated before this process step. However, the mixture composition that enters the PSA is a result of the variations in β. A higher β-value results in an easier PSA process. The final H_2:N_2 ratio shown in figure 4.9b with the adsorbent layer sizing of the base case requires a β-value of at least 2, the higher the value the less adsorbent is necessary. Further influence of β per reactor is given in appendix C. Considering the control and safety aspects of a higher β-value, the lower levelized cost and the higher ammonia yield on the one hand, and the lower CH_4 conversion on the other hand, result in a selected β-value of 2.0.

T_{in}-sensitivity

Low input temperatures require less preheating, however higher input temperatures result in better reaction kinetics. The operating window of an ATR is very specific, at low temperatures hydrocarbon accumulation can lead to coke formation and incomplete reactions. Whereas a temperature that is too high can lead to hydrocarbon cracking also resulting in coke formation. Mirghani (2007) found that the minimum input temperature should be 450 °C to prevent coke formation. The maximum temperature depends on the reactor set-up, in this case the earlier maximum 1323.15 K (1050 °C) limit for the ATR is the main restriction on the input temperature. Figure 4.10a indicates the input temperature should not surpass 873.15 K (600 °C) to respect this thermal limit in the ATR. An advantage of a lower input temperature is a shorter the system start-up and shut-down time.

At higher temperatures, the conversion of methane in the ATR is enhanced. The final operational temperature is limited by the CO_2-purity which is only sufficient at temperatures above 550 ° C, this is shown in figure 4.10b. The higher the temperature the lower the levelized costs and CO_2-emission are. A final input temperature of 600 °C was selected. However, it is important to note that in this research,

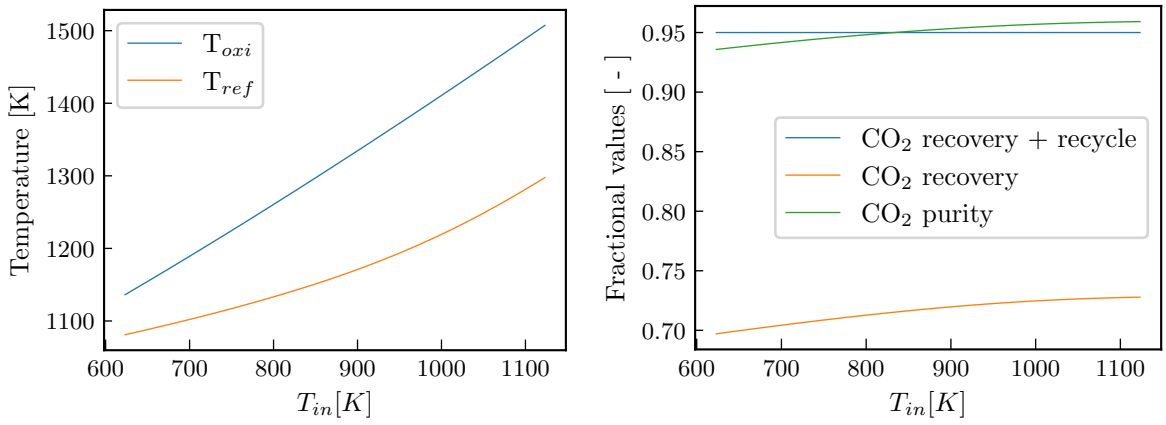

(a) Influence of T_{in} on the peak temperature after oxidation and the output temperature after the reformer bed in the ATR

(b) Influence of T_{in} on the CO_2-purity in absorption process and the recovery

Figure 4.10: Influence of input temperature on reactor performance

heat loss is not accounted for and all residual heat that cannot be reused in the operation is not used for other purposes. The financial implications of raising the temperature should be further investigated along with the heat loss during oxidation and reforming to find the true optimum.

P_{in}-sensitivity

The pressure was varied from 2.1 MPa to 3.5 MPa. High pressure is not advantageous for the equilibrium of the ATR, thermodynamics dictate a shift towards the methane side, however at higher pressure the reaction rate is enhanced. The total molar flowrates after the LTWGS are shown in figure 4.11a. It shows the pressure variation at this scale has minimal influence on the composition. The absolute CH_4-conversion and H_2-yield in the ATR is not affected greatly, and the conversion in the WGS reactors is also affected minimally, however, at higher pressure, the water gas shift units can be sized down due to quicker kinetics which decreases the price. Higher pressure could lead to higher CAPEX costs for other process units for safety measures.

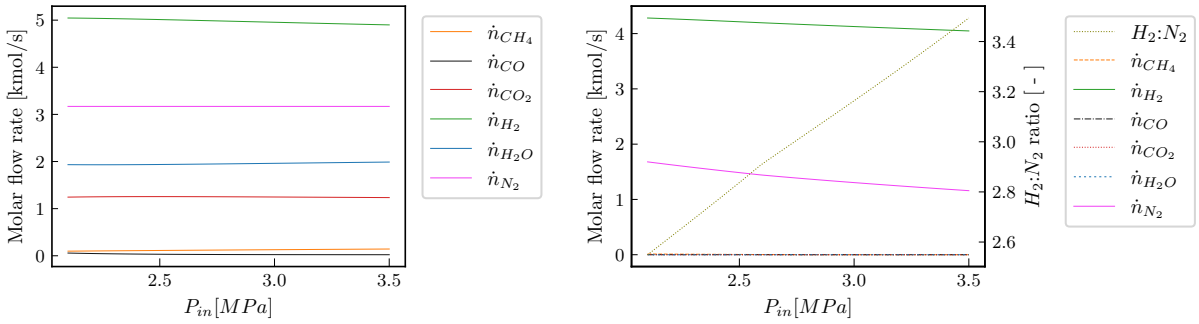

(a) Molar flow rate per component after the low-temperature water gas shift reactor

(b) Molar flow rate of hydrogen and nitrogen and their relative ratio after the PSA

Figure 4.11: Influence of the system input pressure on reactor performance

Financially, the influence of pressure is limited, however to meet the right ammonia synthesis ratio a high pressure is advantageous. The relative N_2-removal in the PSA is higher at a higher pressure compared to the H_2-removal as is visible from figure 4.11b. Generating an excess of H_2 is preferential to an excess of N_2, therefore at higher pressure, it is easier to meet the 3:1 ratio with less hydrogen loss. Otherwise, the adsorbent volume would have to be increased to meet the same specification. The threshold is located around 2.8 MPa. Lowering the pressure further reduces the effectiveness of the separation processes, which could result in the necessity of a vacuum PSA to reach the desired

purity in real life, which would increase the costs significantly. To limit LCOA, and emissions but still meet physical requirements in the process, the pressure is set to this minimum threshold of 2.8 Mpa.

4.2.3. Conclusions for the final operating window

Table 4.1 summarizes the operating parameters for the modelled chain base case. The specific operating specifications per reactor are presented in appendix D in tabulated form. The selected operating conditions fall within the operating safety limits and theoretical boundary conditions whilst still maximizing yield and limiting costs. As a final check, the physical boundaries, not accounted for in the models, were cross-referenced with literature to ensure safe operation. Simeone et al. (2008) presented an operating window for an ATR in which thermal deactivation and coking were avoided. The selected operating window falls within its limits. Past literature has also shown industrial processes are operated in these windows.

Table 4.1: Operating input conditions

Input	value	Unit
$\dot{n}_{CH_4}$	1400	mol/s
α	0.6	[-]
β	2.0	[-]
T_{in}	873.15 / 600	K / ° C
P_{in}	2.8	MPa

4.3. Model performance

The overall performance of the model in the base case is presented in this section. The base case refers to steady-state operation under the previously established operating conditions with a capacity factor of 0.9. Financially, the electricity pricing profile and average carbon intensity of the grid are taken from an in-house TNO projection model of the energy mix by 2030, the IEA pledged scenario fixed pricing for natural gas and carbon emissions are used and the costs for carbon transport and storage is 0.05€/kg CO_2 taken from PORTHOS. To calculate the revenue an ammonia price of 0.472 EUR/kg is used (reflecting current blue ammonia prices corrected for inflation).

4.3.1. Overall performance

The overall chain performance will be evaluated based on the following technical aspects: composition outputs per step, the process efficiency and the indirect and direct emission. Direct emissions refer to the scope one emissions (direct emissions released during the process), for indirect emissions, the scope two emissions are considered (emissions from upstream natural gas production and electricity). After this, the chain will be evaluated on its economic performance through a CAPEX breakdown, the levelized costs, NPV and cumulative cash flows over its lifetime, followed by a sensitivity analysis to reflect the contribution of each financial aspect to the final NPV. It is important to note that in all performance measures, the excess heat and steam are not used for power generation or sold. Therefore there could be additional financial gains in the process not accounted for. Moreover, the costs of carbon storage are not reflected in the financial outcomes.

Technical performance

The technical performance is presented schematically in figure 4.12. Figure 4.12a shows the outcome composition per process step, representing the component conversion and separation per reactor step, the tabulated form can be found in appendix D. In figure 4.12b, the CO_2-equivalent carbon intensity of the process is expressed in kg of CO_2 per kg of NH_3 produced, both the direct and indirect emissions are presented.

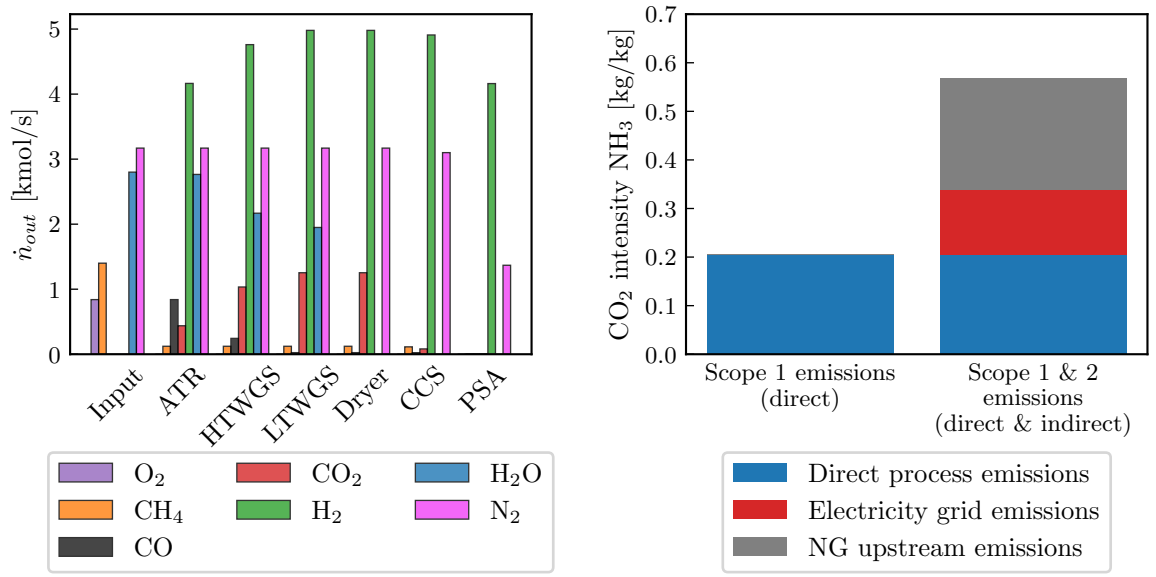

(a) Component composition at the output per process step in steady state operation

(b) Scope 1 (direct emissions) and scope 1 and 2 (direct and indirect emissions) CO_2 intensity of the entire plant per kg of NH_3

Figure 4.12: Technical performance of the blue ammonia plant

This entire process yields an ammonia production of 46.88 kg/s, therefore the capacity of this plant is relatively large (1.478 million tonnes NH_3-capacity per annum). This is equal to a daily capacity of approximately 4000 tonnes, which is slightly higher than the largest single-train ammonia plant (with 3670 tonnes per day). Multiple plants with similar or larger capacities have been realized in the US (CF Industry, 2023) and in Vlaardingen there is already a plant with a 1.8 million tonnes yearly capacity running (Yara, 2023). Therefore proving this capacity is technically feasible and reasonable in the Netherlands. To compare the process performance, the entire process was evaluated on its efficiency. This analysis yielded a thermal efficiency of 74.5 %. Arnaiz del Pozo et al. (2021) found a slightly lower value for the thermal efficiency (65.5 %), this can be due to the large number of idealizations in the reactor models and the extensive purification minimizing the urge requirements. The overall process efficiency (including power consumption) was found to be lower than the value published (65.4 %), with a 59.5 % efficiency in this case. This difference can be explained because Arnaiz del Pozo et al. (2021) assumed the excess steam to be used for power generation, whereas it was disregarded in this research.

Figure 4.12b shows the process has a direct emission of 0.205 kg/kg, Arnaiz del Pozo et al. (2021) found a 0.28 kg/kg direct carbon intensity. When indirect emissions are also included, the process has a 0.567 kg/kg emission intensity. The upstream natural gas emission intensity accounts for 0.230 kg/kg CO_2-equivalent which is higher than the process emission intensity and the indirect electricity emissions also contribute significantly with 0.132 kg/kg. Grey ammonia production has a scope 1 emission of 1.40 kg/kg. If the same natural gas emissions are assumed for grey ammonia as for blue ammonia, the total emission amounts to 1.92 kg CO_2 per kg of ammonia (C. Smith et al., 2020). Blue ammonia results in a 70.5 % emission reduction compared to grey ammonia (scope 1 and 2). If just direct process emissions are considered 85.4% emission reduction is reached.

Economic performance

The system costs were calculated as explained in chapter 3 to evaluate the economic performance. Firstly the CAPEX was calculated, and the outcome is shown in figure 4.13. The graph shows the replacement costs as if they were made in 2030 to make the comparison easier. The ammonia synthesis is significantly more expensive than the other reactors. This is because it also includes the compressor and heat exchanger costs. If all investments were done in 2030 the total CAPEX would amount to 1145

million euros.

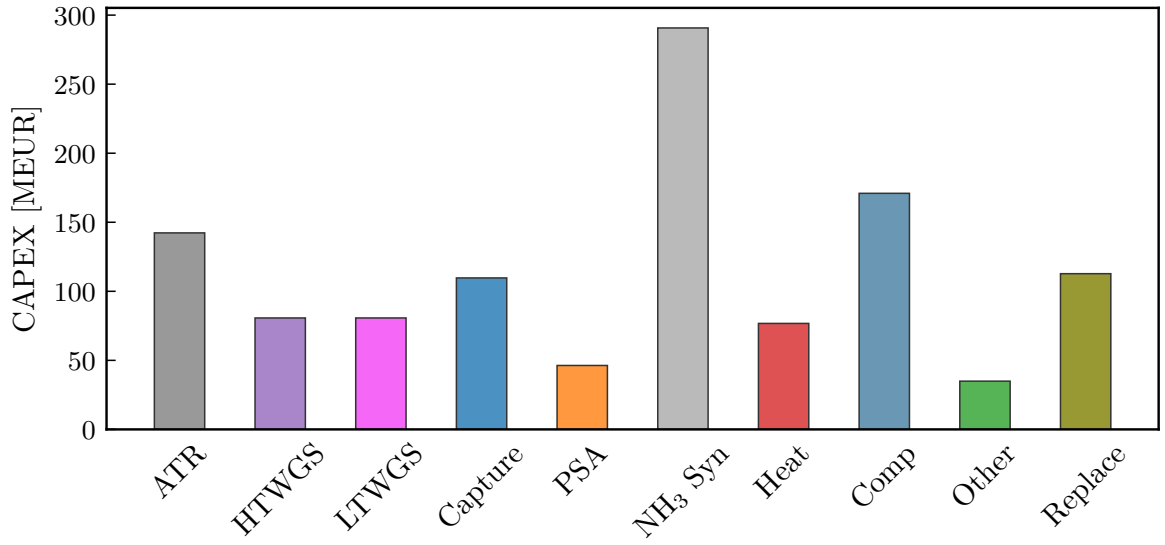

Figure 4.13: CAPEX distribution per process step in MEUR including installation factors in 2030, Other refers to pre-treatment, Replace is the costs of replacements in 2030 currency.

Figure 4.14a shows the total levelized costs and their distribution. The final levelized costs €0.417 per kg of NH_3. When the costs of CO_2 storage are not included, the final levelized costs €0.368 per kg of NH_3. Cloete et al. (2021) found levelized costs for a reference plant with CCS of 0.367 €/kg NH_3 without carbon storage costs therefore confirming the validity of this outcome. The largest contributor to the levelized costs is the natural gas costs with €0.158 per kg NH_3. This is followed by the CAPEX (€0.080), the electricity costs (€0.066), the transport and storage costs for CO_2 (0.0495€), the fixed OPEX (€0.038) and finally the carbon taxes (€0.025).

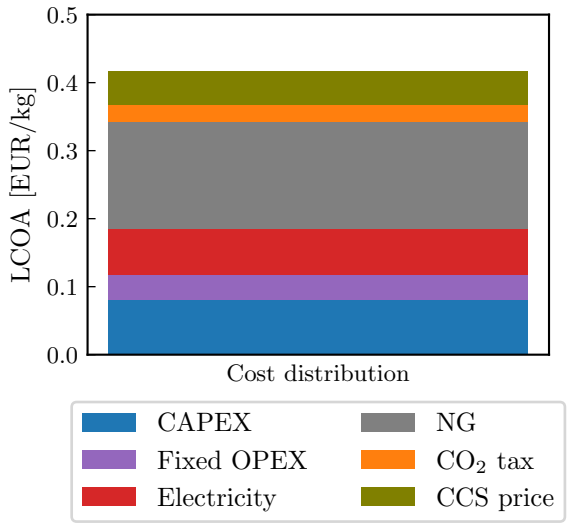

(a) LCOA cost distribution for the base case

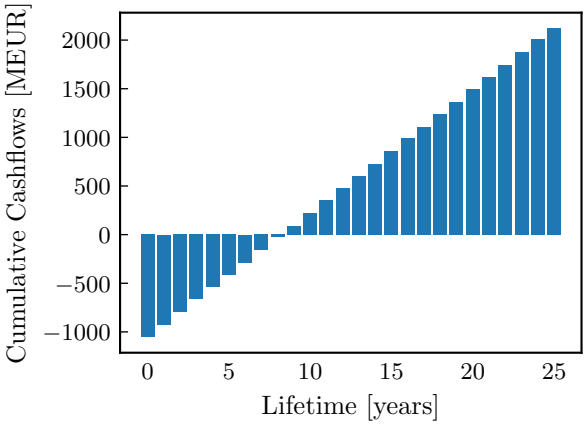

(b) Cumulative cash flows over the plant lifetime

Figure 4.14: Economic performance of the blue ammonia plant

The ammonia price data from S&P Global (2022) for grey and blue ammonia were corrected for inflation resulting in a selling price indication for 2030. This yielded a grey price of 0.428 €/kg NH_3 and

a blue price of €0.472 per kg of NH_3, the latter is used in the calculations for the NPV. The projected price difference does not cover the costs for CO_2 transport and storage. This could be an indication that this blue ammonia price is based on lower capture rates, it has less expensive CO_2 transport and storage or it is partially subsidized.

The blue ammonia price of 0.472 €/kg is used for financial analyses. The cumulative cashflows of the plant are schematically projected in the graph presented in figure 4.14b. This shows the payback time of the system is 9 years. It is also visible that even though the CAPEX costs of the replacements total up to quite a significant amount the investments are quite uniformly spread over the plant lifetime, therefore there are no years in which the plant is projected to have a loss or incurs a significant dent in revenue.

Overall the NPV of the system for the base case conditions is 103.9 million euros. In figure 4.15 the sensitivity of all financial factors is given. This graph shows most influential factor for the NPV is the selling price of ammonia, since this is the only revenue that is generated from the production this is to be expected. If the ammonia prices remain in line with what they are now for grey ammonia (approximately 0.428 €/kg), equal to 90.6% in the graph, a negative NPV (-427.9 million euros) is projected without additional subsidy. At €0.461 per kg price for ammonia (97.7% in the graph), the NPV is equal to zero. Therefore if ammonia prices remain at the grey level, a subsidy of €0.033 per kilogram of NH_3 would be required to break even.

Regarding costs, the natural gas price is the most dominant factor in the price estimation as was already established from the levelized costs. However, in this graph, it is visible that a 4.7% rise in natural gas prices already results in a negative NPV. Over the past few years, the large price fluctuations in the natural gas market have shown that more extreme price increases are feasible. Therefore, coupling the ammonia market to the natural gas price is essential to remain financially viable through any natural gas production route. Currently, this is already the case, as was visible from the ammonia prices during the natural gas crisis (Raghuveer & Wilczewski, 2022).

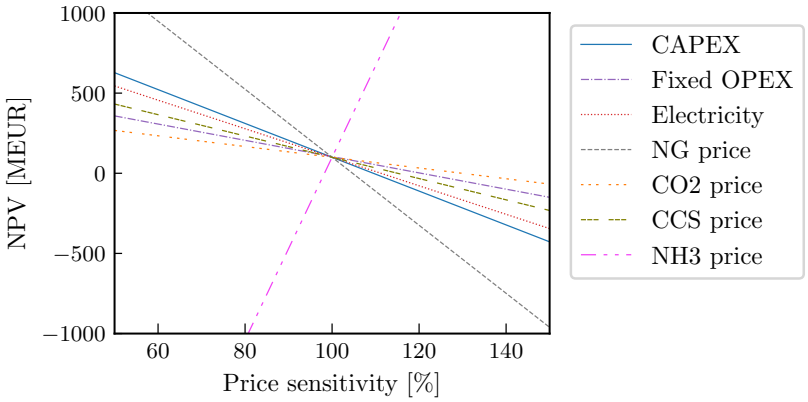

Figure 4.15: NPV sensitivity analysis for all financial factors.
$CAPEX_{base}$= 1033 MEUR initial and 112.8 MEUR replacements, $OPEX_{base}$=63.51 MEUR/year, $electricity_{base}$=41.77 €/MWh, NGbase=22.64 €/MWh, CO_{2base}=0.135 €/kg, CCS_{base}=0.05 €/kg CO_2, NH_{3base}=0.472 €/kg

Conclusions overall performance

The model's technical and financial outcomes are in line with previously published literary values, confirming the model's validity to serve as a basis for different simulations of this process. The system has an overall process efficiency of 59.5% (similar to grey installations) and it produces approximately 4000 tonnes NH_3 daily at full capacity. The CCS leads to a direct scope 1 CO_2-equivalent emission intensity of 0.205 kg/kg NH_3, which is significantly lower than the grey process (an 85% reduction in direct emissions). The natural gas upstream emissions account for the largest emission-intensity contribution if the indirect emissions (scope 2) are also considered. Financially the model gives the levelized costs

of 0.417 €/kg which is within the range published in past research. Finally, the results yield a positive NPV of 103.9 MEUR for an ammonia price of 0.472 €/kg. The NPV is most significantly influenced by the natural gas price (regarding costs) and the ammonia price (overall sensitivity).

4.4. Case 1: Three IEA scenarios

Three IEA policy scenarios are compared in the following section to show the impact of climate policies on the viability and price of commodities. The stated scenario refers to a future landscape in which only the climate policies that are already officially announced or already implemented are considered for future pricing scenarios. The base case is based on the IEA pledged financial scenario, all announced policies are implemented but also the policies required to meet the pledged goals. The NZE scenario refers to one of many paths in which the policies required to reach net zero by 2050 are implemented. Each policy scenario gives a projection for the natural gas price and the carbon taxes, these two parameters are varied and their financial implications are discussed. The equipment price, labour costs and electricity price are kept at the established fixed values. The levelized costs of ammonia in each scenario are compared in figure 4.16.

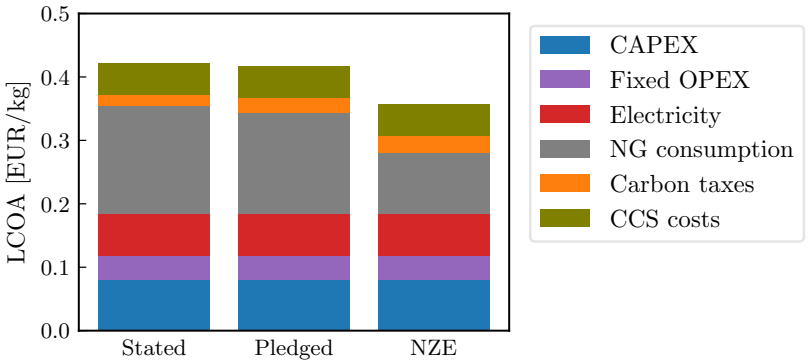

Figure 4.16: LCOA for the three IEA climate scenarios

Table 4.2 summarizes the absolute values of the financial outcome of the IEA scenarios. This table shows that if policies are implemented in line with the net-zero emission scenario the lowest levelized costs and highest NPV for this route of blue ammonia are obtained compared to the other two policy scenarios. Whereas, the stated and pledged scenarios give similar levelized costs and all three scenarios give a positive NPV for an ammonia price of €0.472 per kg of NH_3. The significant reduction of the natural gas price in scenario NZE drives the LCOA reduction. However, the decrease in natural gas prices also affects the grey ammonia price. Therefore in comparison to grey ammonia, the true difference between the three scenarios can be found in the difference in carbon taxes. For grey ammonia, a direct emission of 1.40 kg CO_2 per kg of NH_3 is assumed as opposed to the established 0.206 kg/kg for blue ammonia. In the stated scenario, a €0.11 difference per kg of ammonia is realized through carbon taxes, for the pledged scenario this is €0.16, and for the NZE scenario is €0.17. From this data, it can be concluded that if the additional costs of CCS do not surpass €0.11 per kg of produced ammonia, blue ammonia through this production route can be financially competitive with grey ammonia in all three policy scenarios. The storage and transport costs are 0.06 €/kg NH_3 therefore a minimum 0.05 €/kg margin is left to finance the capture process in each scenario. It is important to note that the pricing of most commodities is in line with the energy price, therefore the implementation of carbon taxes to make low-carbon options financially competitive for ammonia but also for other energy systems most likely will be reflected in the electricity price, equipment price, labour costs but also in the pricing of everyday products. Therefore the broader impact of implementing higher carbon taxes should be considered by policy makers.

The cumulative cashflows for each scenario are shown in figure 4.17. It is visible that the payback time of the NZE scenario is the shortest and the final profit the highest. However, the standard ammonia

Table 4.2: Financial outcome of three IEA scenarios

Outcome	Stated	Pledged	NZE
NPV [MEUR]	54.3	103.9	920.0
LCOA total [€/kg]	0.421	0.417	0.356
LCOA NG costs [€/kg]	0.170	0.158	0.096
LCOA CO_2-taxes [€/kg]	0.017	0.025	0.026
LCOA other [€]/kg]	0.234	0.234	0.234
Payback period [years]	9	9	5

price is heavily correlated to the natural gas price therefore with lower natural gas prices like in the NZE scenario, this will likely also be reflected in the ammonia price, therefore a selling price of 0.472 €/kg NH_3 in the NZE scenario might not be feasible in a competitive market. The levelized costs of the pledged and stated scenarios were similar therefore their cumulative cash flows are also similar. It is important to note that in all three scenarios, with a selling price similar to the current blue ammonia market corrected by inflation, the NVPs are positive (54.3-920.0 MEUR) and the payback time is reasonable (5 - 9 years). From these results, it is visible what the possible effects of policies are on profitability and thereby security of investment in sustainable solutions.

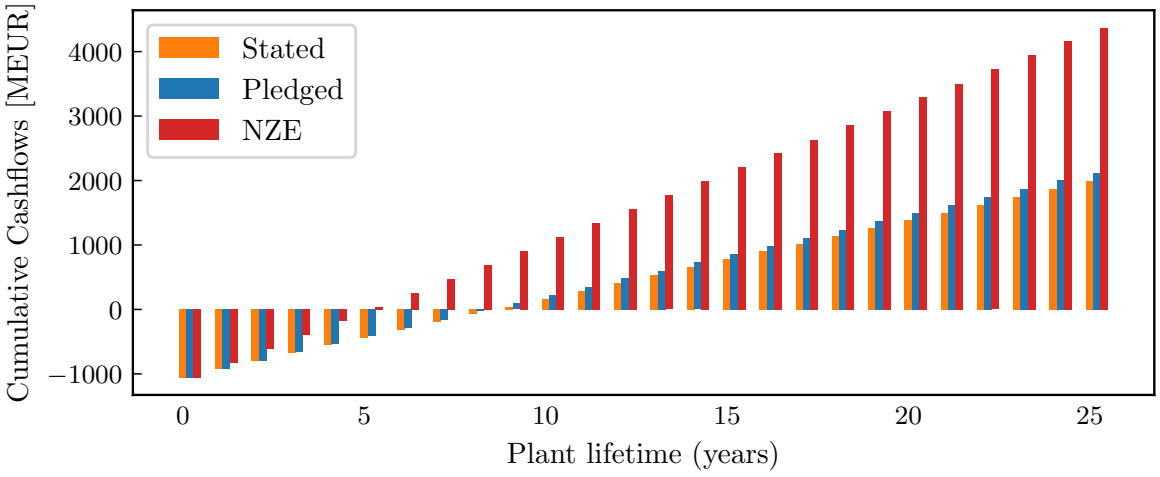

Figure 4.17: Financial prospects over plant lifetime in three IEA climate scenarios

4.4.1. Conclusion IEA climate scenarios

From this case, a few main conclusions can be drawn. Firstly, all three climate cases give a positive NPV, reasonable levelized costs and payback period, therefore regardless of the climate policies implemented, the investment is justifiable at a selling price of €0.472 per kg NH_3. However, to compete with grey hydrogen financially, the increase of carbon taxes has a significant impact in bridging the price gap (with a €0.11 - €0.17 /kg NH_3 buffer for the costs of CCS). The influence of carbon taxes is relatively limited for blue ammonia (2 - 3 cents per kg), the natural gas price however does impact the levelized costs significantly, therefore policies in line with the NZE scenario are very advantageous for the blue ammonia route, however further impact on the electricity prices, CAPEX and OPEX can give a more accurate comparison. These three scenarios show the clear impact policies can have on the financial competitiveness of more sustainable energy systems, but the economic impact of extra taxation on the end consumer should be considered.

4.5. Case 2: Blue vs green

In this case study blue ammonia generated from the base-case scenario is compared to green ammonia for a similar capacity. First, the financial performance of green ammonia is discussed and then it is compared to blue ammonia.

4.5.1. Financial performance green ammonia

First, the CAPEX distribution will be presented, including replacement costs and a short discussion on the CAPEX uncertainty. Thereafter, the sensitivity analysis for all economic factors for green ammonia will be shown graphically, similarly as previously done for blue ammonia, this indicates which costs are most influential in the profitability of green ammonia.

CAPEX distribution green ammonia

The CAPEX distribution for green ammonia is shown in figure 4.18. The total CAPEX distribution consists of three process units. The ammonia synthesis plant is operated in the same fashion as for blue ammonia production case (CAPEX includes auxiliary equipment like compressors). Electrolysis is quite a complex process and the scale of production is very large in this simulation, therefore the CAPEX of the electrolyzer stacks accounts for the majority of the costs with €878.1 million. The initial CAPEX investment for green ammonia is 1168.9 MEUR, which is higher than the initial investment for blue ammonia. Every 7 years the stacks need to be replaced also contributing to additional costs, the total replacement costs over the plant lifetime are valued at 368.8 MEUR in 2030.

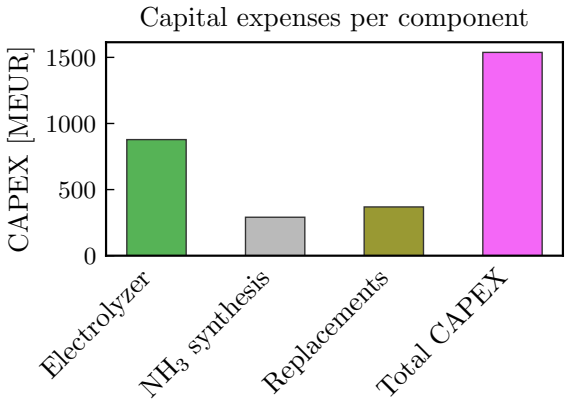

Figure 4.18: CAPEX distribution for green ammonia

The CAPEX costs are dominated by the alkaline electrolyzer costs. The technical landscape of electrolyzers is developing at a fast pace therefore efficiency improvements and economies of scale could prove to decrease the CAPEX significantly. However, because it is a relatively new process, certain effects of up-scaling and unexpected technical hurdles in the development process could lead to unforeseen additional costs. The largest operational electrolysis plant worldwide can supply approximately 1% of the hydrogen necessary to generate this amount of ammonia (IEA, 2022b). Scaling up could result in unexpected additional costs and technical issues. NEOM has announced the construction of a 600-tonne-per-day green hydrogen facility in 2026 (NEOM, 2023), this scale is near to the necessary 730-tonne-per-day hydrogen capacity. In the calculation of the CAPEX for green ammonia, it is important to note that the paper assumes quite a significant learning curve for the evolution of electrolyzer technology over the coming years (Reksten et al., 2022). Cesaro et al. (2021) shows past literature has projected CAPEX costs of 115 - 730 USD/kW for 2030 large-scale installations indicating large uncertainties. The correlation used in this research by Reksten et al. (2022) projects a 320 USD/kW CAPEX for large capacity systems which is approximately 220 USD below the base case projections of 540 USD/kW used by Cesaro et al. (2021). These figures indicate the level of uncertainty in the price development of electrolyzers and the possible optimism in the CAPEX projections assumed in this research. However, due to the rapid technology developments in this field, it is assumed that the manufacturing of electrolyzers with this capacity is possible and is reflected in the CAPEX relation

specified by Reksten et al. (2022).

Financial sensitivity of green ammonia

The financial sensitivity analysis through the NPV evaluation is given in figure 4.19. From this figure, it is visible that the total NPV for green ammonia is negative with a -479.9 MEUR value for the base price values. This is strongly influenced by the ammonia selling price of €0.472 per kg, similar to blue ammonia.

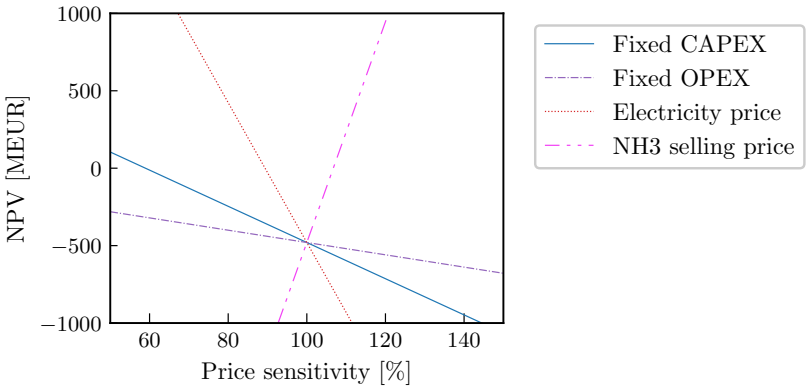

Figure 4.19: Sensitivity analysis of the NPV for green ammonia.
$CAPEX_{base}$=1136.3 MEUR initial and 368.7 MEUR replacements, $OPEX_{base}$=41. MEUR/year, $electricity_{base}$= 41.77 €/MWh, $NH_{3\,base}$= 0.472 €/kg

Figure 4.19 also shows that the electricity price is the main cost driver for green hydrogen and by extension ammonia. To make this system profitable and price-competitive with blue and grey ammonia for the assumed base prices, an additional subsidy is required. It can deduced from this graph that with a 39% CAPEX reduction a positive NPV for green ammonia at a €0.472 selling price can be achieved. However the factor truly dictating the costs is the electricity price, with an 11% decrease in electricity price, the NPV breaks even. This shows that realizing large CAPEX reductions in electrolyzers cannot solely make green ammonia price competitive and profitable. The efficiency of the process would also need to improve to consume less electricity or the electricity price would have to go down. The NPV has a value of zero at an ammonia price of 0.513 €/kg NH_3, indicating a necessity of €0.041 subsidy per kg of ammonia produced to break even. To match the blue ammonia NPV value (104 MEUR), a price of €0.520 is necessary, which is equal to €0.048 per kg NH_3 in subsidy. Once again it is important to emphasize the larger uncertainties in the price evolution of green hydrogen (especially in the Netherlands with large offshore wind capacity) and therefore by extension green ammonia.

4.5.2. Blue and green ammonia comparison

The main comparison criteria are shown in figure 4.20. The levelized costs of green and blue ammonia are shown in figure 4.20a and the total scope 1 and 2 emissions are presented in figure 4.20b. Green ammonia has a levelized cost of €0.461 per kg of ammonia. In other literature, green ammonia had a levelized cost varying between 0.321 - 0.664 in 2030 (Cesaro et al., 2021). Currently, the green ammonia price in Europe is 0.80240 €/kg (S&P Global, 2022) and it is imported. This means the costs of Dutch green ammonia are projected to become close to half of its current selling value by 2030. The levelized costs predicted in this research can be considered slightly optimistic, however still fall well within the range indicated by past research and are therefore considered valid for further comparison.

Blue ammonia has lower levelized costs than green ammonia for the price assumptions of 2030 in the Netherlands. An €0.044 difference per kg between blue and green ammonia is found in this research, which is equal to a 9.3% cost increase. The green ammonia price is mainly driven by the electricity price (0.337 €/kg contribution). Therefore the price development of the electricity market

will play a key role in the feasibility of green ammonia in the longer term, as was also visible from the sensitivity analysis. The CAPEX and fixed OPEX contributions of both technologies are similar. The total additional costs for the CO_2 emitted and the costs for transport and storage add up to 0.075 €/kg which accounts for a significant part of the total levelized costs of blue ammonia (18%). This results in a relatively small cost-gap between blue and green hydrogen by 2030. However, without subsidy, green hydrogen for ammonia production under these circumstances will still not be cost-competitive.

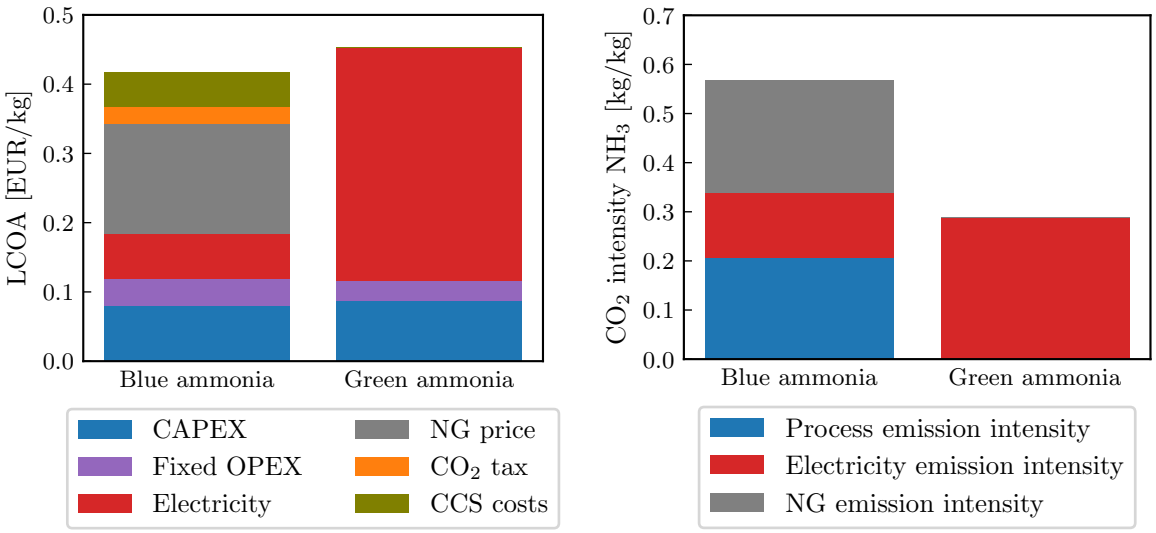

(a) Levelized cost contributions

(b) Total direct and indirect emissions

Figure 4.20: Comparison of blue and green ammonia with levelized costs and CO_2-emissions

The relative emission intensity of the two technologies is shown in figure 4.20b. The graph shows that green ammonia still has some indirect carbon intensity due to the large electricity consumption (0.288 kg/kg). It is important to keep in mind that in this comparison the blue ammonia is generated from grid power whereas green ammonia runs on green power when it is available. This has two main consequences for result interpretation. Firstly, the average indirect electricity emissions per kWh for green ammonia are lower over a yearly profile than for blue therefore the price of electricity in the levelized costs do not scale with the emissions. Secondly, when grid power is used for green ammonia production, it most likely has a higher CO_2-intensity than the average grid intensity which was used in this comparison because these are moments when renewable energy is not available. Therefore the CO_2-intensity might be higher in reality for green ammonia.

Electrolysis at this scale requires more than 5 times the electricity that the blue ammonia production process requires. Therefore if the electrolyzers were powered by the same grid as the blue ammonia, the indirect emission intensity would be 0.671 kg CO_{2eq}, which is higher than the total direct and indirect emission of blue hydrogen, therefore green ammonia in the Netherlands requires a large supply of green electricity to be considered sustainable. On the other hand, in the scenario where blue hydrogen can also be powered by renewable energy, the total direct and indirect emissions are still high due to the upstream NG emissions and direct process emissions. Therefore the share of electricity that is renewable in 2030 has a large impact on which pathway is more sustainable.

It is questionable whether large amounts of green electricity should go to electrolyzers for chemical use if the grid still requires significant decarbonization (Mayer et al., 2023). There are both advantages and disadvantages of producing ammonia through the green route. On the one hand, it can be argued that converting electricity to hydrogen results in efficiency losses as opposed to direct usage of the electricity as electricity. On the other hand, with the large-scale electrification of all other sectors, the overall electricity demand is likely to grow significantly, causing more congestion during peak production or utilization periods. Therefore, it can be argued that steady electricity consumption to make

hydrogen for chemical plants partially relieves the grid from congestion at non-overlapping supply and demand peaks.

This research focuses on the production of ammonia in 2030, this is relatively short-term. Assuming no additional subsidies are introduced, blue ammonia is financially the more justifiable path for low-carbon ammonia production, as it has lower levelized costs and a higher NPV. It also has fewer uncertainties regarding financial and technical developments and is therefore a less risky investment. From an environmental point of view, green ammonia that is produced primarily from renewable energy emits less CO_2. The financial and environmental impact of this route in 2030 is strongly correlated with the upscaling of renewable energy. In the long term, green ammonia will become more feasible as the excess of green energy can used to power processes like this more flexibly and there will be more clarity on the price evolution of electrolyzers and the capacity and price of renewable energy. The limited price gap between green and blue hydrogen production indicates that in the longer term, green hydrogen for ammonia production could overtake the blue hydrogen financially.

4.5.3. Grey ammonia comparison

As also visible in the IEA scenario cases carbon taxes have a significant impact on the financial outcome of the production method. Blue has limited direct emissions over which it pays carbon taxes, green ammonia has no direct emissions and therefore pays no carbon taxes. For a similar grey ammonia production system however, the direct carbon emission would amount to approximately 1.40 kg CO_2 per kg NH_3 which would total up to a 0.189 €/kg NH_3 contribution to the levelized costs due to carbon taxes. Through grey production routes, the electricity consumption of the system is lower and the CAPEX does not include CO_2-compression, the physical absorption tower and Selexol refills therefore lowering costs. However, higher CAPEX costs for the PSA would have to be invested to adsorb all CO_2 to meet purity requirements for ammonia synthesis. All in all, grey ammonia tends to have a lower CAPEX and electricity consumption. The lower electricity price and NG price will also lower the grey ammonia price, but the carbon taxes result in an LCOA increase. Therefore it is assumed the levelized costs of grey ammonia (base case: €0.357 per kg NH_3 (corrected for inflation)) are raised to approximately €0.546, surpassing both the levelized costs of the blue as well as the green ammonia. This comparison is quite crude, however does indicate that, for this timeframe (2030) and the financial assumptions made, both blue and green ammonia can be cost-competitive and possibly even less expensive than grey ammonia. The possible generation of power from the excess heat and pressure in the system is not considered in both the blue and the grey ammonia routes, which could influence the financial outcomes. Regarding emission reduction, scope 1 emissions are reduced by 100% for green ammonia compared to grey, and 86.8% reduction is realized when comparing scope 2 emissions.

4.5.4. Conclusion blue vs green

All in all, it can be concluded from these results that in 2030 blue ammonia is the financially more secure option compared to green ammonia. Blue ammonia has lower projected levelized costs, demands less electricity and has a higher TRL so more initial investment security. Green ammonia is subject to more uncertainties in market and technology development however projections show in the longer term it might overtake blue ammonia prices due to the increasingly lower electricity prices and rapid technical advancements in electrolyzer developments. With the financial and technical assumptions made in this research, green ammonia is not expected to be cost-competitive with blue ammonia by 2030 in the Netherlands without subsidy.

The carbon equivalent emissions of green ammonia are about half of the blue emissions for the base case assumptions. Green ammonia has no direct emissions and if generated mainly from renewable energy has limited indirect emissions. Therefore, grid decarbonization also plays a significant role in the environmental impact of both routes however more significantly impacts the green route. Green ammonia taken from the grid with the projected grid intensity by 2030 emits more CO_2-equivalent emissions than the blue process. Vice versa if the grid is completely decarbonized, blue ammonia still emits carbon directly and through the upstream NG process. Other factors like gird congestion and subsidies can influence the financial and environmental outcomes of both scenarios and should be looked into further.

With the introduction of carbon taxes like in the pledged and NZE emission scenarios blue and green ammonia are cost-competitive with grey ammonia by 2030 under these circumstances. However, increasing the price of ammonia has a direct impact on the farmer and in extension on the everyday consumer as this is compensated in the price of the end product. Large end users are not willing to pay more for fertilizer (Martin, 2023), therefore, additional subsidies might still be necessary to keep the prices low, whilst the market evolves to low-carbon options.

4.6. Case 3: Dynamic operation

Past research indicates the advantages of an autothermal reformer over a steam methane reformer are that reaching high capture rates is often less costly and it can be operated more flexibly. The start-up and shut-down time of an autothermal reformer is shorter because of the quick heat generation by the partial oxidation reaction and the lower initial reactor temperature. Future energy systems will ideally be able to operate at more dynamic levels, this can be on a seasonal, monthly, weekly or even hourly basis depending on the flexibility of the system and the volatility of the feed and product market. The ammonia demand and price over the year tend to be quite steady because the majority of ammonia is sold in term contracts (Yara International ASA, 2022). The natural gas price however could become a more seasonal market due to the increase of demand from domestic use. The Haber-Bosch synthesis reactor is less flexible than the ATR, it is therefore assumed the minimum load capacity of the reactor is limiting.

This case study compares dynamic operations through a discretized monthly varying natural gas feed input. The natural gas feed is inversely varied with the natural gas price: it produces hydrogen at maximum capacity when the price is at its minimum value. The minimum load for the Haber-Bosch was set to 75%. The transient behaviour of the system was disregarded as this was not properly reflected in the model and therefore 12 hours were removed from the yearly operational time to account for these shifts. The natural gas price variation sine function over the year was deduced from 2017 NG selling price data with an amplitude of €1.35. The amplitude of the price was varied more excessively to see the price effect in this case study. Figure 4.21 shows the four case input conditions. The system was resized to meet the same steady-state demand as the base case to properly compare the two cases.

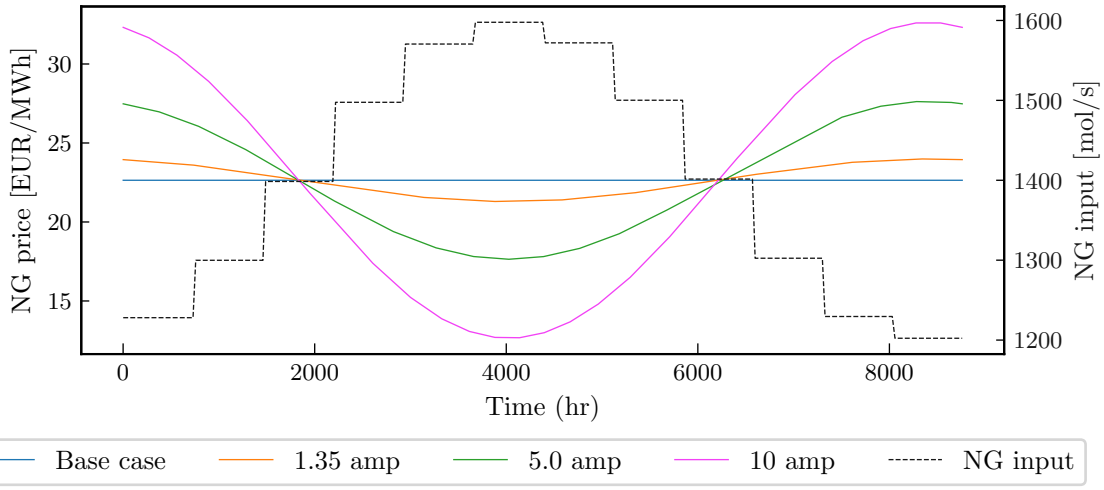

Figure 4.21: Input feed and NG price fluctuation over the year

The plant efficiency for the dynamic operating case is 73.8%, which is lower than the base case with 74.5%. The PSA is sized to meet the needs of the largest flow therefore resulting in more hydrogen loss at lower operation. The sub-models do not fully account for the effects of lower molar flow rates. The impact on heat generation and transfer for example is not accounted for properly. Therefore these

results might still underestimate the negative effects of operating under maximum capacity for the efficiency of the process. On the other hand, the relative catalyst mass per reaction is increased therefore equilibrium is more likely to be reached. All in all, it is expected that the efficiency of the process is lowered by operating at a lower capacity.

4.6.1. Plant CAPEX and OPEX

The CAPEX distribution is shown in figure 4.22. The plant was resized for a larger load this is visible in the CAPEX distribution, all units are sized to the maximum load and additional storage results in a large increase in the total CAPEX costs (1205.2 MEUR). The fixed OPEX is also higher in this case study because it is taken as a percentage of the CAPEX. The storage CAPEX amounts to an additional 70.4 MEUR on top of the original CAPEX, the other 105 MEUR are additional costs for the unit enlargements.

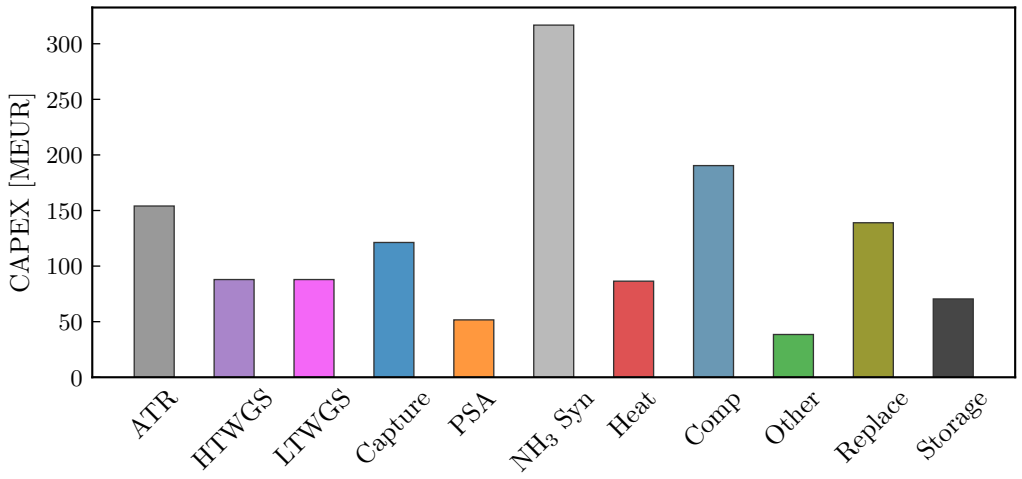

Figure 4.22: CAPEX distribution for the seasonal dynamic operation, same total yearly ammonia production

The variable hourly OPEX over a year is shown in figure 4.23. To portray the effects of dynamic operation on the variable operational costs, the most extreme price fluctuation is depicted. The electricity prices increase in the summer due to the higher load, however, the relative NG costs are lower even though more is consumed. It also shows the extreme fluctuations in the electricity price over a year. Blue ammonia systems based on an ATR and Haber-Bosch reactors are not flexible enough to respond to price impulses at that frequency, therefore the monthly discretization was simulated. An analysis of the impact of dynamic operation at a shorter time frame would require models that more accurately represent the transient behaviour of the system.

4.6.2. Financial outcome

Table 4.3 shows the financial outcome of the different case studies. In all three price scenarios, the lowered variable OPEX does not compensate for the additional CAPEX and fixed OPEX costs of dynamic operation when compared to the base case. The levelized costs of steady-state year-round production versus the levelized costs of dynamic operation result in 0.013-0.018 €/kg difference compared to the base case.

It is important to note that in this study, it is assumed the ammonia demand and price are fixed at one value throughout the year. Therefore, the system perfectly matches demand and supply, in reality, this is often not the case and additional storage is required to meet the fluctuations in the demand. This is not considered in the base case therefore indicating additional costs might be necessary for storage. A storage system that can buffer 5% of the total yearly capacity of this plant, results in a levelized cost contribution of €0.004 per kg (1.2% price increase). Through storage, the system is more flexible to market and demand fluctuations. Moreover, it can serve as a buffer for unexpected maintenance. Therefore further looking into how to optimally match demand, supply, pricing and technical limitations

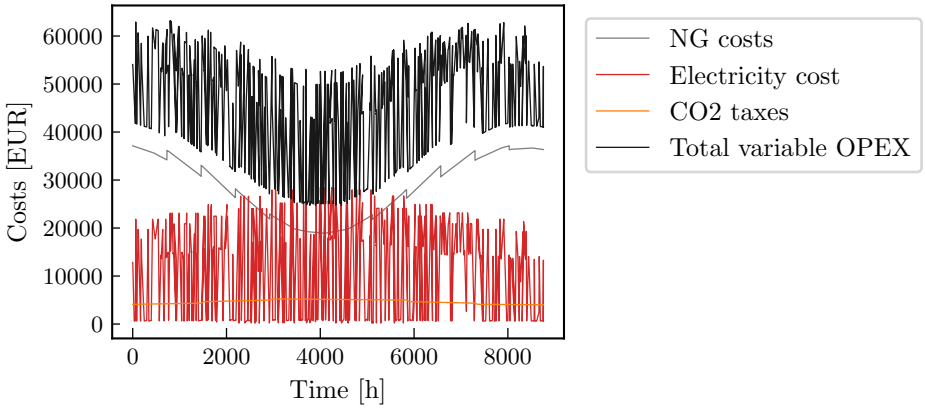

Figure 4.23: Variable hourly OPEX distribution over a year for dynamic operation and a +/-€10 price amplitude in the NG price with an average of 22.64 €/MWh

Table 4.3: Financial outcomes of sine-shaped seasonal pricing of NG with storage to meet steady-state demand

Parameter	Unit	Base case	Fixed price	+/- €1.35 (6%)	+/- €5 (22%)	+/- €10 (44%)
CAPEX	MEUR	1169	1344	1344	1344	1344
NPV	MEUR	104	-177	-169	-145	-113
LCOA	€/kg	0.417	0.439	0.438	0.436	0.434
LCOA CAPEX & OPEX	€/kg	0.118	0.137	0.137	0.137	0.137
LCOA OPEX variable	€/kg	0.141	0.142	0.142	0.142	0.142
LCOA NG	€/kg	0.158	0.160	0.159	0.157	0.155

to maximize profit with storage is an interesting research direction. The +/- €10 scenario is the most economical of the three dynamic scenarios, in this scenario to break even with the base case the entire storage capacity of ammonia should be sold for €0.72 per kg. If the 5% storage is included in the steady-state operation case, all ammonia stored should be sold for €0.63 to break even. This indicates that dynamically operating with storage according to feed price fluctuations is not cost-effective for a steady-state demand when compared to the base case. However, vice versa limiting the storage by matching supply and demand more accurately through dynamic operation might serve as an interesting financial case versus steady-state operation and larger storage requirements.

4.6.3. Conclusion dynamic operation

This case study has shown that for a predictable steady demand, highly seasonal NG pricing (+/- 44%), the dynamic operation through a monthly set point varying from 75%-100% capacity with storage to meet the yearly demand has higher levelized costs than steady state operation with exact supply and demand matching and with a 5% storage to match fluctuations. For smaller scale systems the linearity of the CAPEX sizing is not yet reached so upscaling is relatively economical, therefore offering a possible better use case for this form of dynamic operation. Another more likely scenario in which dynamic operation could be cost-effective is if supply and demand show more fluctuations, thereby operating dynamically can result in smaller storage capacity because supply and demand can be matched more closely. Therefore modelling the transient behaviour and capacity limitations of the reactors to optimize the relative timescale of dynamic operation technically and financially could prove to be interesting.

5 Limitations

The research limitations, their effects and possible solutions are discussed in this section. Firstly, the modelling limitations are discussed; after that, the financial market limitations, and finally the overall result limitations are elaborated on.

5.1. Modelling Limitations

The models presented in chapter 3 each make several assumptions to simplify the complex reactor behaviour into first-order differentials. However, these simplifications accumulate over the process chain and lead to larger uncertainties in the outcome especially when operated near a model's critical boundary conditions.

5.1.1. Feed and product assumptions

The first assumption that was made is that the gasses were considered ideal throughout the entire process. The assumption of an ideal gas can be justified for low pressures or very high temperatures. Therefore in the ATR model, the impact might not be that significant. However, for the water gas shift reactors, the assumption already becomes less accurate and for the separation steps at room temperature the implementation of an equation of state would have most likely improved the accuracy of the outcome.

The second large assumption made throughout the entire chain is that N_2 is inert and only influences the reaction through its partial pressure. The presence of nitrogen dilutes the reactant gasses and thereby limits the interaction between the reactants. This could also result in a rate-limiting effect on the reactions. The limited data on air-blown ATRs makes quantifying the influence of the presence of nitrogen difficult. Insufficient accountability for the possible influence of nitrogen can be considered a limitation of this research. Experimental data on the conversion limitations due to the presence of nitrogen should give a better insight into this effect.

Thirdly, the assumption that all oxygen reacts in the oxidation zone is a limitation. Experimental data shows there are always some traces of oxygen after the ATR. The effect of these traces is not accounted for in this research, however could lead to catalyst degradation and possible safety hazards or unwanted side reactions if not monitored properly.

5.1.2. Reactor assumptions

In each reactor model, the assumption was made the reactor had the ideal conditions. This entails the catalyst is uniformly dispersed, all active sites are accessible, the catalyst does not degrade over its lifetime, the reactor is perfectly adiabatic and only axial dispersion was accounted for. In reality, fabricating a reactor that meets all these conditions is impossible. However, the validity of the assumptions was partially checked through the sub-model validations with industrial values. This showed a constant overestimation of the conversion but the error was never larger than 6%, which was most likely due to

the idealization of the reactor. For process design and simulations at this fidelity level, this error level is acceptable and uncertainty as a result of the assumptions is warranted. For a more detailed reactor design in a later design stage, however, a complex model is recommended.

These ideal reactors also assume full equilibrium is always reached which is another limitation leading to more optimistic conversion rates. Reactors are likely to not reach the equilibrium conditions that are modelled here because of physical constraints not modelled: e.g. local variations in conditions, catalyst degradation, mass transfer limitations, no heat loss and transport phenomena. The implementation of more boundary conditions, based on industrial data, could more accurately portray the non-idealities in these models.

5.1.3. Separation assumptions

For the separation steps relatively crude models were selected, therefore the uncertainty in these models is more significant. For physical absorption assuming Henry's law is applicable throughout the entire column is considered a limitation as this process is more complex in actuality. To reduce the effect of this limitation the boundary condition of a maximum absorption of 95% was set. This improved the physical meaningfulness of the outcome however the profile becomes non-linear at an earlier stage in the absorption column which was not accounted for resulting in a limitation in the accuracy of the necessary Selexol flow rate. Improving the physical absorption model's robustness to reflect reality near the critical zone would improve the accuracy of the carbon reduction outcome.

The PSA was also simplified quite intensively. The largest limitation lies in the assumption the adsorbent mass is linearly proportional to the loading that followed from the competitive Langmuir isotherms. In reality, this loading will never be reached and every adsorption will create a new balance in the isothermal loading. This model assumes all sites are occupied and that the adsorption has a linear relationship with the adsorbent mass. Due to the lack of accurate simplified mathematical models for a PSA, this was deemed the most appropriate option as it still captured some of the apparent thermodynamics. However, this model and specifically these assumptions are considered a large limitation. There might be some discrepancies in the required adsorbent mass and thereby the replacement costs.

5.2. Financial market limitations

Future price assumptions are subject to large uncertainties which is another limitation. The price prognoses for the future are highly speculatory and often have very large standard deviations. Market developments are very unpredictable due to socio-political factors. Regulations and the development of newer technologies also remain uncertain. The sensitivity analyses given in chapter 4 show the possible financial influence of variations in these assumptions. The NPV and levelized costs are very sensitive to certain price deviations, thereby strongly influencing profitability.

5.2.1. CAPEX and fixed OPEX prices

The CAPEX price and thereby indirectly the fixed OPEX price are based on published correlations. These correlations are often quite crude because they are based on limited industrial data and are relatively generic so they are broadly applicable. To get a more accurate CAPEX indication vendor quotes and industrial surveys should be obtained for the specific application and size. For green ammonia, the uncertainty in the development of the technology forms a critical limitation in the accuracy of the CAPEX, more so than for blue which contains more established process units. Moreover, the fixed OPEX for both the blue and green process chains were taken as a percentage of the fixed CAPEX. In larger-scale systems, the linearity of this assumption might overestimate or underestimate the costs.

5.2.2. Variable OPEX

For the base case the natural gas price projections were taken from the IEA pledged scenario. However, in 2005 two hurricanes spiked natural gas prices and more recently, the COVID-pandemic and the Ukraine war have shown that the natural gas market can be very unpredictable and is subject to major (geo)political and environmental influences. Therefore the large possible deviation in natural gas prices is considered a limitation. In this research, it is assumed to be a fixed price with a relatively low value compared to the current market. The financial viability of blue ammonia versus green ammonia

depends highly on the natural gas market, therefore this limitation should be considered explicitly when interpreting the results. In the comparison of grey to blue hydrogen both production methods are affected similarly by natural gas pricing so variations should still yield the same relative results.

The future electricity mix and thereby the market price is also subject to uncertainties which results in a limitation. The price of electricity is likely to become more volatile however grid congestion might also form a restriction in these price developments. In this research the electricity price is assumed to be correlated to the grid price, however the role of PPAs might increase. This could result in a steady off-take of electricity against a fairly stable price.

Finally, the ammonia price is another limitation. The assumption is made ammonia can be sold for €0.472 per kg, this gives a positive NPV. If this price is lowered to match competing prices the profitability without subsidies is strongly influenced. At slightly lower ammonia prices the NPV becomes negative rapidly. Moreover, this research focuses on local blue versus green ammonia production. A possible import market for green and blue ammonia is not considered. Imports will most likely gain market share if the CAPEX for electrolyzers, the electricity price and the storage and transport costs go down for green hydrogen or the natural gas price geographical fluctuations become more extreme resulting in very low-cost blue hydrogen. Finally, the large-scale import of ammonia as a hydrogen carrier is also a feasible route due to the Dutch energy deficit, besides the conversion to hydrogen, this ammonia will then also be utilized directly. All three scenarios could render local Dutch blue hydrogen for ammonia production obsolete.

5.3. Calculation and Case studies

The calculations also have limitations. The LCOA and NPV calculations include a 10% discount factor, however, the possible price evolution of the feed, electricity and carbon taxes is not considered. Over the plant's lifetime, a further fluctuation of the natural gas price and electricity prices is quite likely. Moreover, there might be an increase in carbon taxes or an additional subsidy over the lifetime of the plant that is not properly accounted for in the current calculations.

For the entire process, it is assumed heat integration is possible and that no pinch points occur. A more detailed heat integration research should be executed to see if the found surplus in this research reflects reality and if the exclusion of pinch points is valid. Moreover, if there is indeed a heat surplus, this can be used to generate power or the excess heat can be sold, contributing to the profitability of the system. Other researchers have found this has a significant financial impact. Therefore the seclusion of a detailed heat integration and power co-generation analysis is considered a large limitation.

Finally, the interpretation of each case also has limitations. Firstly, the three IEA pricing scenarios are hypothetical possible paths for the whole of Europe, therefore local policies and pricing could be variable and other routes to reach climate goals could influence the financial conclusions drawn in this research. In the green versus blue case, the green ammonia route does not include the necessary ASU or purchase of pure nitrogen in the cost analysis, nor are other electrolyzer models that are projected to become more economical in the long term considered. In the dynamic operation, more thorough relationships on the transient behaviour of the different process steps would have improved the validity of the outcome. For all case studies a steady-state demand is assumed, however in reality there are peak demand scenarios and volatile pricing over the year therefore forming a limitation, especially in the dynamic operation in which a system with and without storage are compared. Lastly, in all simulations cooling water was not accounted for.

All in all, several uncertainties in this research result in limitations in the interpretability of the results. However, through awareness of these limitations, bounded conclusions can be drawn and the results can be translated to different use cases by adding the right boundary conditions.

6

Conclusion and recommendations

6.1. Conclusion

The energy transition is gaining momentum due to the severity of climate change. Low-carbon hydrogen is projected to play a large role in the transition as both an energy carrier as well as fulfilling its traditional role as feedstock for multiple large-scale industrial processes. Two relatively mature low-carbon options for producing hydrogen are traditional production methods from fossil fuels with carbon capture and storage (blue hydrogen) and electrolysis powered by renewable electricity (green hydrogen). Past research has shown blue hydrogen is often economically more favourable in the short term but generates more emissions than truly green hydrogen.

One of the main hydrogen-consuming industrial processes is the production of ammonia. Ammonia is mainly used to produce fertilizer, with the growing population the fertilizer demand is likely to grow over the coming decade regardless of the production methods of hydrogen. Therefore creating a low-carbon production process for ammonia is important to limit the environmental effects. Most future energy systems are focused on low-carbon solutions.

Additionally, future energy systems are expected to require the integration of multiple energy solutions to be sustainable, affordable, reliable and flexible at the same time. Models that accurately predict the behaviour of these systems can accelerate the transition and help more accurately predict the effects of dynamic parameters on a system's technical and economic performance. This led to the research question: What influence do operating conditions and financial scenarios have on an economic and technical level for a physically modelled, flexible multi-commodity system for blue hydrogen used to produce ammonia?

The research focuses on blue hydrogen produced through a large-scale air-blown ATR, used to generate ammonia through the Haber-Bosch process in the Netherlands in 2030. The carbon that is produced in the process is captured and sent to a storage location (PORTHOS). The plant consists of an autothermal reformer, two water gas shifts, an absorption column and stripper for CO_2-capture and a PSA to purify the hydrogen, it is then sent to the Haber-Bosch process to produce ammonia. Auxiliary process steps consist of a desulphurization unit, a pre-reformer, a furnace, heat exchangers, compressors and a dehydration unit.

All process units were modelled in Python separately, and after validation per sub-model, they were integrated into one chain to form a blue hydrogen process block. The CAPEX and fixed OPEX costs were calculated for the appropriate capacity (720 tonne/day of H_2; which is equivalent to 4000 tonne/-day of NH_3) for the base case. The variable OPEX was calculated based on the operational conditions and the market conditions. Next, the entire chain was evaluated both on technical grounds and financial grounds for different input parameters to see the influence on the system and select the proper operating conditions. A complete base case evaluation of the system was executed and finally, three case study simulations were run.

The sub-models were compared to existing literature and industrial data to validate them. The models showed the expected theoretical behaviour and yielded similar outputs to the available data. The largest deviation was 6%, thereby confirming the applicability of these models for simulation purposes. The operational window selection was based on the financial performance, emission intensity and technical limitations in the reactor models. From these sensitivity analyses, it can also be concluded that the α-value (oxygen-to-carbon ratio) and T_{in} (the input temperature) are the most influential parameters regarding the final performance of the process, however, internal reactor limitations restrict their value. Therefore the final operational window was set to an α-value of 0.6, a β-value (steam-to-methane ratio) of 2.0, a T_{in} (input temperature) of 873.15K (600 °C) and a P_{in} value (input pressure) of 2.8 MPa.

The entire model performance evaluation results in a daily production of approximately 4000 t/-day of NH_3 at an overall process efficiency of 59.1%. The process direct emission intensity (scope 1) amounts to 0.205 $kg_{CO_{2(eq)}}$ / kg_{NH_3}. The total emissions when upstream emissions and grid intensity are accounted for amount to 0.567 $kg_{CO_{2(eq)}}/kg_{NH_3}$, primarily caused by upstream natural gas emissions. Regarding direct emissions, the utilization of blue hydrogen results in an 85% reduction compared to grey ammonia. The model gives in levelized costs of ammonia at €0.417 per kg of NH_3, resulting in an NPV of 103.9 MEUR with a payback time of 9 years. The base case economic assumptions are an ammonia selling price of €0.472; a natural gas price and carbon taxes at 22.64 €/MWh and 0.135 €/kg_{CO2} respectively, taken from the IEA pledged scenario; an average electricity price of 41.77 €/MWh and carbon transport and storage price of 0.05 €/kg_{CO_2}. The NPV is most severely influenced by the selling price of ammonia and the purchasing price of natural gas, therefore coupling the blue ammonia market to the natural gas market, similar to what is already the case for grey ammonia reduces the financial risk but also indicates the strong dependence on the development of the natural gas market.

Three IEA policy scenarios were compared to see the effect of policies on the economic feasibility of the process. These scenarios assume in a more proactive pricing policy to fight climate change, the natural gas price will shrink. Therefore the total levelized costs of blue ammonia are significantly lower for the NZE scenario (-15%) than for the pledged scenario. In all three scenarios, the NPV value is positive. It can be concluded that the role of policymakers in the energy transition has a substantial influence on whether low-carbon options can become price-competitive with grey. The grey ammonia price increases by at least €0.11 per kg of NH_3 in all three scenarios due to carbon taxes. If the capture costs of CO_2 do not surpass €0.05 per kg of ammonia, blue ammonia can become price competitive with grey ammonia. However, more sustainable energy scenarios are likely to also influence the price evolution of electricity and the CAPEX and fixed OPEX of systems, therefore these broader cost implications should be taken into consideration as well as the overall impact on everyday pricing for consumers.

The second case study compares the production of ammonia through blue and green hydrogen routes. It can be concluded that under the base case economic conditions, the green ammonia route will not yet be financially competitive with the blue route in 2030. The levelized costs of green ammonia modelled in this research amount to 0.461 €/kg in the pledged scenario with an NPV of -480 MEUR indicating under these circumstances without additional subsidy, green ammonia is not profitable. From the sensitivity analysis, it can be concluded that at this scale, the electricity price pre-dominantly impacts the costs of the system, and the ammonia selling price drives the profitability. The direct emissions of green ammonia are zero, the indirect emissions however are strongly correlated to the electricity source it is connected to. Under the assumed circumstances of a partially renewable source, the emission intensity is 0.228 kg/kg and blue ammonia has approximately double the indirect emissions. How electricity sources are best allocated with the increase of renewables also impacts the sustainability of all production paths. Therefore the evolution of the electricity market pricing, electricity allocations and grid intensity will play a key role in the financial viability and environmental impact of green ammonia compared to blue ammonia. Environmentally blue and grey ammonia both reduce emissions by 86% and 100% respectively when only scope 1 emissions are considered, financially, this research indicates both process methods can become cost-competitive with grey by 2030 in the pledged scenario of carbon taxes.

Finally, the dynamic operation to take advantage of the possible natural gas price seasonality is

considered. This case study leads to the conclusion that the costs of the additional capacity required in the reactors and the storage do not compensate for the cost savings on natural gas and electricity throughout the year. The process efficiency is slightly lower for dynamic operation, the true effect of dynamic operation might be larger because the models make simplifications and transient behaviour in the reactors is not accounted for. From this case study, it can be concluded that dynamic operation at advantageous tariffs with storage to meet a steady-state demand is not financially superior to the steady-state operation of the system. However, for a non-steady demand pattern, the comparison should be made between steady-state production with storage and a direct supply and demand matching system through dynamic operation.

The research limitations were classified into three types: modelling limitations, financial limitations and overall result limitations. the main modelling limitations were the simplifications of the models through assumptions that could result in more optimistic conversion rates. The financial limitations refer to the large uncertainties in the development of future markets. The result limitations refer to the method of calculating the final results in which certain process aspects were neglected and for result interpretation, the results must be considered under the specific boundary conditions of this research.

Overall this research has yielded a flexible blue hydrogen model that can relatively accurately predict reactor behaviour and by extension be used for different flexible economic and technical simulations. From the simulations, multiple conclusions regarding reactor and system behaviour can be drawn. The performance of blue hydrogen production through an ATR to make ammonia is most impacted by the input temperature and oxygen-to-carbon ratio however internal reactor limits play a role. This confirms both internal physics per reactor and the integrated process chain need to be considered simultaneously to evaluate the system's performance. The natural gas price and ammonia price need to remain linked for blue ammonia to be profitable, these are the two most influential economic factors. To become cost-competitive with grey ammonia, the implementation of carbon taxes or subsidies is necessary. Blue ammonia under the technical and economic circumstances assumed in this research offers lower levelized costs and more investment security than green ammonia in 2030, suggesting investing in blue hydrogen to produce ammonia is more cost-effective than green ammonia in the short term. However green ammonia emits less carbon, the green ammonia levelized costs are driven by the electricity price and ammonia price. In comparison with grey ammonia, green and blue hydrogen both are environmentally superior and in all three carbon-tax scenarios considered under the simulated conditions, they are cost-competitive with grey hydrogen for the production of ammonia. Lastly, this research shows that monthly dynamic operation based on natural gas price fluctuations with additional storage for a steady-state demand is financially not justifiable compared to steady-state operation.

6.2. Recommendations

Further research recommendations were comprised in light of the results that follow from this research and the identified limitations. Firstly, focusing on the sub-models, it is recommended that they are further developed through data-driven validation, which can also serve as the basis for correction factors to compensate for the simplifications. In line with this, it is recommended to quantify and rank the influence of each reactor assumption, to account for the largest sensitivity first. Secondly, further research is required to prove that in reality, the theoretical 3:1 ratio of H_2:N_2 is possible in the PSA. Further research is also required as to the effect of the presence of nitrogen in the system on both heat transfer and conversion rates. Finally, regarding modelling, further research should be conducted into the transient behaviour of each reactor. This will lead to better quantification of the effects of dynamic operation and its limitations. It can also be used to optimize dynamic operations to match supply and demand more thoroughly or respond to market shifts more adequately.

For the entire process chain, the integration of heat and the possible co-generation of power is neglected. These two factors could prove to have significant financial influence therefore their effect on the profitability and operation of the system requires additional research. Blue hydrogen production generates large upstream emissions through NG, additional research should be done on how to lower this amount. Furthermore, the comparison made to grey hydrogen-based ammonia was quite crude therefore modelling grey hydrogen through SMR to make a proper comparison would give a better

indication of the true financial comparison. Moreover, further research should be conducted on the optimization of the chain, both regarding design and operation, through the comparison of an air-blown system with an oxygen-blown system including ASU for example.

Financially, it is recommended to access industrial data through surveys and vendor quotes to confirm the CAPEX and fixed OPEX evaluation of the system. Moreover, besides a discount rate of 10%, looking further into the market projections beyond 2030 to account for market evolution over the plant's lifetime could offer interesting perspectives for both low-carbon solutions. Especially, a more thorough projection of the development of the electricity market regarding grid intensity, congestion and pricing would clarify which pathway is truly financially and environmentally superior. Moreover, the effect of the rapidly changing import markets of natural gas, ammonia and hydrogen, should be further investigated. This could prove to make local production in the Netherlands obsolete. Furthermore, the financial influence of carbon taxes on all commodity prices should be further researched before implementing further carbon taxes. Overall, more research into market development to strengthen the assumptions in this research would result in additional credibility of the absolute financial results.

References

Aasberg-Petersen, K., Bak Hansen, J. H., Christensen, T. S., Dybkjaer, I., Christensen, P. S., Stub Nielsen, C., Winter Madsen, S. E., & Rostrup-Nielsen, J. R. (2001). Technologies for large-scale gas conversion. *Applied Catalysis A: General*, *221*(1-2). https://doi.org/10.1016/S0926-860X(01)00811-0

Adams, T. A., & Barton, P. I. (2009). A dynamic two-dimensional heterogeneous model for water gas shift reactors. *International Journal of Hydrogen Energy*, *34*(21). https://doi.org/10.1016/j.ijhydene.2009.08.045

Adams, T. A., Salkuyeh, Y. K., & Nease, J. (2014). Processes and simulations for solvent-based CO2 capture and syngas cleanup. In *Reactor and process design in sustainable energy technology*. https://doi.org/10.1016/B978-0-444-59566-9.00006-5

Ahn, H., Kapetaki, Z., Brandani, P., & Brandani, S. (2014). Process simulation of a dual-stage selexol unit for pre-combustion carbon capture at an IGCC power plant. *Energy Procedia*, *63*. https://doi.org/10.1016/j.egypro.2014.11.182

Amadeo, N. E., & Laborde, M. A. (1995). Hydrogen production from the low-temperature water-gas shift reaction: Kinetics and simulation of the industrial reactor. *International Journal of Hydrogen Energy*, *20*(12). https://doi.org/10.1016/0360-3199(94)00130-R

Amhamed, A. I., Shuibul Qarnain, S., Hewlett, S., Sodiq, A., Abdellatif, Y., Isaifan, R. J., & Alrebei, O. F. (2022). Ammonia Production Plants - A Review. *Fuels*, *3*(3), 408–435.

Amirshaghaghi, H., Zamaniyan, A., Ebrahimi, H., & Zarkesh, M. (2010). Numerical simulation of methane partial oxidation in the burner and combustion chamber of autothermal reformer. *Applied Mathematical Modelling*, *34*(9). https://doi.org/10.1016/j.apm.2009.10.039

Arent, D. J., Bragg-Sitton, S. M., Miller, D. C., Tarka, T. J., Engel-Cox, J. A., Boardman, R. D., Balash, P. C., Ruth, M. F., Cox, J., & Garfield, D. J. (2021). Multi-input, Multi-output Hybrid Energy Systems. *Joule*, *5*(1), 47–58. https://doi.org/10.1016/j.joule.2020.11.004

Armijo, J., & Philibert, C. (2020). Flexible production of green hydrogen and ammonia from variable solar and wind energy: Case study of Chile and Argentina. *International Journal of Hydrogen Energy*, *45*(3). https://doi.org/10.1016/j.ijhydene.2019.11.028

Arnaiz del Pozo, C., Cloete, S., & Alvaro, A. J. (2021). Standard Economic Assessment (SEA) Tool.

Aromada, S. A., Eldrup, N. H., Normann, F., & Øi, L. E. (2020). Techno-economic assessment of different heat exchangers for co2 capture. *Energies*, *13*(23). https://doi.org/10.3390/en13236315

Asaro, M., & Smith, R. M. (2013). Gas to Liquid Technologies. In *Fossil energy*. https://doi.org/10.1007/978-1-4614-5722-0{_}8

Ashkanani, H. E., Wang, R., Shi, W., Siefert, N. S., Thompson, R. L., Smith, K., Steckel, J. A., Gamwo, I. K., Hopkinson, D., Resnik, K., & Morsi, B. I. (2020). Levelized Cost of CO2 Captured Using Five Physical Solvents in Pre-combustion Applications. *International Journal of Greenhouse Gas Control*, *101*. https://doi.org/10.1016/j.ijggc.2020.103135

Ávila-Neto, C. N., Dantas, S. C., Silva, F. A., Franco, T. V., Romanielo, L. L., Hori, C. E., & Assis, A. J. (2009). Hydrogen production from methane reforming: Thermodynamic assessment and autothermal reactor design. *Journal of Natural Gas Science and Engineering*, *1*(6). https://doi.org/10.1016/j.jngse.2009.12.003

Bahadori, A., & Kashiwao, T. (2019). Modeling and analysis of hydrogen production in steam methane reforming (SMR) process. *Petroleum Science and Technology*, *37*(12). https://doi.org/10.1080/10916466.2019.1587466

Bharadwaj, S. S., & Schmidt, L. D. (1995). Catalytic partial oxidation of natural gas to syngas. *Fuel Processing Technology*, *42*(2-3). https://doi.org/10.1016/0378-3820(94)00098-E

Biesheuvel, P. M., & Kramer, G. J. (2003). Two-section reactor model for autothermal reforming of methane to synthesis gas. *AIChE Journal*, *49*(7). https://doi.org/10.1002/aic.690490719

Bodhankar, P., Patnaik, S., & Kale, G. R. (2021). Thermodynamic analysis of autothermal steam-reforming of methane for ammonia production. *International Journal of Energy Research*, *45*(5). https://doi.org/10.1002/er.6283

Bonnet-Cantalloube, B., Espitalier-Noël, M., Ferrari de Carvalho, P., Fonseca, J., & Pawelec, G. (2023, March). *Clean ammonia in the future energy system* (tech. rep.). Europe Hydrogen.

Boon, J., Van Dijk, E., Pirgon-Galin, Ö., Haije, W., & Van Den Brink, R. (2009). Water-gas shift kinetics over fecr-based catalyst: Effect of hydrogen sulphide. *Catalysis Letters*, *131*(3-4). https://doi.org/10.1007/s10562-009-0090-0

Bukkholm, I. S., Hektor, E. A., Jones, C. L., & Kimpton, S. K. (2021, November). *Blue hydrogen for a low-carbon energy future* (tech. rep.). DNV. Hovik.

Burgers, I., Dehdari, L., Xiao, P., Li, K. G., Goetheer, E., & Webley, P. (2022). Techno-economic analysis of PSA separation for hydrogen/natural gas mixtures at hydrogen refuelling stations. *International Journal of Hydrogen Energy*, *47*(85). https://doi.org/10.1016/j.ijhydene.2022.08.175

Callaghan, C. A. (2006). Kinetics and Catalysis of the Water-Gas-Shift Reaction: A Microkinetic and Graph Theoretic Approach. *Department of Chemical Engineering*, *Ph. D. The*.

Campanari, S., Chiesa, P., Manzolini, G., & Bedogni, S. (2014). Economic analysis of CO2 capture from natural gas combined cycles using Molten Carbonate Fuel Cells. *Applied Energy*, *130*. https://doi.org/10.1016/j.apenergy.2014.04.011

Carapellucci, R., & Giordano, L. (2020). 0378-7753/© 2020 Elsevier B.V. All rights reserved.Steam, dry and autothermal methane reforming for hydrogen production: A thermodynamic equilibrium analysis. *Journal of Power Sources*, *469*.

Cesaro, Z., Ives, M., Nayak-Luke, R., Mason, M., & Bañares-Alcántara, R. (2021). Ammonia to power: Forecasting the levelized cost of electricity from green ammonia in large-scale power plants. *Applied Energy*, *282*. https://doi.org/10.1016/j.apenergy.2020.116009

CF Industry. (2023). Ammonia Production.

Cha, J., Park, Y., Brigljević, B., Lee, B., Lim, D., Lee, T., Jeong, H., Kim, Y., Sohn, H., Mikulčić, H., Lee, K. M., Nam, D. H., Lee, K. B., Lim, H., Yoon, C. W., & Jo, Y. S. (2021). An efficient process for sustainable and scalable hydrogen production from green ammonia. *Renewable and Sustainable Energy Reviews*, *152*. https://doi.org/10.1016/j.rser.2021.111562

Chai, S., Zhang, G., Li, G., & Zhang, Y. (2021). Industrial hydrogen production technology and development status in China: a review. https://doi.org/10.1007/s10098-021-02089-w

Cheema, I. I., & Krewer, U. (2018). Operating envelope of Haber-Bosch process design for power-to-ammonia. *RSC Advances*, *8*(61). https://doi.org/10.1039/c8ra06821f

ChemAnalyst. (2023, September). Global Ammonia Market Analysis: Plant Capacity, Production, Operating Efficiency, Foreign Trade, Demand & Supply, End-User Industries, Sales Channel, Company Share, Regional Demand, 2015-2030.

Chen, C. (2005, December). *A Technical and Economic Assessment of CO2 Capture Technology for IGCC Power Plants* [Doctoral dissertation, Carnegie Mellon University].

Chen, D., Lødeng, R., Omdahl, K., Anundskås, A., Olsvik, O., & Holmen, A. (2001). A model for reforming on Ni catalyst with carbon formation and deactivation. *Studies in Surface Science and Catalysis*, *139*. https://doi.org/10.1016/s0167-2991(01)80185-3

Chen, S. H., Chiou-Wei, S. Z., & Zhu, Z. (2022). Stochastic seasonality in commodity prices: the case of US natural gas. *Empirical Economics*, *62*(5). https://doi.org/10.1007/s00181-021-02094-4

Choi, Y., & Stenger, H. G. (2003). Water gas shift reaction kinetics and reactor modeling for fuel cell grade hydrogen. *Journal of Power Sources*, *124*(2). https://doi.org/10.1016/S0378-7753(03)00614-1

Christian Enger, B., Lødeng, R., & Holmen, A. (2008). A review of catalytic partial oxidation of methane to synthesis gas with emphasis on reaction mechanisms over transition metal catalysts. https://doi.org/10.1016/j.apcata.2008.05.018

Cloete, S., Arnaiz del Pozo, C., & Jiménez Álvaro, Á. (2022). System-friendly process design: Optimizing blue hydrogen production for future energy systems. *Energy*, *259*, 124954. https://doi.org/10.1016/j.energy.2022.124954

Cloete, S., Khan, M. N., Nazir, S. M., & Amini, S. (2021). Cost-effective clean ammonia production using membrane-assisted autothermal reforming. *Chemical Engineering Journal*, *404*. https://doi.org/10.1016/j.cej.2020.126550

Collodi, G., Azzaro, G., Ferrari, N., & Santos, S. (2017). Techno-economic Evaluation of Deploying CCS in SMR Based Merchant H2 Production with NG as Feedstock and Fuel. *Energy Procedia*, *114*. https://doi.org/10.1016/j.egypro.2017.03.1533

Darazz, A., & Al-Obaidan, A. (2013). What is the best comperssor for our applications, centrifugal or reciprocating. *SPE Kuwait Oil and Gas Show and Conference*.

De Groote, A. M., & Froment, G. F. (1996). Simulation of the catalytic partial oxidation of methane to synthesis gas. *Applied Catalysis A: General*, *138*(2). https://doi.org/10.1016/0926-860X(95)00299-5

De Jong, C. (2020, August). *PPA Insights: Valuing long-term investments and PPA contracts* (tech. rep.). Kyos.

De Smet, C. R., De Croon, M. H., Berger, R. J., Marin, G. B., & Schouten, J. C. (2001). Design of adiabatic fixed-bed reactors for the partial oxidation of methane to synthesis gas. Application to production of methanol and hydrogen for fuel-cells. *Chemical Engineering Science*, *56*(16). https://doi.org/10.1016/S0009-2509(01)00130-0

De Souza, T. L., Rossi, C. D. C. R. D. S., Alonso, C. G., Guirardello, R., Cabral, V. F., Fernandes-Machado, N. R. C., Specchia, S., Zabaloy, M. S., & Cardozo-Filho, L. (2014). Thermodynamic analysis of autothermal reforming of methane via entropy maximization: Hydrogen production. *International Journal of Hydrogen Energy*, *39*(16). https://doi.org/10.1016/j.ijhydene.2014.03.078

de Groot, M. T., Kraakman, J., & Garcia Barros, R. L. (2022). Optimal operating parameters for advanced alkaline water electrolysis. *International Journal of Hydrogen Energy*, *47*(82). https://doi.org/10.1016/j.ijhydene.2022.08.075

Detz, R., Weeda, M., & van Stralen, J. (2020, July). *Hydrogen in the Netherlands: A review of recent Dutch scenario studies* (tech. rep.). TNO. Amsterdam.

Detz, R., Lenzmann, F., Sijm, J., & Weeda, M. (2019). *Future role of Hydrogen in the Netherlands* (tech. rep.). TNO. Amsterdam.

Devkota, S. (2019). Basic Plant Design of High-Temperature Water Gas Shift Reaction.

Dickel, R. (2020). *Blue hydrogen as an enabler of green hydrogen : the case of Germany*.

Dincer, I., & Acar, C. (2014). Review and evaluation of hydrogen production methods for better sustainability. *International Journal of Hydrogen Energy*, *40*(34). https://doi.org/10.1016/j.ijhydene.2014.12.035

Douglas, J. M. (1985). A hierarchical decision procedure for process synthesis. *AIChE Journal*, *31*(3). https://doi.org/10.1002/aic.690310302

Douglas, J. (1988). *Conceptual design of chemical processes*. McGraw-Hill Book Company.

Dybkjaer, I. (1995). Tubular reforming and autothermal reforming of natural gas - an overview of available processes. *Fuel Processing Technology*, *42*(2-3). https://doi.org/10.1016/0378-3820(94)00099-F

EIA. (2023). Natural gas explained.

Ersoz, A., Olgun, H., & Ozdogan, S. (2006). Reforming options for hydrogen production from fossil fuels for PEM fuel cells. *Journal of Power Sources*, *154*(1). https://doi.org/10.1016/j.jpowsour.2005.02.092

EZK. (2023, July). *Nationaal plan energiesysteem* (tech. rep.). Ministerie van Economische Zaken en Klimaat.

Fahim, M. A., Alsahhaf, T. A., & Elkilani, A. (2010). *Fundamentals of Petroleum Refining*. https://doi.org/10.1016/C2009-0-16348-1

Fatou Gómez, J., Jayashankar G.J., Dussi, S., Poort, J., González Díez, N., & Buijs, L. (2022). Digital models, shadows and twins: physics and data integration using PyDOLPHIN. *"Empowering Industry" Digital Energy session*.

Fazioli, R., & Pantaleone, F. (2021). Macroeconomic factors influencing public policy strategies for blue and green hydrogen. *Energies*, *14*(23). https://doi.org/10.3390/en14237938

Fladmark, B., & Grimstad, G. B. (2013). *Seasonality in Natural Gas Prices* [Doctoral dissertation, NORWEGIAN SCHOOL OF ECONOMICS].

Fuller, J., & Spence, E. (2020, June). *PORTHOS CCS – TRANSPORT AND STORAGE (T&S) TARIFF REVIEW* (tech. rep.). XODUS Advisory.

Garcia, H. E., Mohanty, A., Lin, W.-C., & Cherry, R. S. (2013). Dynamic analysis of hybrid energy systems under flexible operation and variable renewable generation – Part I: Dynamic performance analysis. *Energy*, *52*, 1–16. https://doi.org/10.1016/j.energy.2013.01.022

Guo, W., Feng, F., Song, G., Xiao, J., & Shen, L. (2012). Simulation and energy performance assessment of CO2 removal from crude synthetic natural gas via physical absorption process. *Journal of Natural Gas Chemistry*, *21*(6). https://doi.org/10.1016/S1003-9953(11)60412-X

Guthrie, K. M. (1969). Capital Cost Estimating. *Chemical Engineer*, *76*(6). https://doi.org/10.1021/ie50502a032

Halabi, M. H., de Croon, M. H., van der Schaaf, J., Cobden, P. D., & Schouten, J. C. (2008). Modeling and analysis of autothermal reforming of methane to hydrogen in a fixed bed reformer. *Chemical Engineering Journal*, *137*(3). https://doi.org/10.1016/j.cej.2007.05.019

Hamelinck, C. N., & Faaij, A. P. (2002). Future prospects for production of methanol and hydrogen from biomass. *Journal of Power Sources*, *111*(1). https://doi.org/10.1016/S0378-7753(02)00220-3

Hla, S. S., Park, D., Duffy, G. J., Edwards, J. H., Roberts, D. G., Ilyushechkin, A., Morpeth, L. D., & Nguyen, T. (2009). Kinetics of high-temperature water-gas shift reaction over two iron-based commercial catalysts using simulated coal-derived syngases. *Chemical Engineering Journal*, *146*(1). https://doi.org/10.1016/j.cej.2008.09.023

Hoang, D. L., Chan, S. H., & Ding, O. L. (2006). Hydrogen production for fuel cells by autothermal reforming of methane over sulfide nickel catalyst on a gamma alumina support. *Journal of Power Sources*, *159*(2). https://doi.org/10.1016/j.jpowsour.2005.11.094

Hydrogen Council. (2022, January). Hydrogen Council membership grows to more than 130 members, with eleven new companies committing to foster development of the hydrogen economy. https://hydrogencouncil.com/en/hydrogen-council-membership-grows-to-more-than-130-members-with-twelve-new-companies-committing-to-foster-development-of-the-hydrogen-economy/#:~:text=The%20Hydrogen%20Council%20now%20includes,and%20one%20new%20investor%3A%20Temasek.

IEA. (2019a). *Global Energy & CO2 Status Report 2019 – Analysis* (tech. rep.). IEA.

IEA. (2019b). Putting CO2 to Use Creating Value from emissions. *IEA Publications*.

IEA. (2019c). *The Future of Hydrogen* (tech. rep. No. June).

IEA. (2021). Ammonia Technology Roadmap; Towards more Sustainable Nitrogen Fertilizer Production. *International Energy Agency*.

IEA. (2022a). *Global Hydrogen Review 2022* (tech. rep.).

IEA. (2022b). Hydrogen projects database public version.

IEA. (2022c). International Energy Agency (IEA) World Energy Outlook 2022. Https://Www.Iea.Org/Reports/World-Energy-Outlook-2022/Executive-Summary

IEA. (2023a, February). *Gas Market Report, Q1-2023* (tech. rep.). International Energy Agency.

IEA. (2023b, September). *Global Hydrogen Review 2023* (tech. rep.). International Energy Agency.

IEAGHG. (2017, February). *Techno-Economic Evaluation of HYCO Plant Integrated to Ammonia/Urea or Methanol Production with CCS* (tech. rep.). IEA greenhouse gas R&D programme.

INDEXBOX. (2022). *EU - Anhydrous Ammonia - Market Analysis, Forecast, Size, Trends and Insights* (tech. rep.). IndexBox, Inc.

IPCC Working Group II. (2022). IPCC AR6 Working Group II: Summary for policymakers: Climate Change 2022, Impacts, Adaptation anf Vulnerability. In *Contribution of working group ii to the sixth assessment report of the intergovernmental panel on climate change*.

Jansen, D., Gazzani, M., Manzolini, G., Dijk, E. V., & Carbo, M. (2015). Pre-combustion CO2 capture. *International Journal of Greenhouse Gas Control*, *40*. https://doi.org/10.1016/j.ijggc.2015.05.028

Kapetaki, Z., Brandani, P., Brandani, S., & Ahn, H. (2015). Process simulation of a dual-stage Selexol process for 95% carbon capture efficiency at an integrated gasification combined cycle power plant. *International Journal of Greenhouse Gas Control*, *39*. https://doi.org/10.1016/j.ijggc.2015.04.015

Katebah, M., Al-Rawashdeh, M., & Linke, P. (2022). Analysis of hydrogen production costs in Steam-Methane Reforming considering integration with electrolysis and CO2 capture. *Cleaner Engineering and Technology*, *10*. https://doi.org/10.1016/j.clet.2022.100552

Khojasteh Salkuyeh, Y., Saville, B. A., & MacLean, H. L. (2017). Techno-economic analysis and life cycle assessment of hydrogen production from natural gas using current and emerging technologies. *International Journal of Hydrogen Energy*, *42*(30). https://doi.org/10.1016/j.ijhydene.2017.05.219

Kim, S., Dean, A. M., & Bae, J. (2013). Coupled transport and kinetics in the mixing region for hydrocarbon autothermal reforming applications. *International Journal of Hydrogen Energy*, *38*(36). https://doi.org/10.1016/j.ijhydene.2013.09.119

Klijn, H. (2023). Ammonia and the Netherlands. *Ammonia Energy APAC 2023*.

Klotsche, K., Micus, F., Thomas, C., & Hesse, U. (2019). Waste Heat Recovery for Reciprocating Compressors. *IOP Conference Series: Materials Science and Engineering*, *604*(1). https://doi.org/10.1088/1757-899X/604/1/012085

Krishnan, S., Koning, V., Theodorus de Groot, M., de Groot, A., Mendoza, P. G., Junginger, M., & Kramer, G. J. (2023). Present and future cost of alkaline and PEM electrolyser stacks. *International Journal of Hydrogen Energy*, *48*(83). https://doi.org/10.1016/j.ijhydene.2023.05.031

Kumar, R., Kumar, A., & Pal, A. (2020). An overview of conventional and non-conventional hydrogen production methods. *Materials Today: Proceedings*, *46*. https://doi.org/10.1016/j.matpr.2020.08.793

Latham, D. A., McAuley, K. B., Peppley, B. A., & Raybold, T. M. (2011). Mathematical modeling of an industrial steam-methane reformer for on-line deployment. *Fuel Processing Technology*, *92*(8). https://doi.org/10.1016/j.fuproc.2011.04.001

Le Chatelier, H. L. (1884). Comptes Rendus. *Journal of the French Academy of Sciences*, *99*, 786–789.

Lee, K., Liu, X., Vyawahare, P., Sun, P., Elgowainy, A., & Wang, M. (2022). Techno-economic performances and life cycle greenhouse gas emissions of various ammonia production pathways including conventional, carbon-capturing, nuclear-powered, and renewable production. *Green Chemistry*, *24*(12). https://doi.org/10.1039/d2gc00843b

Li, Y., Wang, Y., Zhang, X., & Mi, Z. (2008). Thermodynamic analysis of autothermal steam and CO2 reforming of methane. *International Journal of Hydrogen Energy*, *33*(10). https://doi.org/10.1016/j.ijhydene.2008.02.051

Luberti, M., & Ahn, H. (2022). Review of Polybed pressure swing adsorption for hydrogen purification. https://doi.org/10.1016/j.ijhydene.2022.01.147

Luyben, W. L. (2018). Capital cost of compressors for conceptual design. *Chemical Engineering and Processing - Process Intensification*, *126*. https://doi.org/10.1016/j.cep.2018.01.020

Lyons, M., Durrant, P., & Kochhar, K. (2021). *Reaching zero with renewables - Capturing Carbon*. International Renewable Energy Agency.

Lyons, S., Durusut, E., & Moore, I. (2018, December). *Industrial Fuel Switching Market Engagement Study* (tech. rep.). Element Energy, Jacobs. Cambridge.

Ma, R., Xu, B., & Zhang, X. (2019). Catalytic partial oxidation (CPOX) of natural gas and renewable hydrocarbons/oxygenated hydrocarbons—A review. https://doi.org/10.1016/j.cattod.2019.06.025

Mac Dowell, N., Sunny, N., Brandon, N., Herzog, H., Ku, A. Y., Maas, W., Ramirez, A., Reiner, D. M., Sant, G. N., & Shah, N. (2021). The hydrogen economy: A pragmatic path forward. *Joule*, *5*(10). https://doi.org/10.1016/j.joule.2021.09.014

Madejski, P., Chmiel, K., Subramanian, N., & Kuś, T. (2022). Methods and Techniques for CO2 Capture: Review of Potential Solutions and Applications in Modern Energy Technologies. https://doi.org/10.3390/en15030887

Malischek, R., & McCulloch, S. (2021, April). *The world has vast capacity to store CO2: Net zero means we'll need it* (tech. rep.). IEA. Paris.

Manfren, M. (2012). Multi-commodity network flow models for dynamic energy management – Mathematical formulation. *Energy Procedia*, *14*, 1380–1385. https://doi.org/10.1016/j.egypro.2011.12.1105

Maroño, M., Ruiz, E., Sánchez, J. M., Martos, C., Dufour, J., & Ruiz, A. (2009). Performance of Fe-Cr based WGS catalysts prepared by co-precipitation and oxi-precipitation methods. *International Journal of Hydrogen Energy*, *34*(21). https://doi.org/10.1016/j.ijhydene.2009.08.068

Martin, P. (2023, October). Fertiliser production is an obvious use case for green hydrogen, so why are producers more likely to want blue?

Mayer, P., Ramirez, A., Pezzella, G., Winter, B., Sarathy, S. M., Gascon, J., & Bardow, A. (2023). Blue and green ammonia production: A techno-economic and life cycle assessment perspective. *iScience*, *26*(8). https://doi.org/10.1016/j.isci.2023.107389

Mehanovic, D., Al-Haiek, A., Leclerc, P., Rancourt, D., Fréchette, L., & Picard, M. (2023). Energetic, GHG, and economic analyses of electrified steam methane reforming using conventional re-

former tubes. *Energy Conversion and Management*, *276*. https://doi.org/10.1016/j.enconman.2022.116549

Meloni, E., Martino, M., & Palma, V. (2020). A short review on ni based catalysts and related engineering issues for methane steam reforming. https://doi.org/10.3390/catal10030352

Mendes, D., Chibante, V., Mendes, A., & Madeira, L. M. (2010). Determination of the low-temperature water-gas shift reaction kinetics using a cu-based catalyst. *Industrial and Engineering Chemistry Research*, *49*(22). https://doi.org/10.1021/ie101137b

Ministry van Economic Affairs and Climate Policy. (2022). Does less Russian gas mean more gas from Groningen? *Government of the Netherlands*.

Mirghani, M. (2007). *Modelling and simulation of autothermal reformer for synthesis gas production* [Doctoral dissertation, UNIVERSITI TEKNOLOGI PETRONAS].

Moe, J. (1962). Design of water-gas shift reactors. *Chemical Engineering Progress*, *58*, 33–36.

Mohajerani, S., Kumar, A., & Oni, A. O. (2018). A techno-economic assessment of gas-to-liquid and coal-to-liquid plants through the development of scale factors. *Energy*, *150*. https://doi.org/10.1016/j.energy.2018.03.005

Møller, K. T., Jensen, T. R., Akiba, E., & Li, H. w. (2017). Hydrogen - A sustainable energy carrier. *Progress in Natural Science: Materials International*, *27*(1). https://doi.org/10.1016/j.pnsc.2016.12.014

Morgan, E. R., Manwell, J. F., & McGowan, J. G. (2017). Sustainable Ammonia Production from U.S. Offshore Wind Farms: A Techno-Economic Review. https://doi.org/10.1021/acssuschemeng.7b02070

Muradov, N. (2014). *Liberating Energy from Carbon: Introduction to Decarbonization* (Vol. 22).

Muradov, N. (2017). Low to near-zero CO2 production of hydrogen from fossil fuels: Status and perspectives. https://doi.org/10.1016/j.ijhydene.2017.04.101

Nakaten, N., Schlüter, R., Azzam, R., & Kempka, T. (2014). Development of a techno-economic model for dynamic calculation of cost of electricity, energy demand and CO2 emissions of an integrated UCG-CCS process. *Energy*, *66*. https://doi.org/10.1016/j.energy.2014.01.014

Nandakumar, N., & Annaswamy, A. M. (2017). Impact of increased renewables on natural gas markets in eastern United States. *Journal of Modern Power Systems and Clean Energy*, *5*(3). https://doi.org/10.1007/s40565-017-0292-1

NEOM. (2023, May). NEOM GREEN HYDROGEN COMPANY COMPLETES FINANCIAL CLOSE AT A TOTAL INVESTMENT VALUE OF USD 8.4 BILLION IN THE WORLD'S LARGEST CARBON-FREE GREEN HYDROGEN PLANT.

Noelker, K., & Johanning, J. (2010). Autothermal reforming: a flexible syngas route with future potential. *NITROGEN & SYNGAS 2010 International Conference*.

Nosherwani, S. A., & Neto, R. C. (2021). Techno-economic assessment of commercial ammonia synthesis methods in coastal areas of Germany. *Journal of Energy Storage*, *34*. https://doi.org/10.1016/j.est.2020.102201

Oni, A. O., Anaya, K., Giwa, T., Di Lullo, G., & Kumar, A. (2022). Comparative assessment of blue hydrogen from steam methane reforming, autothermal reforming, and natural gas decomposition technologies for natural gas-producing regions. *Energy Conversion and Management*, *254*. https://doi.org/10.1016/j.enconman.2022.115245

Oshiro, K., & Fujimori, S. (2022). Role of hydrogen-based energy carriers as an alternative option to reduce residual emissions associated with mid-century decarbonization goals. *Applied Energy*, *313*. https://doi.org/10.1016/j.apenergy.2022.118803

Padurean, A., Cormos, C. C., & Agachi, P. S. (2012). Pre-combustion carbon dioxide capture by gas-liquid absorption for Integrated Gasification Combined Cycle power plants. *International Journal of Greenhouse Gas Control*, *7*. https://doi.org/10.1016/j.ijggc.2011.12.007

Pagani, G., Acar, C., & Hajimolana, Y. (2022). GREEN HYDROGEN FOR AMMONIA PRODUCTION - A CASE FOR THE NETHERLANDS. *Proceedings of WHEC 2022 - 23rd World Hydrogen Energy Conference: Bridging Continents by H2*.

Palma, V., Ruocco, C., Martino, M., Meloni, E., & Ricca, A. (2017). Structured catalyst for process intensification in hydrogen production by reforming processes. In *Hydrogen production, separation and purification for energy*. https://doi.org/10.1049/pbpo089e{_}ch1

Park, S., Shin, Y., Jeong, E., & Han, M. (2023). Techno-economic analysis of green and blue hybrid processes for ammonia production. *Korean Journal of Chemical Engineering*. https://doi.org/10.1007/s11814-023-1520-1

Park, Y., Moon, D. K., Kim, Y. H., Ahn, H., & Lee, C. H. (2014). Adsorption isotherms of CO2, CO, N2, CH4, Ar and H2 on activated carbon and zeolite LiX up to 1.0 MPa. *Adsorption*, *20*(4). https://doi.org/10.1007/s10450-014-9608-x

Parkinson, B., Balcombe, P., Speirs, J. F., Hawkes, A. D., & Hellgardt, K. (2019). Levelized cost of CO2 mitigation from hydrogen production routes. *Energy Environ. Sci.*, *12*, 19–40.

Pashchenko, D., & Gnutikova, M. (2021). Thermodynamic Analysis Of Carbon Formation Conditions In A Steam Methane Reforming Process. *Thermal Science*, *25*(5 Part B). https://doi.org/10.2298/TSCI190404136P

PexaPark. (2023). *In-depth Insights to PPA Markets and Structures* (tech. rep.).

Phan, T. S., Pham Minh, D., Espitalier, F., Nzihou, A., & Grouset, D. (2022). Hydrogen production from biogas: Process optimization using ASPEN Plus®. *International Journal of Hydrogen Energy*, *47*(100). https://doi.org/10.1016/j.ijhydene.2022.01.100

Piña, J., & Borio, D. O. (2006). Modeling and simulation of an autothermal reformer. *Latin American Applied Research*, *36*(4).

PORTHOS. (2020, June). *Vragen en antwoorden over de Porthos-infrastructuur* (tech. rep.). Royal HaskoningDHV.

PORTHOS. (2023). PORTHOS Project.

Rabenstein, G., & Hacker, V. (2008). Hydrogen for fuel cells from ethanol by steam-reforming, partial-oxidation and combined auto-thermal reforming: A thermodynamic analysis. *Journal of Power Sources*, *185*(2). https://doi.org/10.1016/j.jpowsour.2008.08.010

Rachford, H., & Rice, J. (1952). Procedure for use of electrical digital computers in calculating flash vaporization hydrocarbon equilibrium. *Journal of Petroleum Technology*, 19.

Raghuveer, T., & Wilczewski, W. (2022, May). U.S. ammonia prices rise in response to higher international natural gas prices.

Ratnasamy, C., & Wagner, J. (2009). Water gas shift catalysis. https://doi.org/10.1080/01614940903048661

Raza, A., Gholami, R., Rezaee, R., Rasouli, V., & Rabiei, M. (2019). Significant aspects of carbon capture and storage – A review. https://doi.org/10.1016/j.petlm.2018.12.007

Reddy, G. K., & Smirniotis, P. G. (2015). *Water Gas Shift Reaction: Research Developments and Applications*. https://doi.org/10.1016/C2013-0-09821-0

Reksten, A. H., Thomassen, M. S., Møller-Holst, S., & Sundseth, K. (2022). Projecting the future cost of PEM and alkaline water electrolysers; a CAPEX model including electrolyser plant size and technology development. *International Journal of Hydrogen Energy*, *47*(90). https://doi.org/10.1016/j.ijhydene.2022.08.306

Rice, S. F., & Mann, D. P. (2007). Autothermal Reforming of Natural Gas to Synthesis Gas. *Sandia Report*, *125*(April).

Rosner, F., Rao, A., & Samuelsen, S. (2020). Water gas shift reactor modelling and new dimensionless number for thermal management/design of isothermal reactors. *Applied Thermal Engineering*, *173*. https://doi.org/10.1016/j.applthermaleng.2020.115033

Rostrup-Nielsen, J., & Christiansen, L. J. (2011). *Concepts in Syngas Manufacture*.

Rother, J., & Fieback, T. (2013). Multicomponent adsorption measurements on activated carbon, zeolite molecular sieve and metal-organic framework. *Adsorption*, *19*(5). https://doi.org/10.1007/s10450-013-9527-2

Rouwenhorst, K., Krzywda, P., Benes, N., Mul, G., & Lefferts, L. (2021). Ammonia Production Technologies. In *Techno-economic challenges of green ammonia as an energy vector*. https://doi.org/10.1016/b978-0-12-820560-0.00004-7

Rovere, A. (2019, December). *AUTOTHERMAL REFORMING PLANT WITH CCS: TECHNO-ECONOMIC INVESTIGATION* [Doctoral dissertation, Politecnico di Torino].

Rowshanzamir, S., Safdarnejad, S. M., & Eikani, M. H. (2012). A CFD model for methane autothermal reforming on Ru/γ- Al 2O3 catalyst. *Procedia Engineering*, *42*. https://doi.org/10.1016/j.proeng.2012.07.390

Ruettinger, W., Ilinich, O., & Farrauto, R. J. (2003). A new generation of water gas shift catalysts for fuel cell applications. *Journal of Power Sources*, *118*(1-2). https://doi.org/10.1016/S0378-7753(03)00062-4

Ruthven, D. M., Farooq, S., & Knaebel, K. S. (1996). *Pressure swing adsorption*. John Wiley & Sons.

Sakurai, H., Ueda, A., Kobayashi, T., & Haruta, M. (1997). Low-temperature water-gas shift reaction over gold deposited on TiO2. *Chemical Communications*, (3). https://doi.org/10.1039/a606192c

Schaaf, T., Grünig, J., Schuster, M. R., Rothenfluh, T., & Orth, A. (2014). Methanation of CO2 - storage of renewable energy in a gas distribution system. *Energy, Sustainability and Society*, *4*(1). https://doi.org/10.1186/s13705-014-0029-1

Shi, L., Bayless, D. J., & Prudich, M. E. (2009). A CFD model of autothermal reforming. *International Journal of Hydrogen Energy*, *34*(18). https://doi.org/10.1016/j.ijhydene.2009.07.039

Siang, T., Jalil, A., Liew, S., Owgi, A., & Rahman, A. (2022). A review on state-of-the-art catalysts for methane partial oxidation to syngas production. *Catalysis Reviews*, 1–57. https://doi.org/10.1080/01614940.2022.2072450

Simeone, M., Salemme, L., Scognamiglio, D., Allouis, C., & Volpicelli, G. (2008). Effect of water addition and stoichiometry variations on temperature profiles in an autothermal methane reforming reactor with Ni catalyst. *International Journal of Hydrogen Energy*, *33*(4). https://doi.org/10.1016/j.ijhydene.2007.12.034

Simon, C. M., Smit, B., & Haranczyk, M. (2016). PyIAST: Ideal adsorbed solution theory (IAST) Python package. *Computer Physics Communications*, *200*. https://doi.org/10.1016/j.cpc.2015.11.016

Sircar, S. (2007). PRESSURE SWING ADSORPTION TECHNOLOGY FOR HYDROGEN PURIFICATION - A STATUS REVIEW. https://doi.org/10.1142/9789812770264{_}0002

Sjardin, M., Damen, K. J., & Faaij, A. P. (2006). Techno-economic prospects of small-scale membrane reactors in a future hydrogen-fuelled transportation sector. *Energy*, *31*(14). https://doi.org/10.1016/j.energy.2005.12.004

Smith, C., Hill, A. K., & Torrente-Murciano, L. (2020). Current and future role of Haber-Bosch ammonia in a carbon-free energy landscape. *Energy and Environmental Science*, *13*(2). https://doi.org/10.1039/c9ee02873k

Smith, M. W., & Shekhawat, D. (2011). Chapter 5 - Catalytic Partial Oxidation. In Dushyant Shekhawat, James J. Spivey, & David A. Berry (Eds.), *Fuel cells: Technologies for fuel processing* (pp. 73–128). Elsevier B.V.

Smith R J, B., Loganathan, M., & Shantha, M. S. (2010). A review of the water gas shift reaction kinetics. https://doi.org/10.2202/1542-6580.2238

Song, C., Liu, Q., Ji, N., Kansha, Y., & Tsutsumi, A. (2015). Optimization of steam methane reforming coupled with pressure swing adsorption hydrogen production process by heat integration. *Applied Energy*, *154*. https://doi.org/10.1016/j.apenergy.2015.05.038

S&P Global. (2022). Ammonia Fertilizer Market and Price Analysis.

Spath, P. L., & Dayton, D. C. (2003). Preliminary Screening – Technical and Economic Assessment of Synthesis Gas to Fuels and Chemicals with Emphasis on the Potential for Biomass-Derived Syngas. *National Renewable Energy Laboratory*, (December). https://doi.org/10.2172/15006100

Speight, J. G. (2023). Production of bio-syngas and bio-hydrogen by gasification. In R. Luque, C. S. K. Lin, K. Wilson, & C. Du (Eds.), *Handbook of biofuels production* (pp. 419–448). Woodhead Publishing. https://doi.org/10.1016/B978-0-323-91193-1.00006-8

Tennyson, R. N., & Schaaf, R. P. (1977). GUIDELINES CAN HELP CHOOSE PROPER PROCESS FOR GAS-TREATING PLANTS. *Oil and Gas Journal*, *75*(2).

Tetteh, D., & Salehi, S. (2023). The Blue Hydrogen Economy:A Promising Option for the Near-to-Mid-Term Energy Transition. *Journal of Energy Resources Technology*, *145*(4).

Towler, G., & Sinnott, R. (2013). *Chapter 19 - Heat-Transfer Equipment*.

Tran, A., Aguirre, A., Durand, H., Crose, M., & Christofides, P. D. (2017). CFD modeling of a industrial-scale steam methane reforming furnace. *Chemical Engineering Science*, *171*. https://doi.org/10.1016/j.ces.2017.06.001

Verleysen, K., Parente, A., & Contino, F. (2021). How sensitive is a dynamic ammonia synthesis process? Global sensitivity analysis of a dynamic Haber-Bosch process (for flexible seasonal energy storage). *Energy*, *232*. https://doi.org/10.1016/j.energy.2021.121016

Vernon, P. D. F., Green, M. L. H., Cheetham, A. K., & Ashcroft, A. T. (1990). Partial oxidation of methane to synthesis gas. *Catalysis Letters*, *6*(2), 181–186. https://doi.org/10.1007/BF00774718

Voldsund, M., Jordal, K., & Anantharaman, R. (2016). Hydrogen production with CO2 capture. https://doi.org/10.1016/j.ijhydene.2016.01.009

Xu, J., & Froment, G. F. (1989). Methane Steam Reforming , Methanation and Water-Gas Shift : 1 . Intrinsic Kinetics. *AIChE Journal*, *35*(1).

Yan, Y., Li, H., Li, L., Zhang, L., & Zhang, J. (2018). Properties of methane autothermal reforming to generate hydrogen in membrane reactor based on thermodynamic equilibrium model. *Chemical Engineering and Processing - Process Intensification*, *125*. https://doi.org/10.1016/j.cep.2018.01.010

Yara. (2023). Productie-eenheid Sluiskil.

Yara International ASA. (2022, June). Yara Clean Ammonia - Capital Markets Day.

York, A. P., Xiao, T., & Green, M. L. (2003). Brief overview of the partial oxidation of methane to synthesis gas. *Topics in Catalysis*, *22*(3-4). https://doi.org/10.1023/A:1023552709642

Yousefi, S. H., Groenenberg, R., Koornneef, J., Juez-Larré, J., & Shahi, M. (2023). Techno-economic analysis of developing an underground hydrogen storage facility in depleted gas field: A Dutch case study. *International Journal of Hydrogen Energy*, *48*(74). https://doi.org/10.1016/j.ijhydene.2023.04.090

Yu, C. H., Huang, C. H., & Tan, C. S. (2012). A review of CO2 capture by absorption and adsorption. https://doi.org/10.4209/aaqr.2012.05.0132

Zahedi nezhad, M., Rowshanzamir, S., & Eikani, M. H. (2009). Autothermal reforming of methane to synthesis gas: Modeling and simulation. *International Journal of Hydrogen Energy*, *34*(3). https://doi.org/10.1016/j.ijhydene.2008.11.091

A

PORTHOS CO_2 specifications

CO_2 specifications

Component	Mole Base
CO_2	≥ 95%
H_2O	≤ 70 ppm
Sum [H_2+N_2+Ar+CH_4+CO+O_2]	≤ 4%
H_2	≤ 0.75%
N_2	≤ 2.4%
Ar	≤ 0.4%
CH_4	≤ 1%
CO	≤ 750 ppm
O_2	≤ 40 ppm
Total sulfur-contained compounds (COS, DMS, H_2S, SOx, Mercaptan)	≤ 20 ppm Of which H_2S ≤ 5 ppm
Total NOx	≤ 5 ppm
Total aliphatic hydrocarbons (C2 to C10)[i]	≤ 1200 ppm
Total aromatic hydrocarbons (C6 to C10, incl. BTEX)[i]	≤ 0.1 ppm
Total volatile organic compounds[ii] (excl. methane, total aliphatic HC (C2 to C10), methanol, ethanol, and aldehydes)	≤ 10 ppm
Total aldehyde compounds	≤ 10 ppm
Ethanol	≤ 20 ppm
Methanol	≤ 620 ppm
Hydrogen cyanide (HCN)	≤ 2 ppm
Total amine compounds	≤ 1 ppm
Total glycol compounds	Follow dew point specification
Ammonia (NH_3)	≤ 3 ppm
Total carboxylic acid and amide compounds	≤ 1 ppm
Total phosphorus-contained compounds	≤ 1 ppm
Toxic compounds[iii]	
Dew point limit value measurement (for all liquids, i.e. for complete CO_2 composition)	< -10 °C (at 20 bara)

Note i: Specification values are molecular based
Note ii: VOC definition according to Dutch policy
Note iii: Toxic compounds: although CO_2 and other gases like i.e. H_2 and N_2 can form a risk of asphyxiation, Porthos would like to know other components within the stream which impose a risk on personal safety to be taken into account in Porthos HSE policy

B

Reactor validation

B.1. ATR

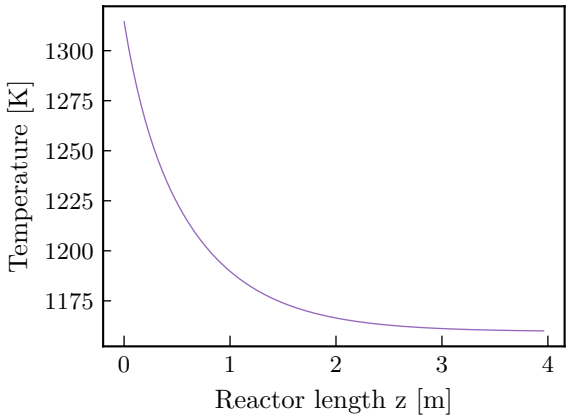

Figure B.1: Temperature profile over the reactor length of the ATR

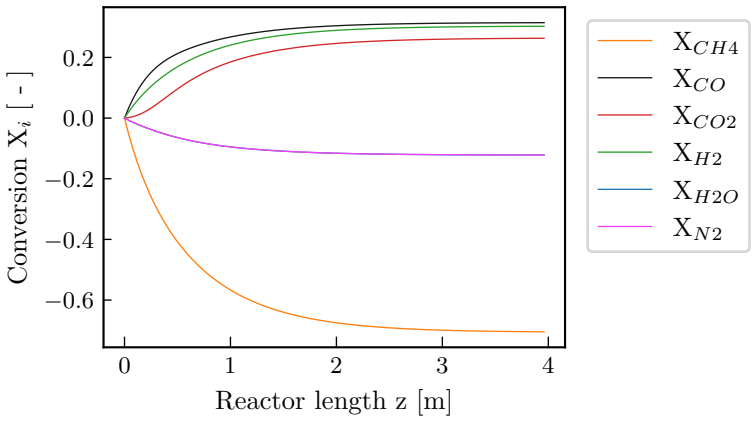

Figure B.2: Conversion per component over the reactor length of the ATR

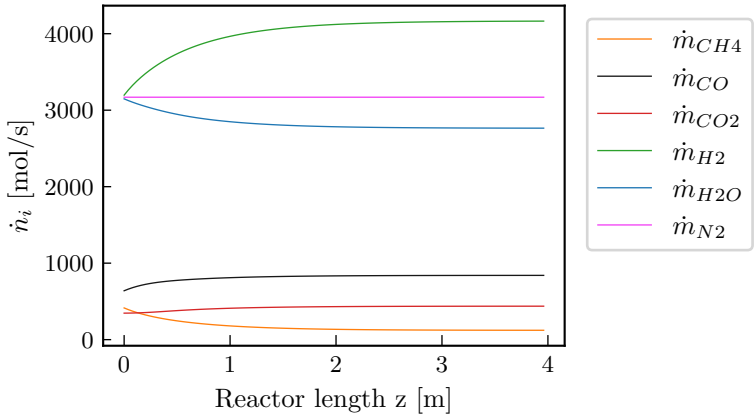

Figure B.3: Molar flow rate per component over the reactor length of the ATR

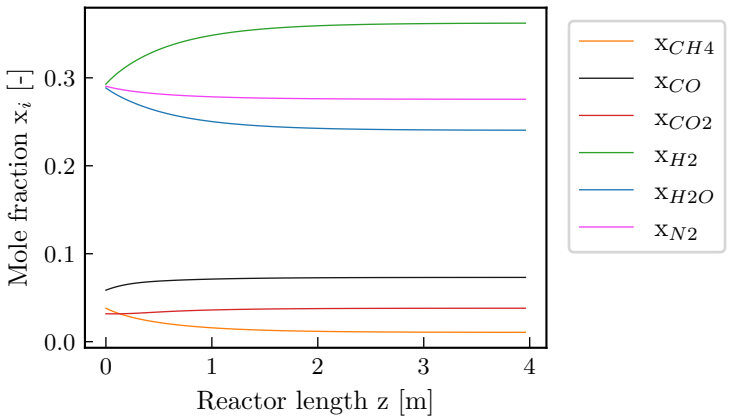

Figure B.4: Mole fraction per component over the reactor length of the ATR

B.2. HTWGS

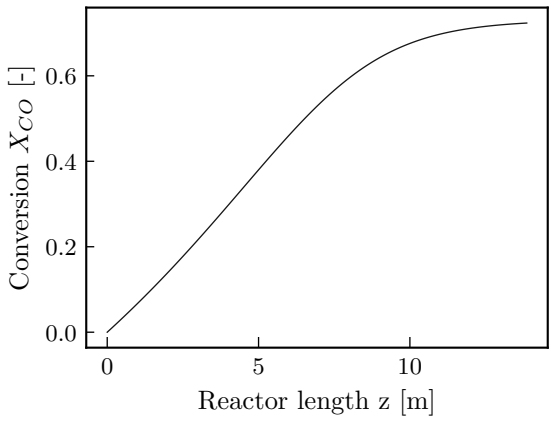

Figure B.5: Conversion per component over the reactor length of the HTWGS

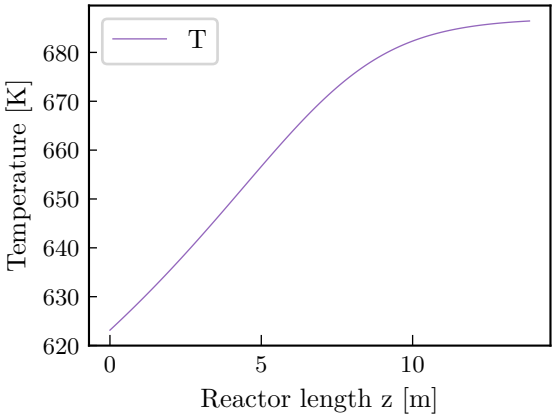

Figure B.6: Temperature profile over the reactor length of the HTWGS

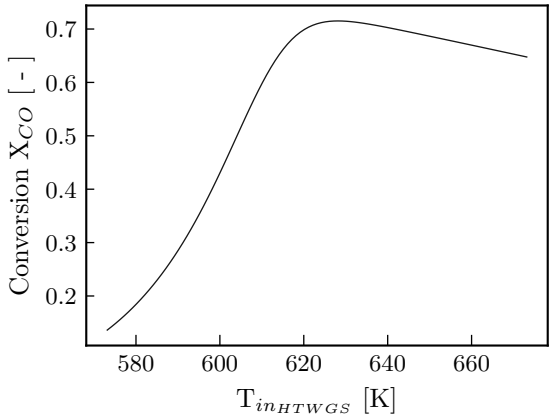

Figure B.7: Input temperature sensitivity over the conversion, optimum temperature around 623.15 K

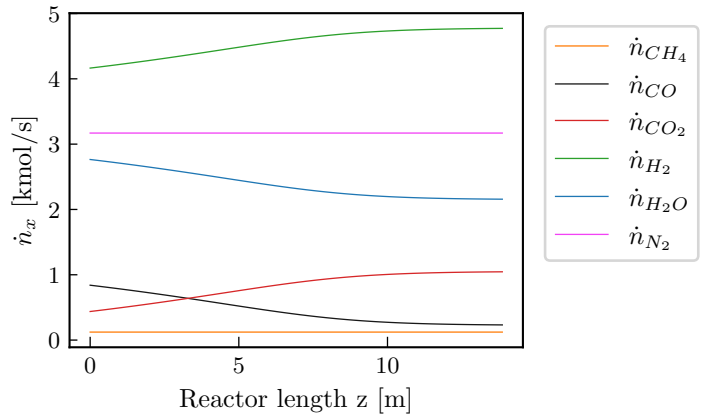

Figure B.8: Molar flow rate per component over the reactor length of the HTWGS

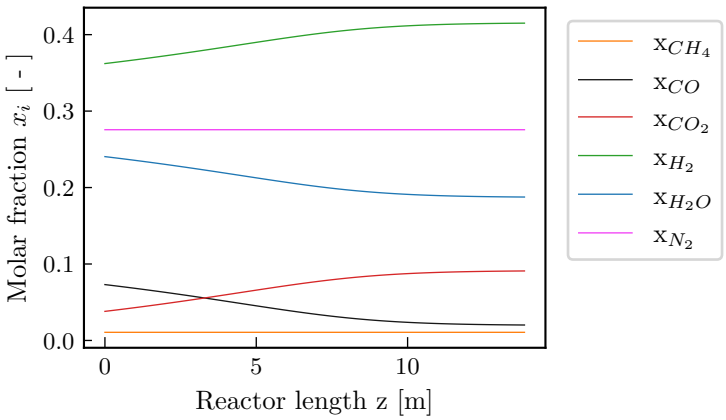

Figure B.9: Mole fraction per component over the reactor length of the HTWGS

B.3. LTWGS

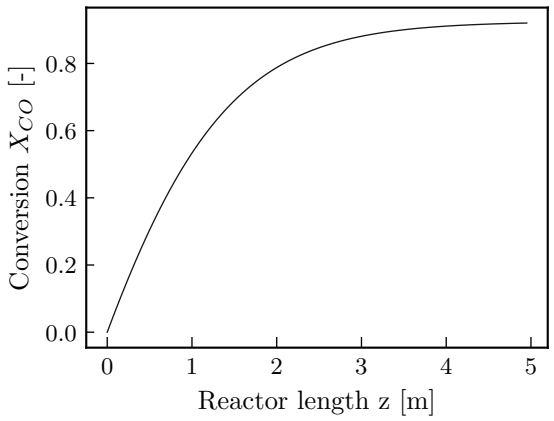

Figure B.10: Conversion per component over the reactor length of the LTWGS

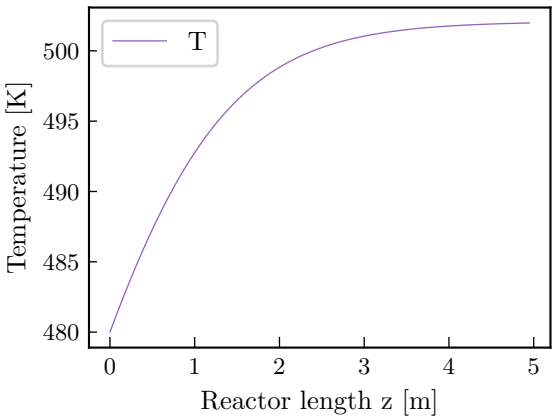

Figure B.11: Temperature profile over the reactor length of the LTWGS

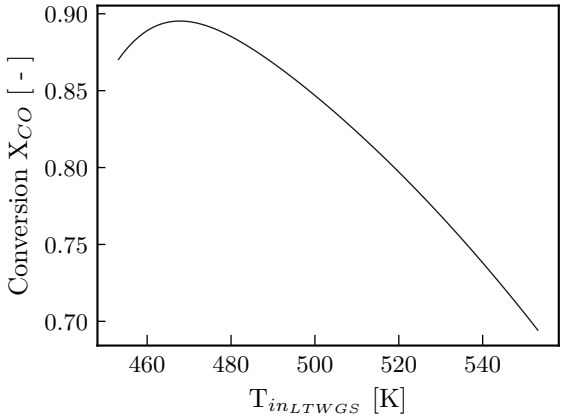

Figure B.12: Input temperature sensitivity over the conversion, optimum temperature around 473.15K

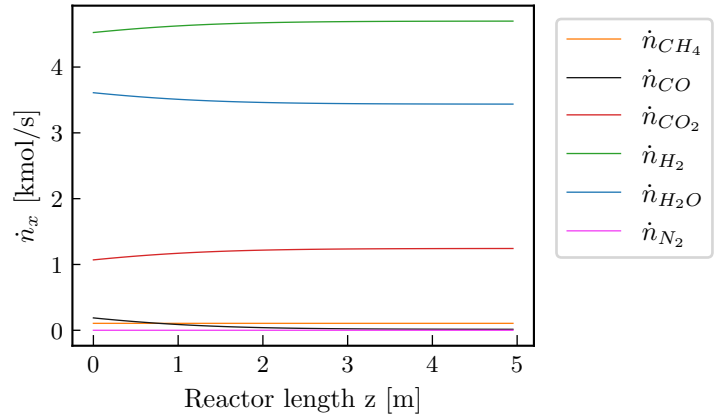

Figure B.13: Molar flow rate per component over the reactor length of the LTWGS

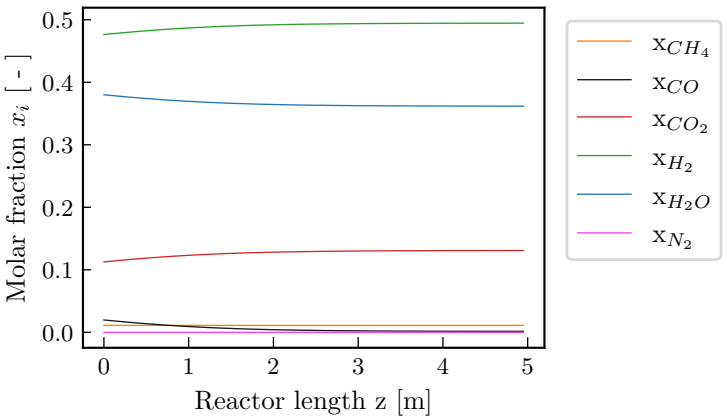

Figure B.14: Mole fraction per component over the reactor length of the LTWGS

B.4. Absorption tower and stripper

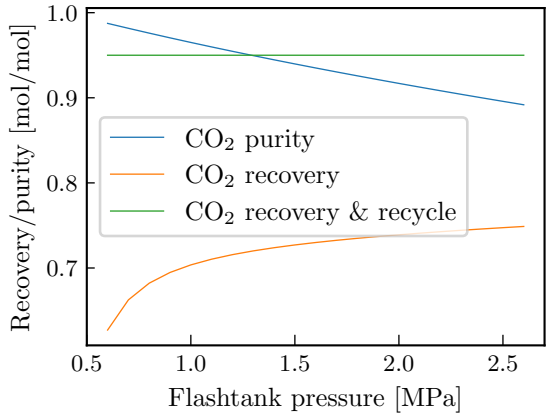

Figure B.15: Adsorbent loading on activated carbon

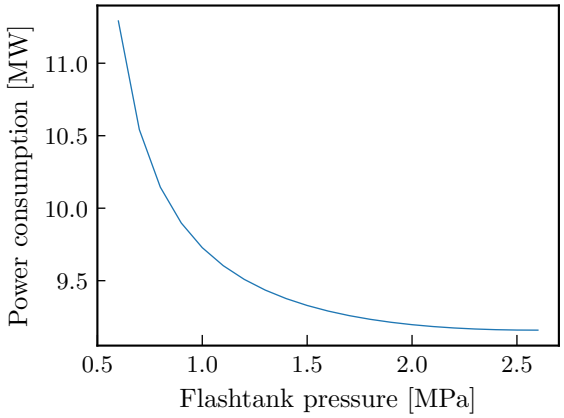

Figure B.16: Power consumption for physical absorption versus flash tank pressure

B.5. PSA

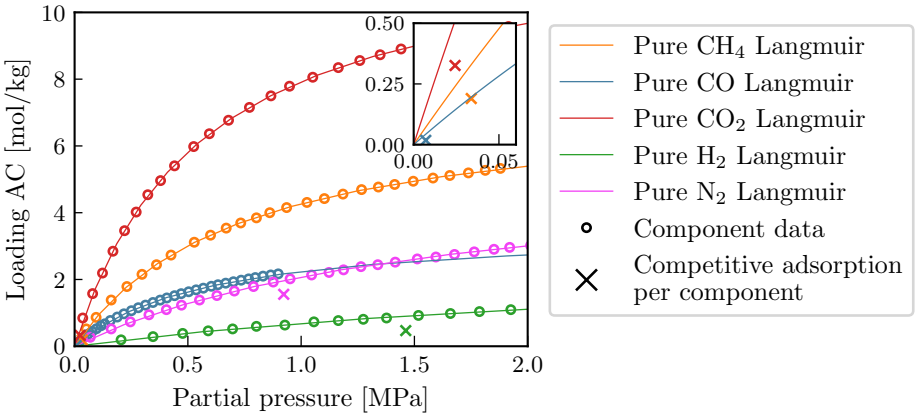

Figure B.17: Adsorbent loading on activated carbon

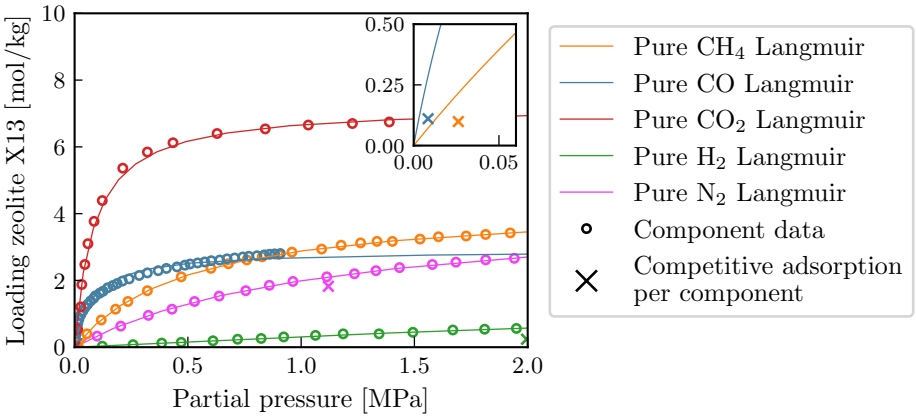

Figure B.18: Adsorbent loading on zeolite X13

C

Reactor sensitivity

C.1. ATR

C.1.1. α-sensitivity

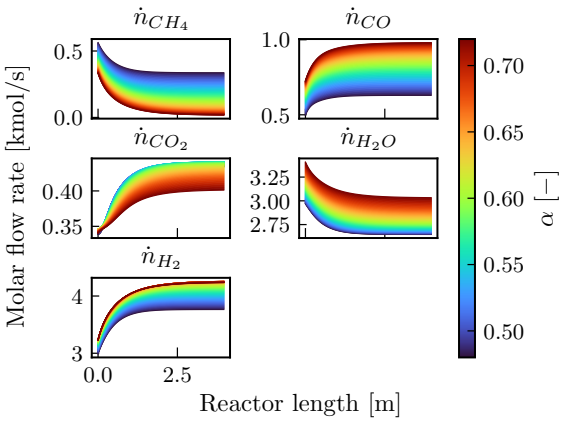

(a) Component composition sensitivity

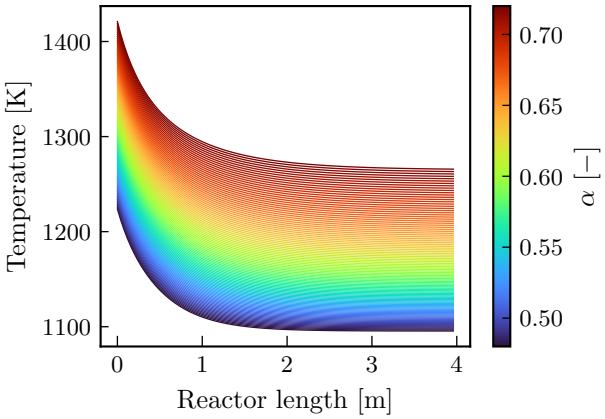

(b) Temperature profile sensitivity

Figure C.1: ATR sensitivity to α over the length of the reactor

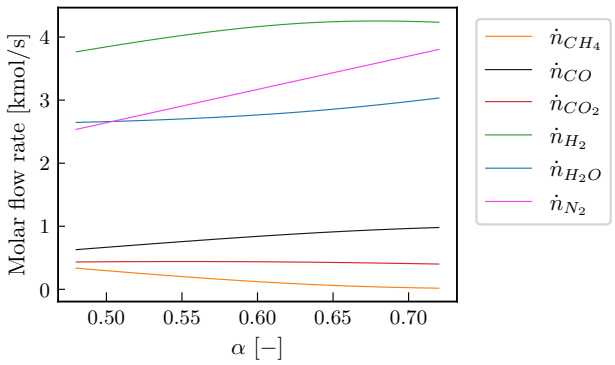

(a) ATR output molar flow rate per component

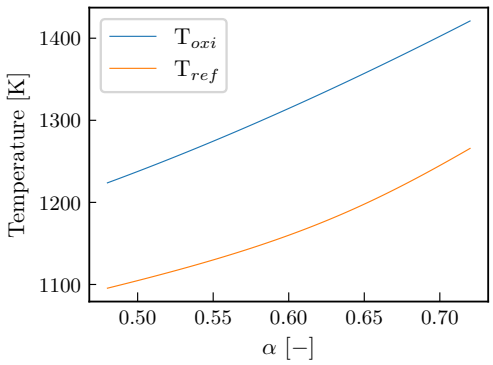

(b) Peak oxidation temperature and reformer output temperature

Figure C.2: ATR reactor output sensitivity for α

C.1.2. β-sensitivity

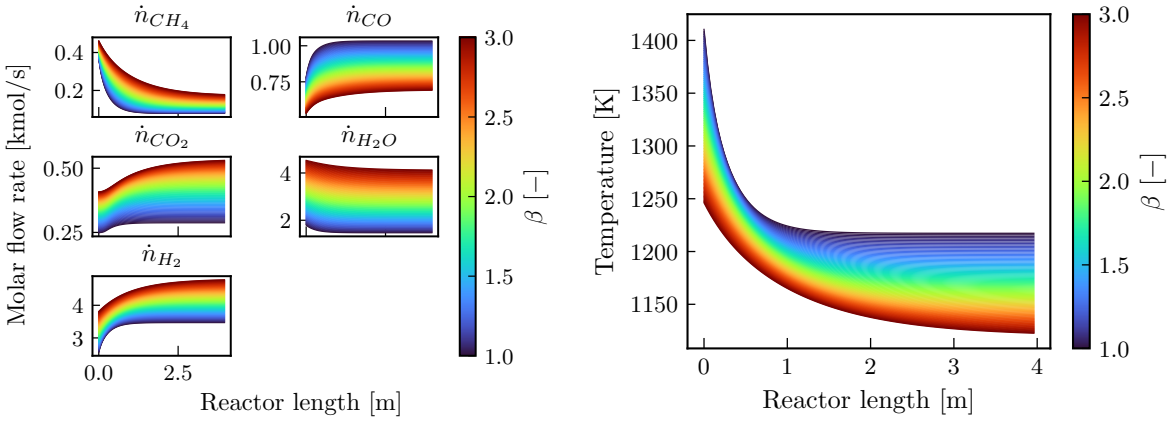

(a) Component composition sensitivity

(b) Temperature profile sensitivity

Figure C.3: ATR sensitivity to β over the length of the reactor

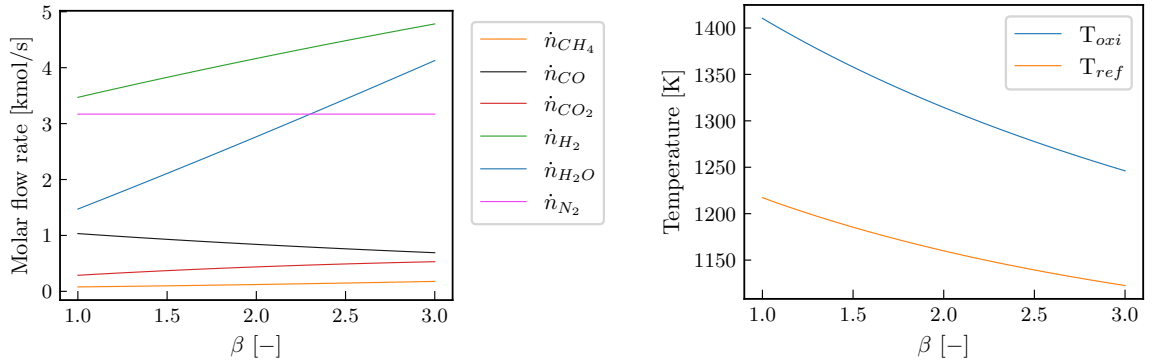

(a) ATR output molar flow rate per component

(b) Peak oxidation temperature and reformer output temperature

Figure C.4: ATR reactor output sensitivity for β

C.1.3. T_{in}-sensitivity

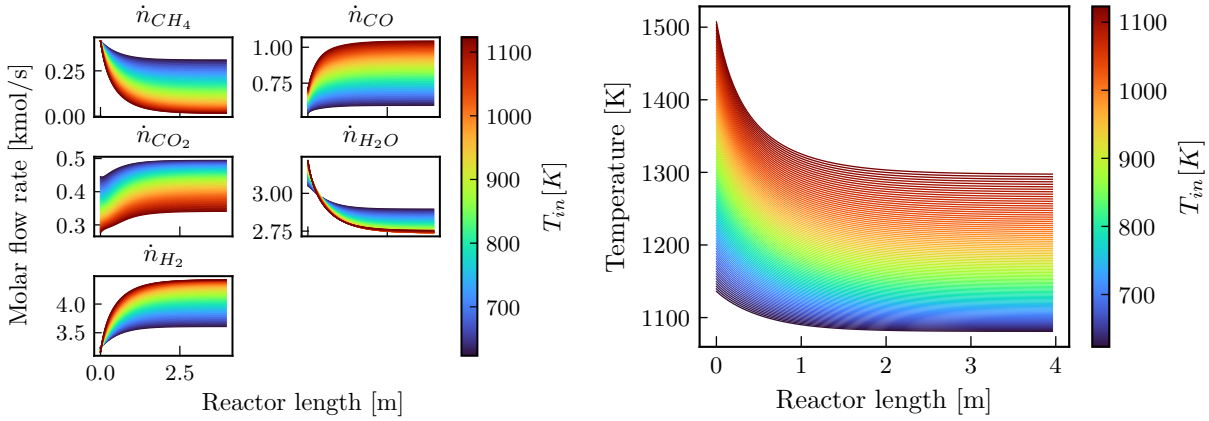

(a) Component composition sensitivity

(b) Temperature profile sensitivity

Figure C.5: ATR sensitivity to T_{in} over the length of the reactor

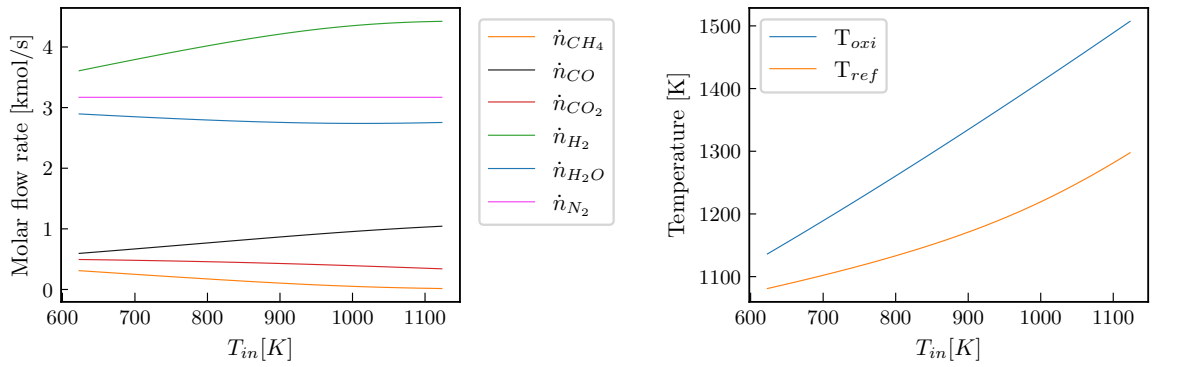

(a) ATR output molar flow rate per component

(b) Peak oxidation temperature and reformer output temperature

Figure C.6: ATR reactor output sensitivity for T_{in}

C.1.4. P_{in}-sensitivity

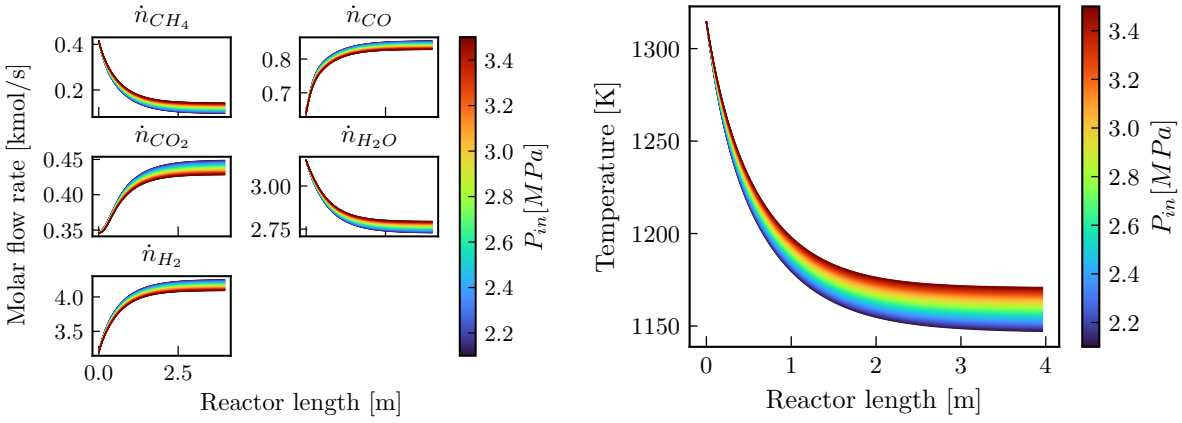

(a) Component composition sensitivity

(b) Temperature profile sensitivity

Figure C.7: ATR sensitivity to P_{in} over the length of the reactor

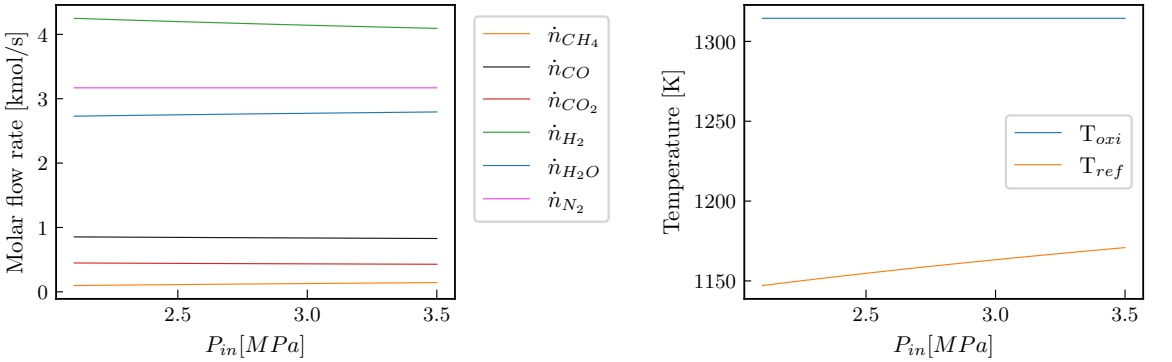

(a) ATR output molar flow rate per component

(b) Peak oxidation temperature and reformer output temperature

Figure C.8: ATR reactor output sensitivity for P_{in}

C.2. HTWGS

C.2.1. α-sensitivity

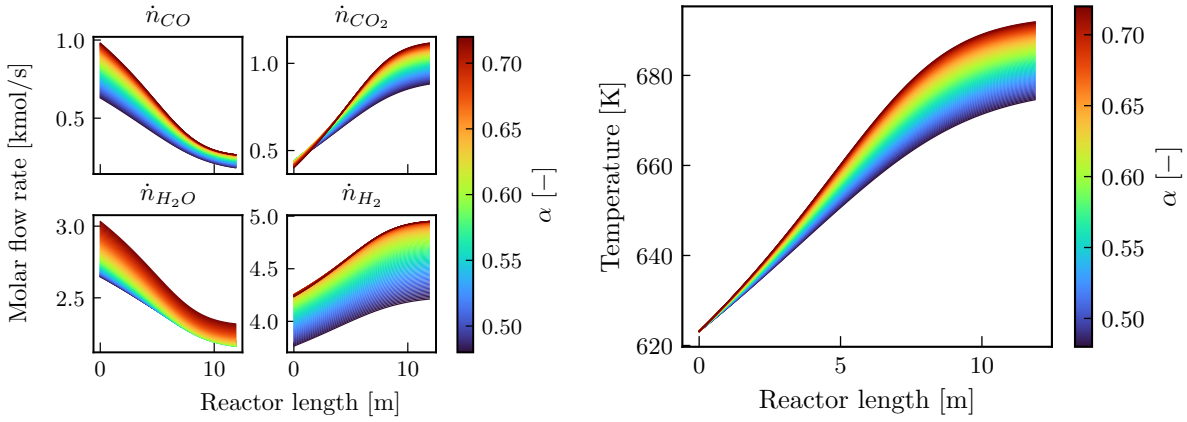

(a) Component composition sensitivity

(b) Temperature profile sensitivity

Figure C.9: HTWGS sensitivity to α over the length of the reactor

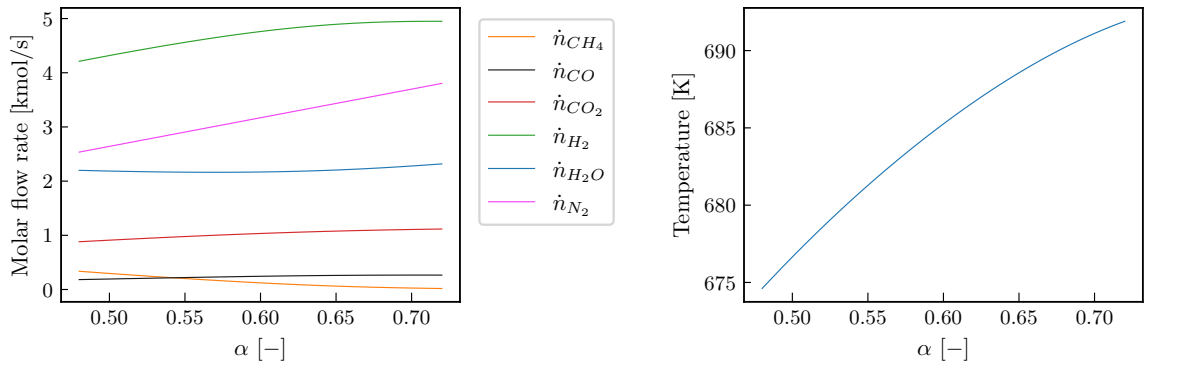

(a) HTWGS output molar flow rate per component

(b) HTWGS output temperature at input temperature of 623.15 K

Figure C.10: HTWGS reactor output sensitivity for α

C.2.2. β-sensitivity

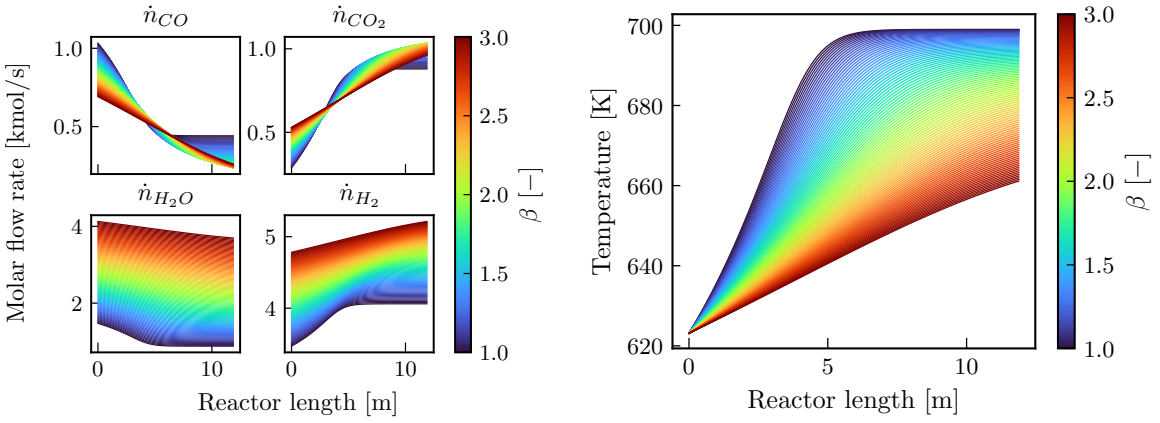

(a) Component composition sensitivity

(b) Temperature profile sensitivity

Figure C.11: HTWGS sensitivity to β over the length of the reactor

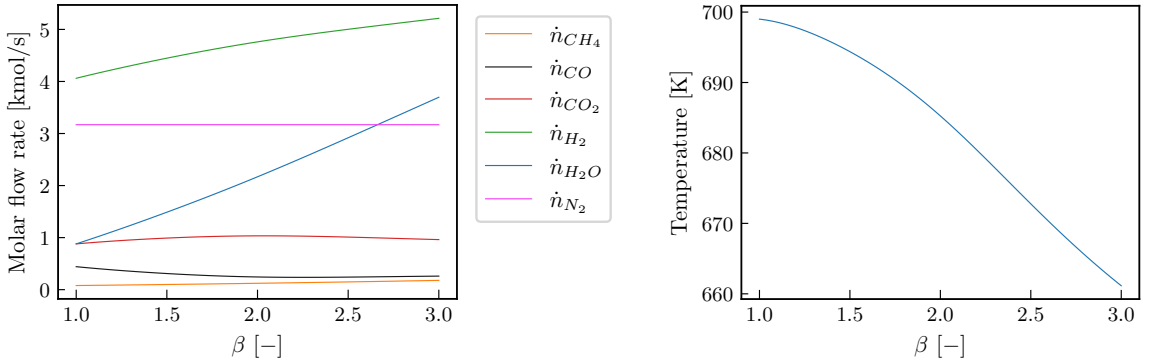

(a) HTWGS output molar flow rate per component

(b) HTWGS output temperature at input temperature of 623.15 K

Figure C.12: HTWGS reactor output sensitivity for β

C.2.3. T_{in}-sensitivity

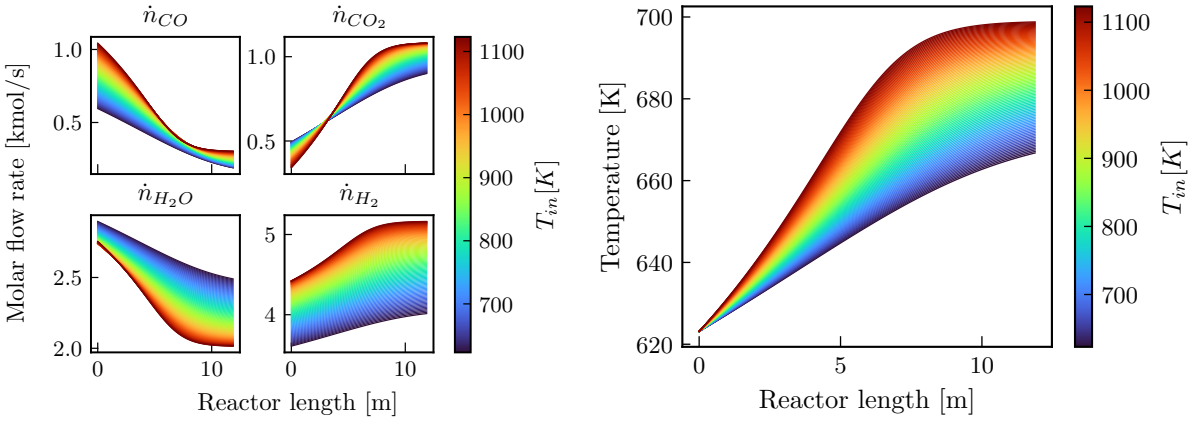

(a) Component composition sensitivity

(b) Temperature profile sensitivity

Figure C.13: HTWGS sensitivity to T_{in} over the length of the reactor

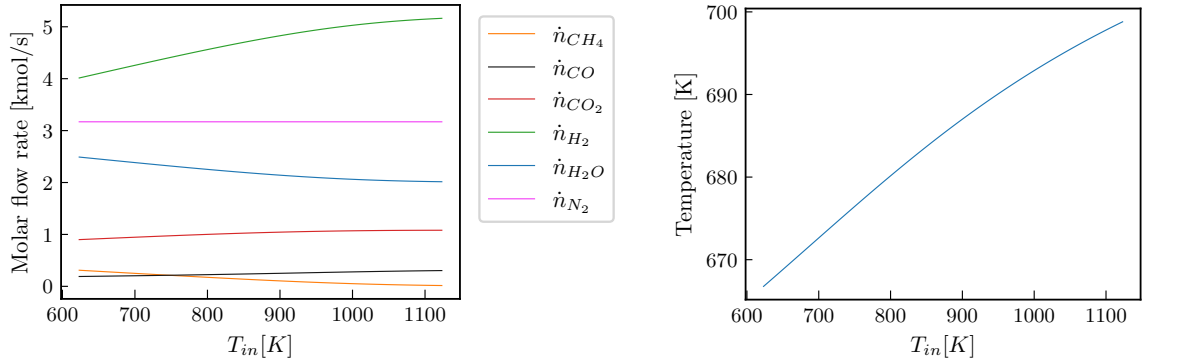

(a) HTWGS output molar flow rate per component

(b) HTWGS output temperature at input temperature of 623.15 K

Figure C.14: HTWGS reactor output sensitivity for T_{in}

C.2.4. P_{in}-sensitivity

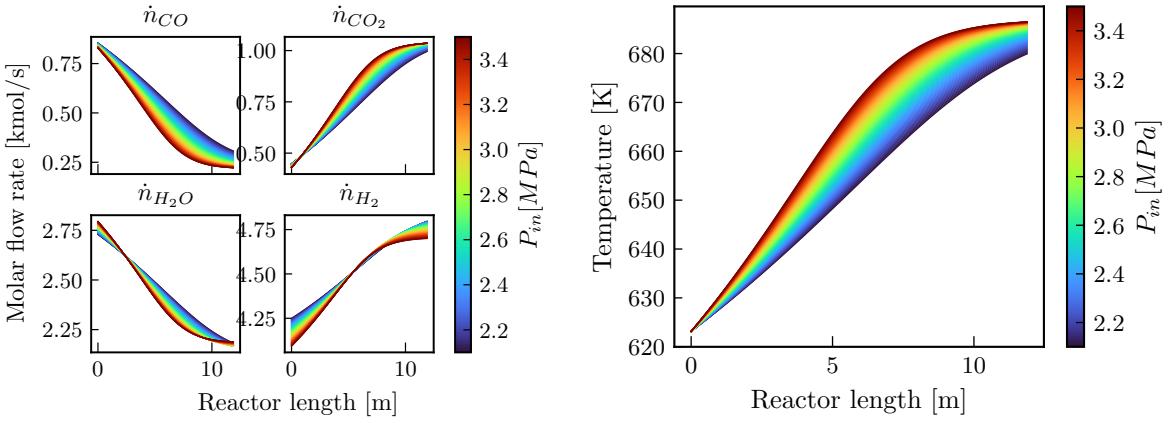

(a) Component composition sensitivity

(b) Temperature profile sensitivity

Figure C.15: HTWGS sensitivity to P_{in} over the length of the reactor

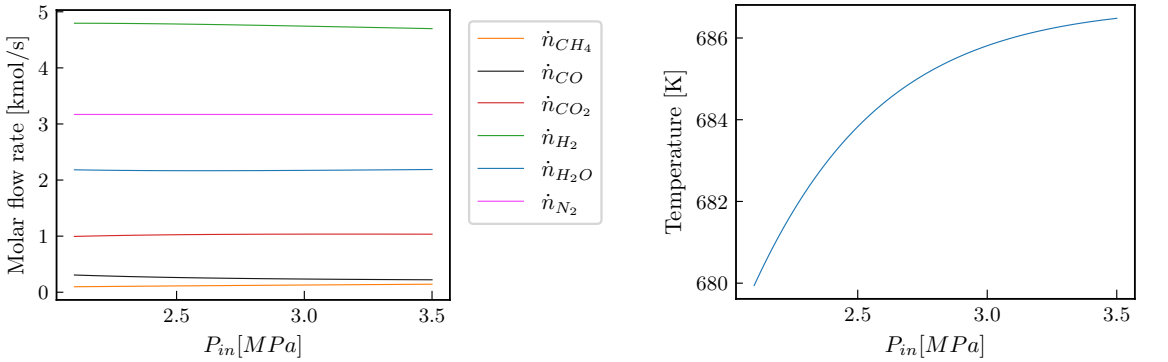

(a) HTWGS output molar flow rate per component

(b) HTWGS output temperature at input temperature of 623.15 K

Figure C.16: HTWGS reactor output sensitivity for P_{in}

C.3. LTWGS

C.3.1. α-sensitivity

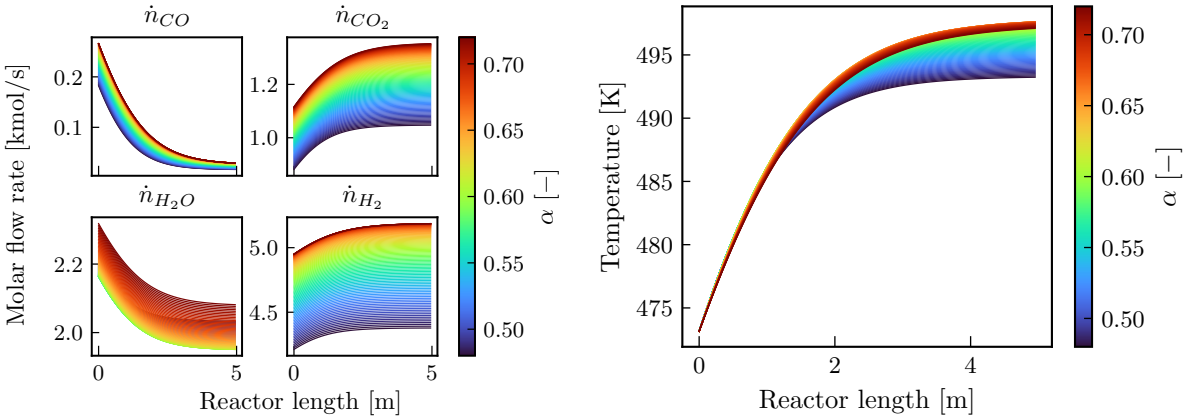

(a) Component composition sensitivity

(b) Temperature profile sensitivity

Figure C.17: LTWGS sensitivity to α over the length of the reactor

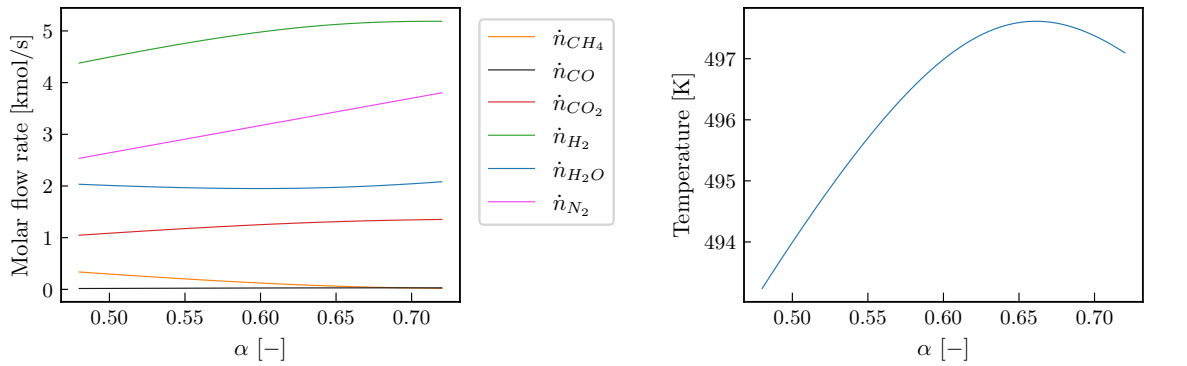

(a) LTWGS output molar flow rate per component

(b) LTWGS output temperature at input temperature of 473.15 K

Figure C.18: LTWGS reactor output sensitivity for α

C.3.2. β-sensitivity

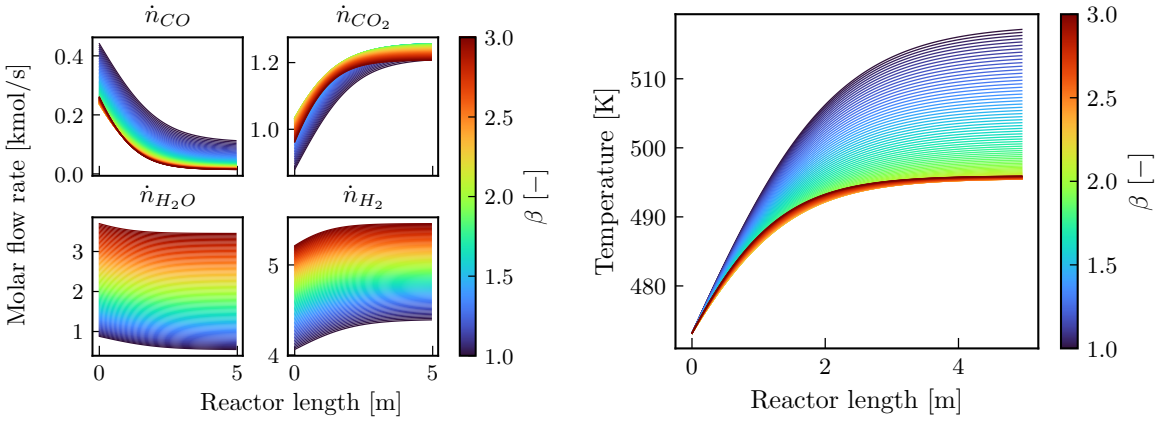

(a) Component composition sensitivity

(b) Temperature profile sensitivity

Figure C.19: LTWGS sensitivity to β over the length of the reactor

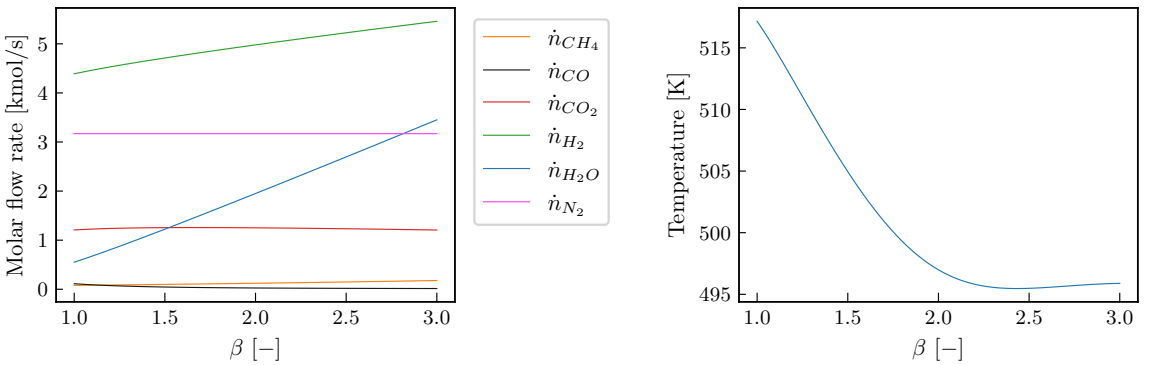

(a) LTWGS output molar flow rate per component

(b) LTWGS output temperature at input temperature of 473.15 K

Figure C.20: LTWGS reactor output sensitivity for β

C.3.3. T_{in}-sensitivity

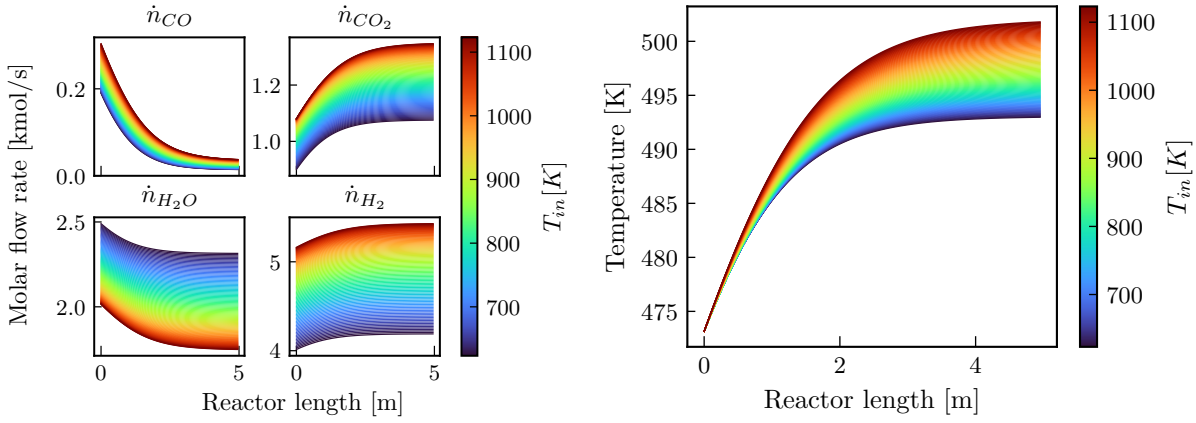

(a) Component composition sensitivity

(b) Temperature profile sensitivity

Figure C.21: LTWGS sensitivity to T_{in} over the length of the reactor

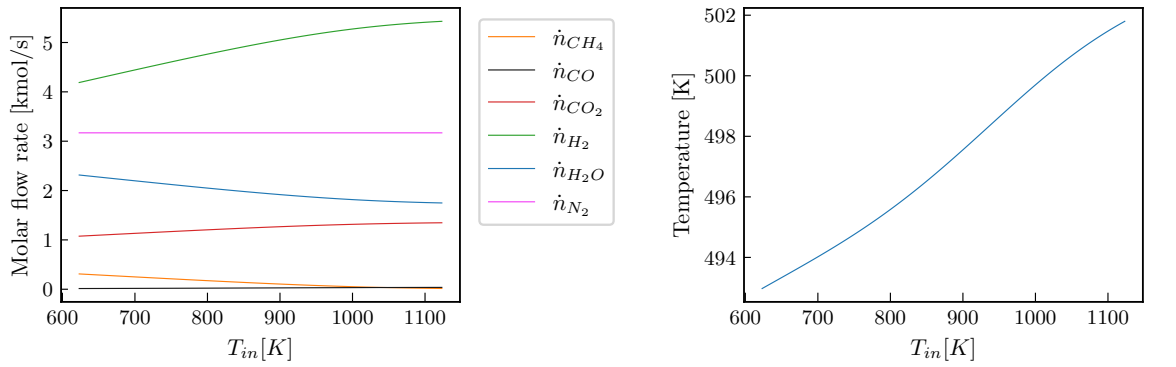

(a) LTWGS output molar flow rate per component

(b) Peak oxidation temperature and reformer output temperature

Figure C.22: LTWGS reactor output sensitivity for T_{in}

C.3.4. P_{in}-sensitivity

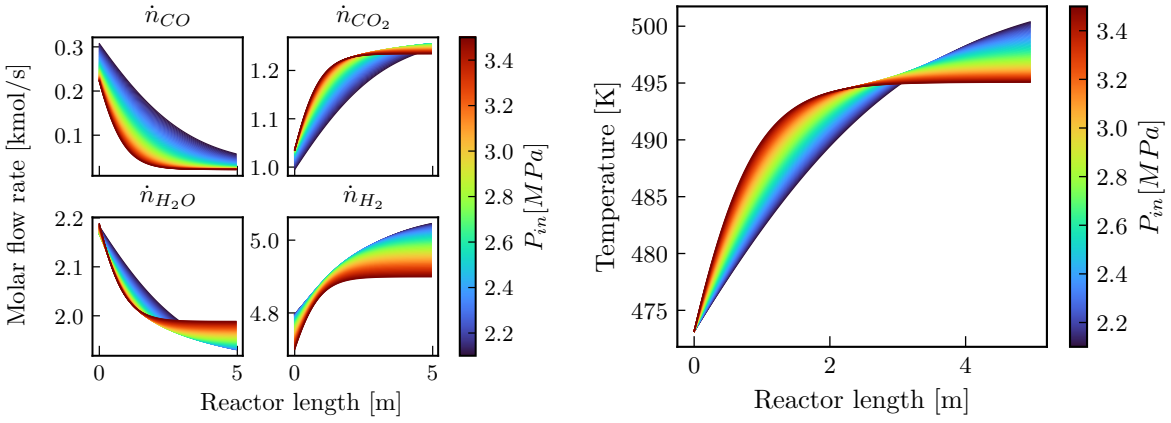

(a) Component composition sensitivity

(b) Temperature profile sensitivity

Figure C.23: LTWGS sensitivity to P_{in} over the length of the reactor

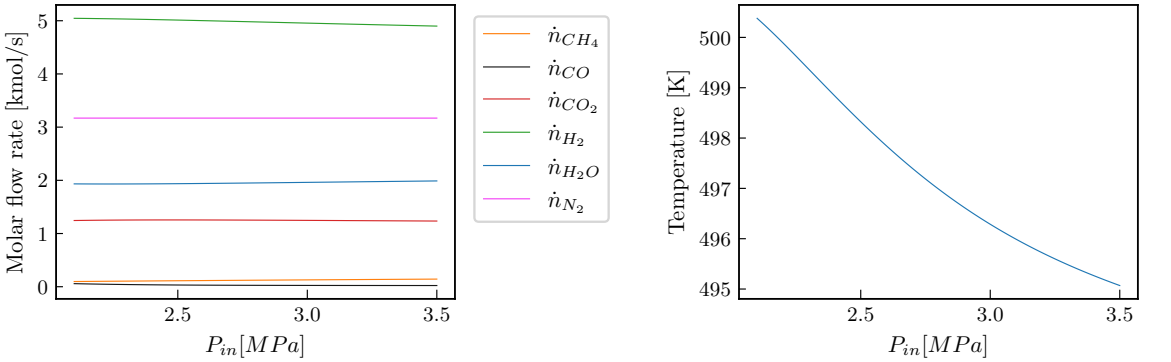

(a) LTWGS output molar flow rate per component

(b) LTWGS output temperature at input temperature of 473.15 K

Figure C.24: LTWGS reactor output sensitivity for P_{in}

C.4. Absorption tower and stripper

C.4.1. α-sensitivity

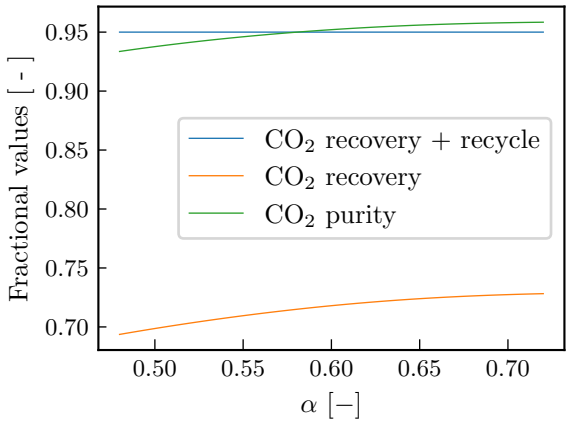

Figure C.25: Purity and recovery as a function of α

C.4.2. β-sensitivity

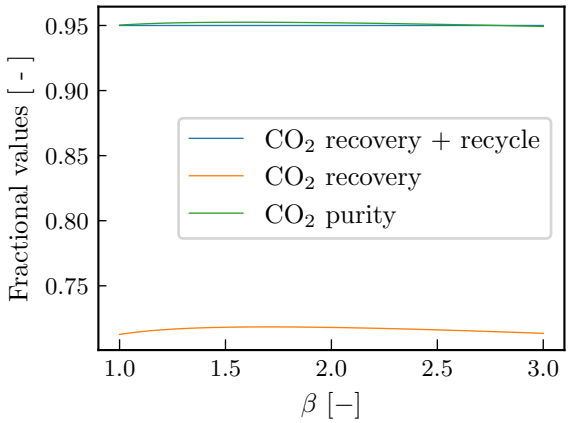

Figure C.26: Purity and recovery as a function of β

C.4.3. T_{in}-sensitivity

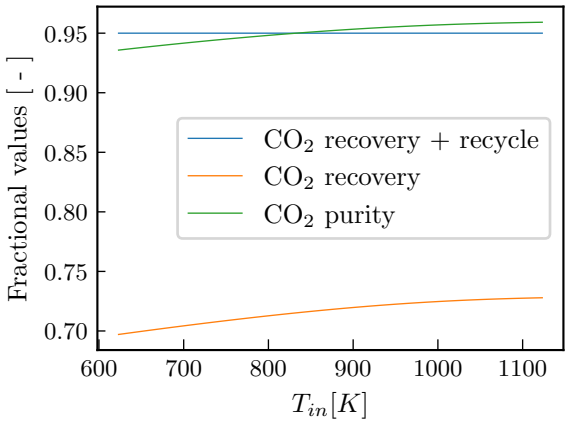

Figure C.27: Purity and recovery as a function of T_{in}

C.4.4. P_{in}-sensitivity

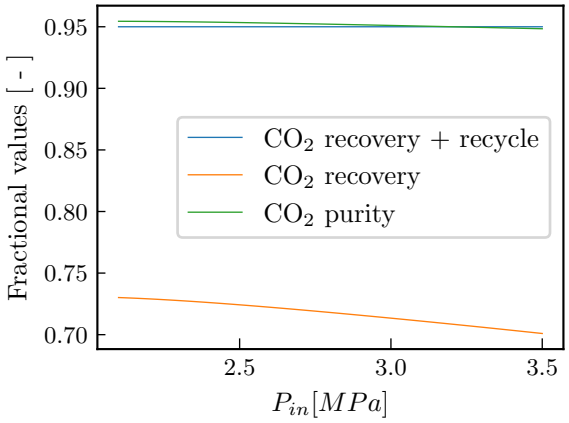

Figure C.28: Purity and recovery as a function of P_{in}

C.5. PSA

C.5.1. α-sensitivity

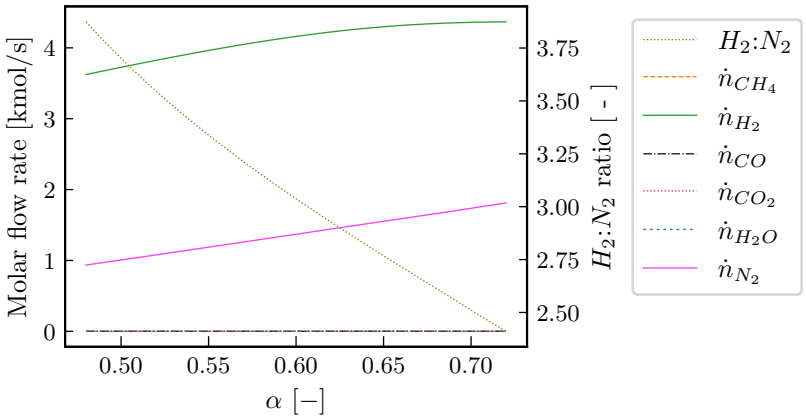

Figure C.29: Molar flow rates at the output of the PSA and the relative H_2:N_2 ratio (ratio 3 is preferential) as a function of α

C.5.2. β-sensitivity

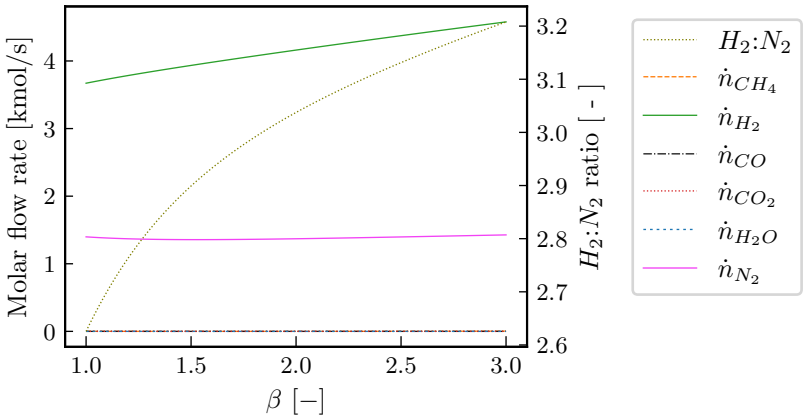

Figure C.30: Molar flow rates at the output of the PSA and the relative H_2:N_2 ratio (ratio 3 is preferential) as a function of β

C.5.3. T_{in}-sensitivity

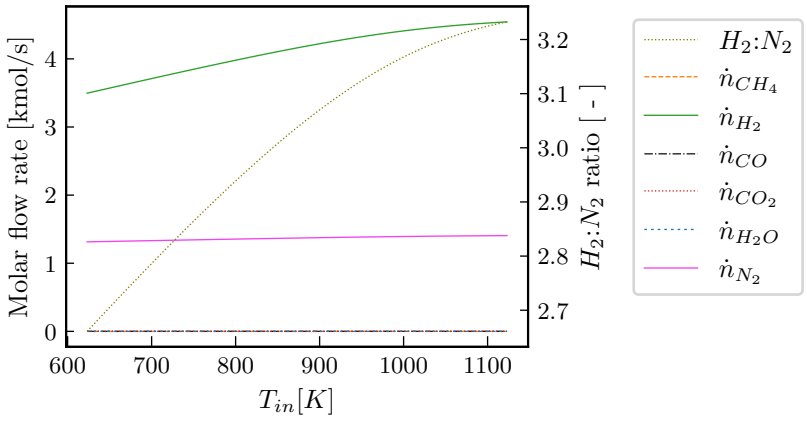

Figure C.31: Molar flow rates at the output of the PSA and the relative H_2:N_2 ratio (ratio 3 is preferential) as a function of T_{in}

C.5.4. P_{in}-sensitivity

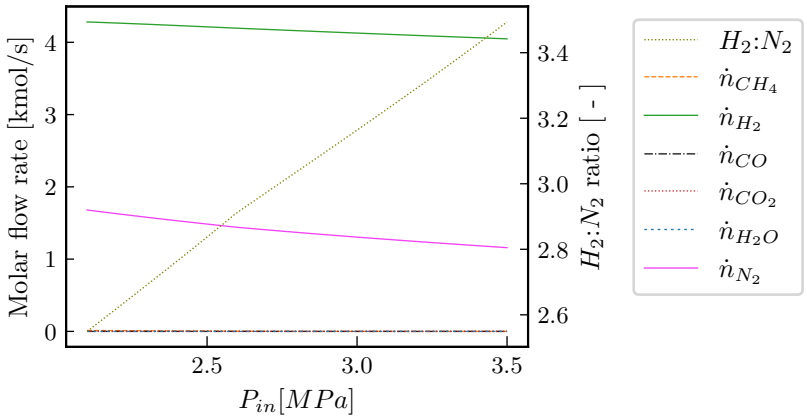

Figure C.32: Molar flowrates at the output of the PSA and the relative H_2:N_2 ratio (ratio 3 is preferential) as a function of P_{in}

C.6. Overall sensitivity

C.6.1. α-sensitivity

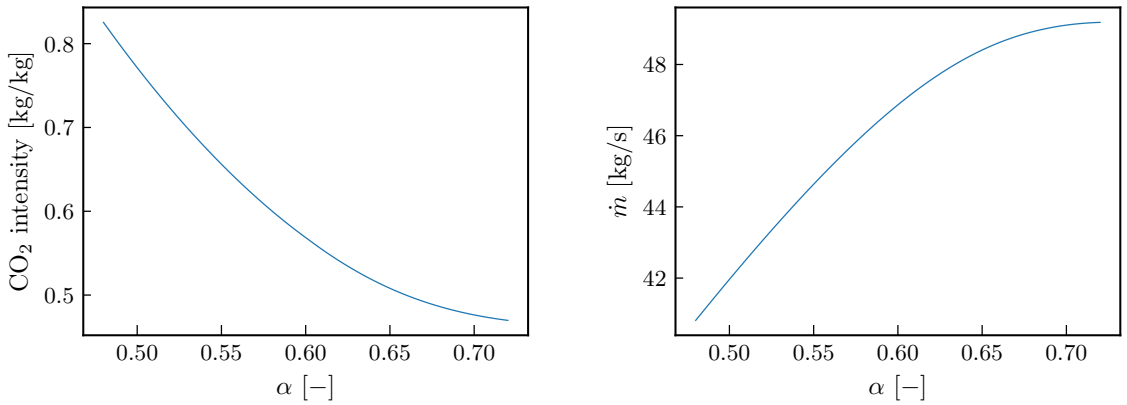

(a) System direct carbon emissions as a function of α (oxygen-to-carbon ratio)

(b) Mass flow rate of ammonia as a function of α (oxygen-to-carbon ratio)

Figure C.33: Influence of α (oxygen-to-carbon ratio) on system performance

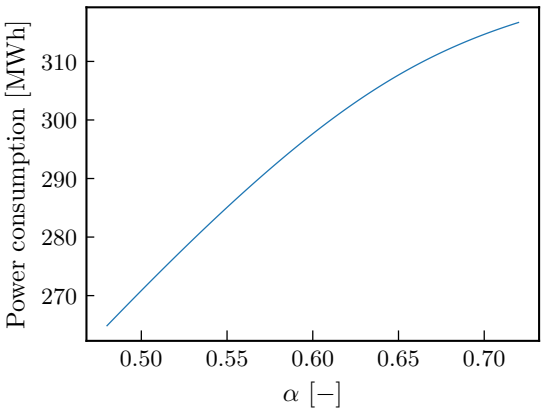

Figure C.34: System power consumption as a function of α (oxygen-to-carbon ratio)

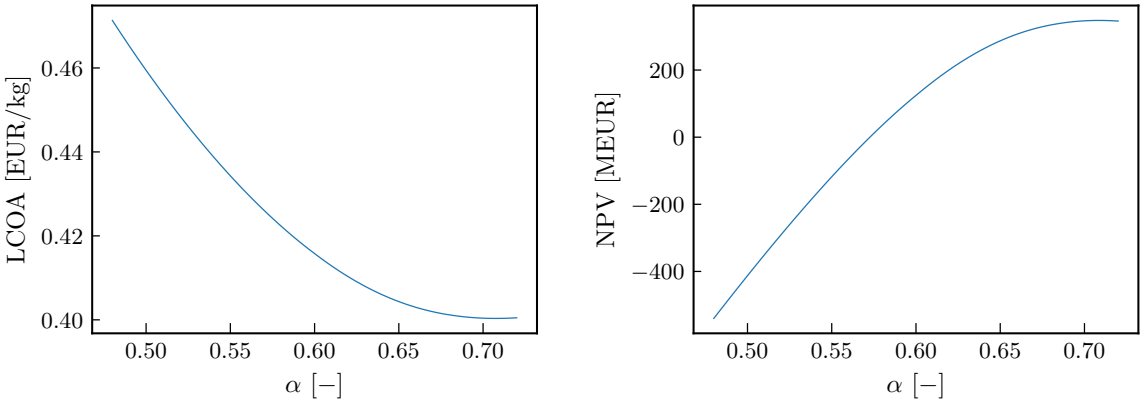

(a) LCOA as a function of α (oxygen-to-carbon ratio)

(b) NPV as a function of α (oxygen-to-carbon ratio)

Figure C.35: Influence of α (oxygen-to-carbon ratio) on the financial performance of the system

C.6.2. β-sensitivity

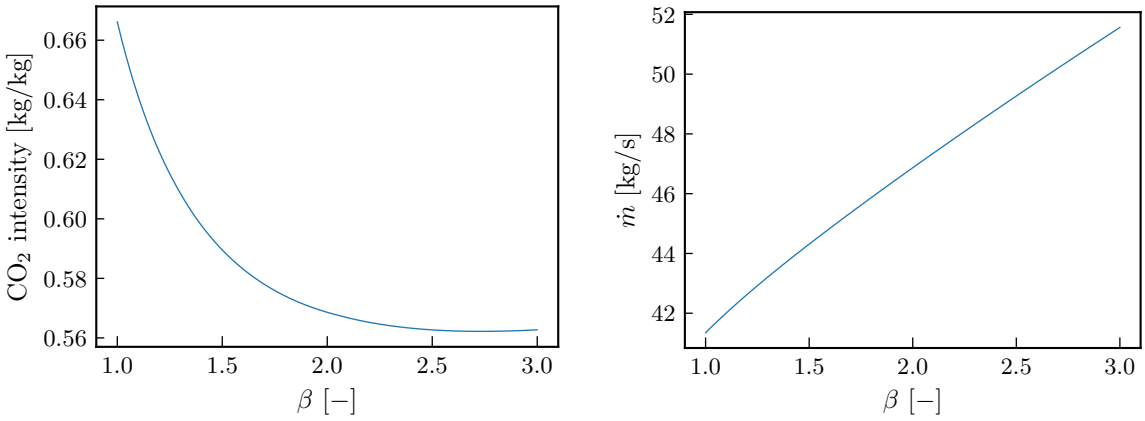

(a) System direct carbon emissions as a function of β

(b) Mass flow rate of ammonia as a function of β

Figure C.36: Influence of β on system performance

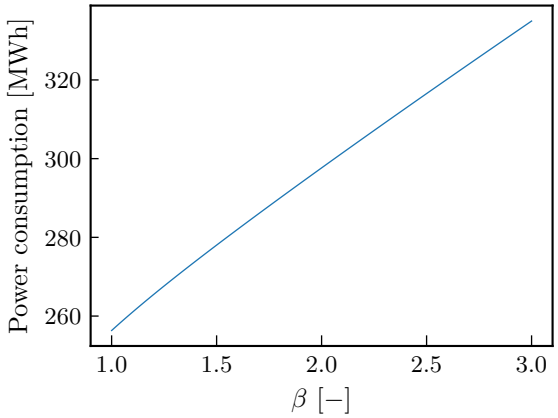

Figure C.37: System power consumption as a function of β

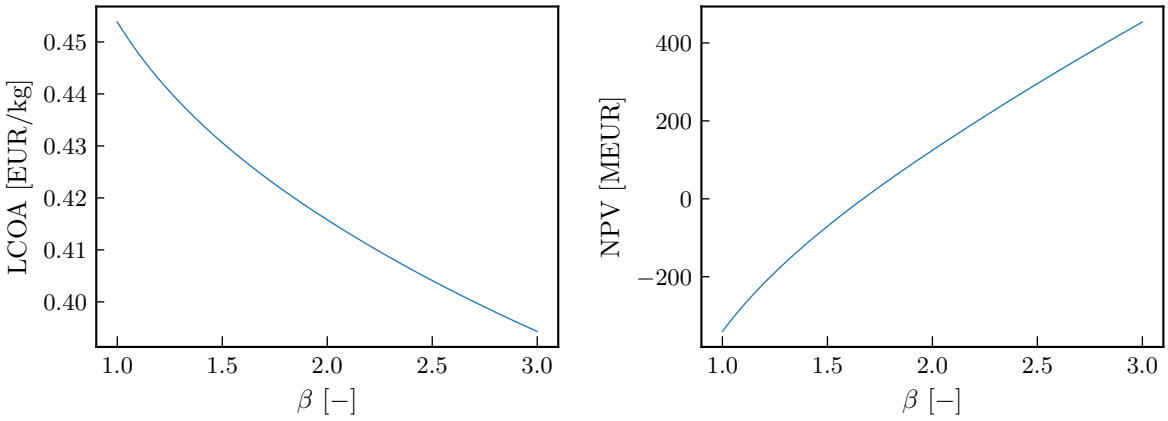

(a) LCOA as a function of β

(b) NPV as a function of β

Figure C.38: Influence of β on the financial performance of the system

C.6.3. T_{in}-sensitivity

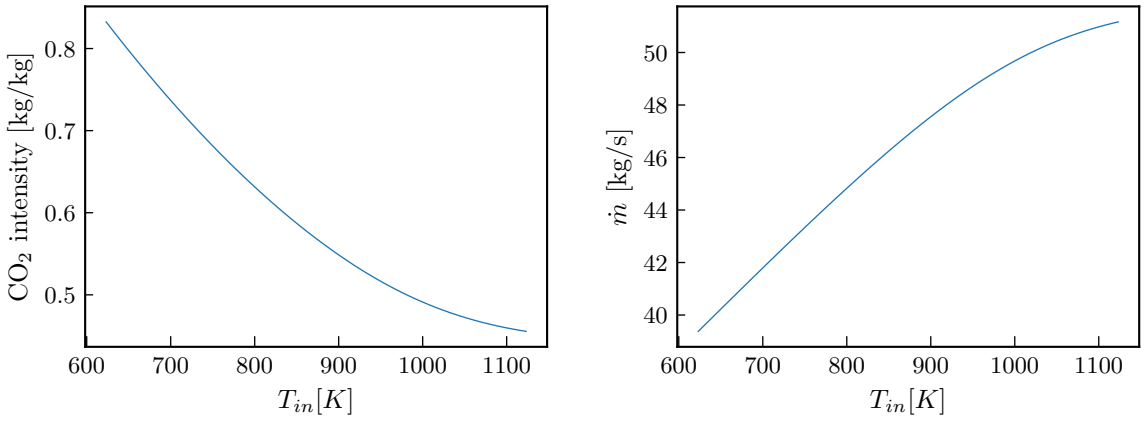

(a) System direct carbon emissions as a function of T_{in}

(b) Mass flow rate of ammonia as a function of T_{in}

Figure C.39: Influence of T_{in} on system performance

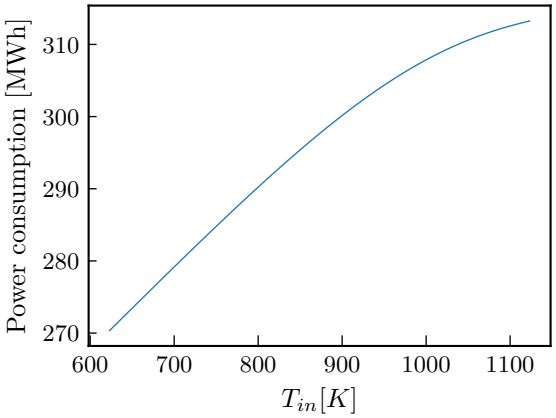

Figure C.40: System power consumption as a function of T_{in}

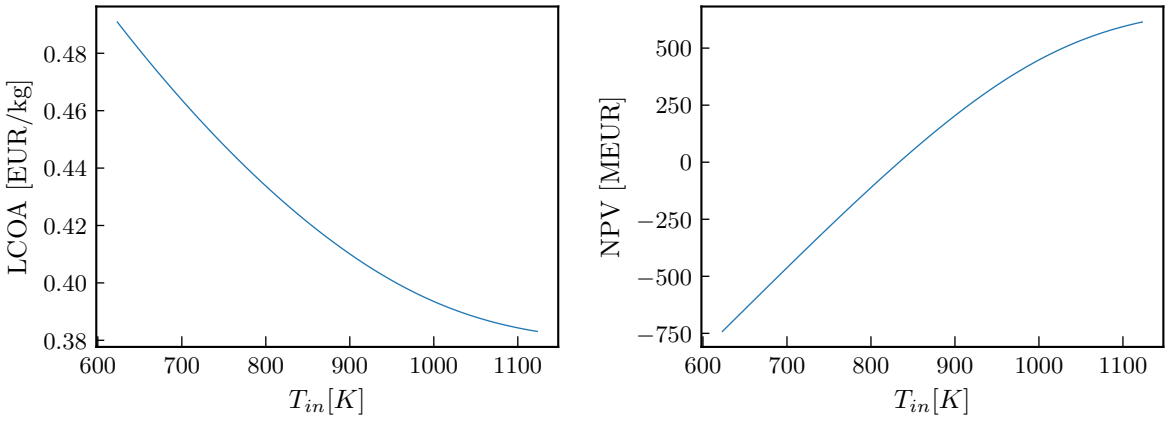

(a) LCOA as a function of T_{in}

(b) NPV as a function of T_{in}

Figure C.41: Influence of T_{in} on the financial performance of the system

C.6.4. P_{in}-sensitivity

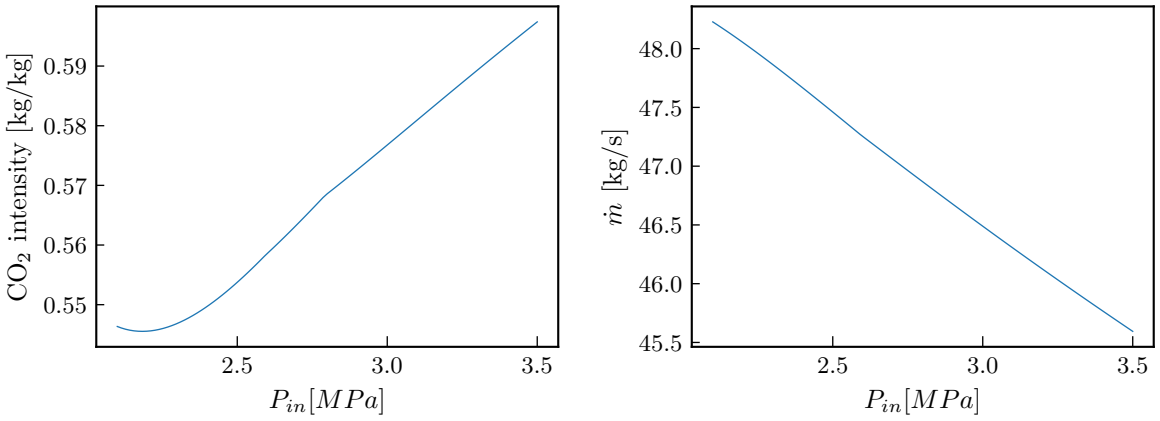

(a) System direct carbon emissions as a function of P_{in}

(b) Mass flow rate of ammonia as a function of P_{in}

Figure C.42: Influence of P_{in} on system performance

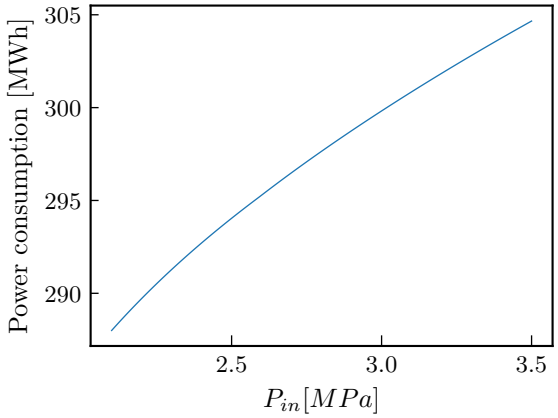

Figure C.43: System power consumption as a function of P_{in}

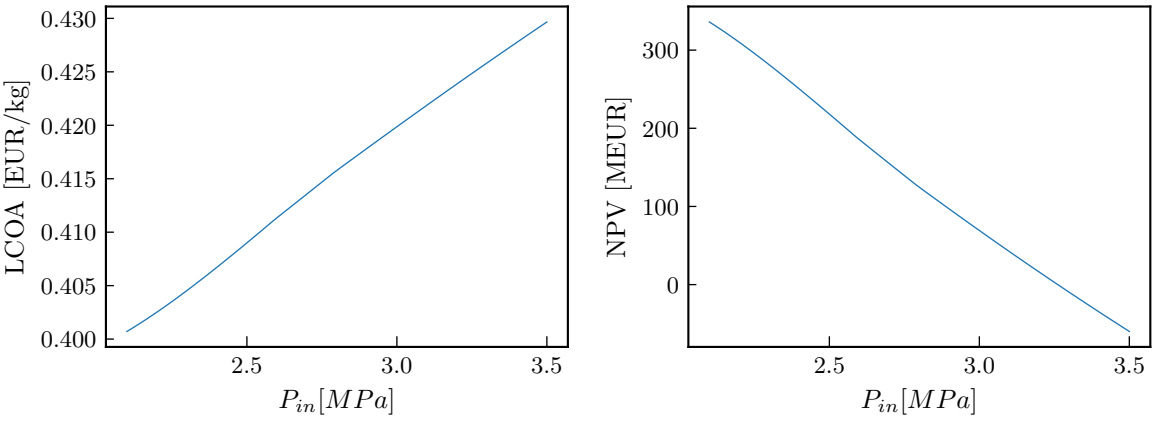

(a) LCOA as a function of P_{in}

(b) NPV as a function of P_{in}

Figure C.44: Influence of P_{in} on the financial performance of the system

D

Overall system performance and conditions

Table D.1: Component output molar flow rates in mol/s per process step.

Component	Input	ATR	HTWGS	LTWGS	Dehydration	Selexol absorption	PSA	Furnace	Haber-Bosch
CH_4	1400	122	122	122	122	113	0	113	0
CO	0	840	244	25	25	24	0	24	0
CO_2	0	437	1033	1253	1253	82	0	82	0
H_2	0	4164	4760	4980	4980	4909	4162	747	42
H_2O	2800	2765	2169	1949	0	0	0	0	0
N_2	3170	3170	3170	3170	3170	3100	1368	1732	0
O_2	840	0	0	0	0	0	0	0	0
NH_3	0	0	0	0	0	0	0	0	2752
Total	8210	11498	11498	11499	9550	8228	5530	2698	2793

Table D.2: Reactor input temperature and pressure

Process step	Input temperature [K]	Input Pressure [MPa]
ATR	873.15	2.8
HTWGS	623.15	2.65
LTWGS	473.15	2.55
Phys abs	298.15	2.45
PSA	298.15	2.45
NH3 synthesis	713.15	20.0
CO2 compression	298.15	3.5

E

Case study - Green versus Blue

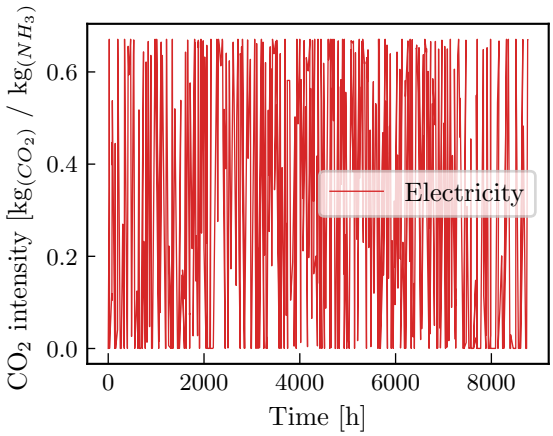

(a) Hourly carbon production of the process over the year for green hydrogen with an integrated windfarm, a 0 carbon intensity refers ammonia production from fully green electricity.

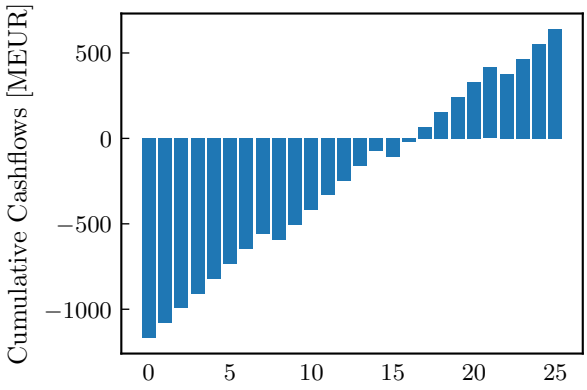

(b) Cumulative cash flow green ammonia, confirming the losses made at an NH_3 selling price of 0.419 €/kg.

Figure E.1: Green ammonia production relative carbon emissions and cumulative cashflows over its lifetime.

F

Case study - Dynamic operation

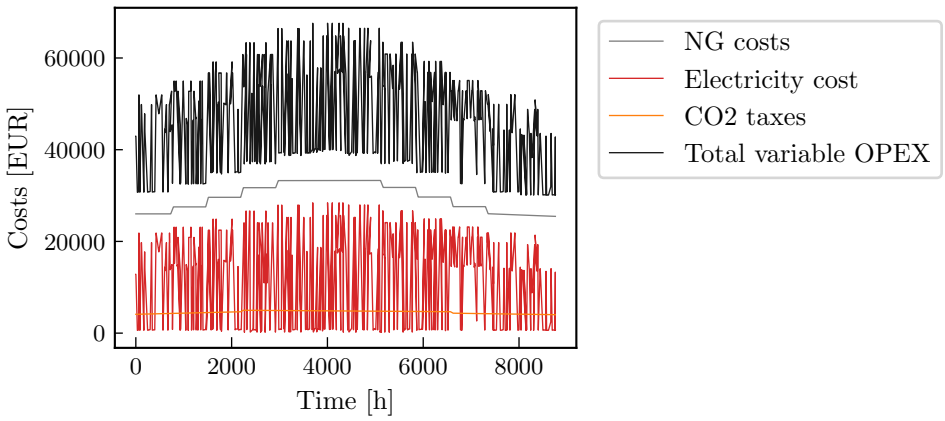

(a) Dynamic operation with fixed NG price of 22.64 €/MWh

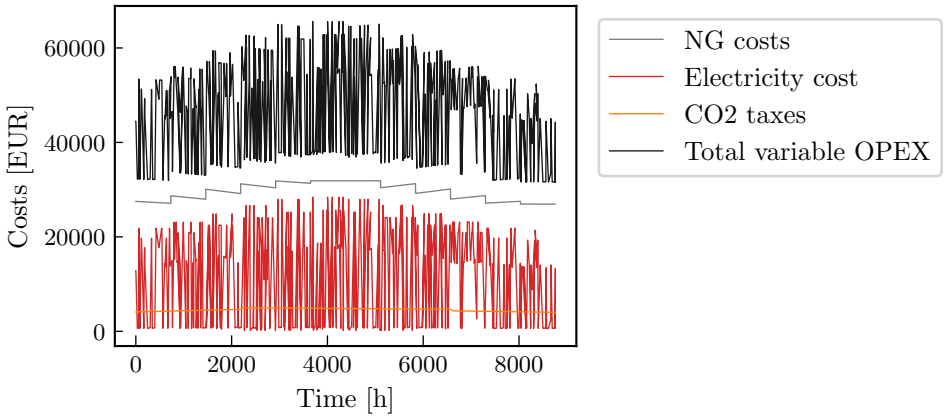

(b) Dynamic operation with seasonal NG price with amplitude 1.35 €/MWh around average 22.64 €/MWh NG price

Figure F.1: The different hourly Variable OPEX distributions

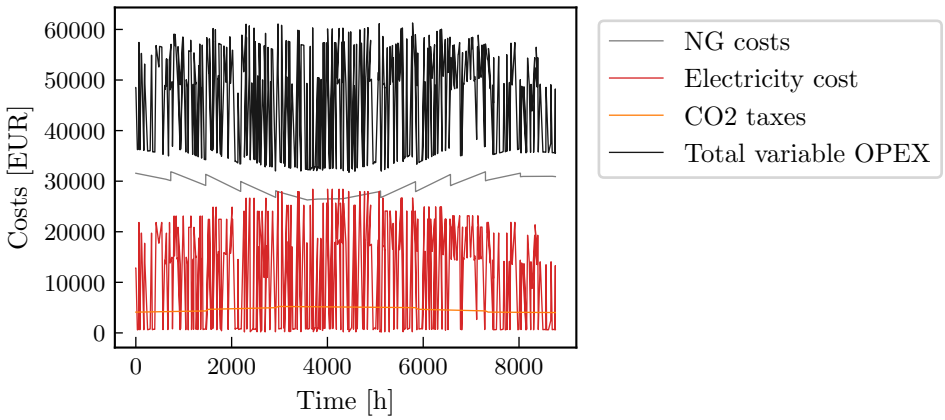

(a) Dynamic operation with seasonal NG price with amplitude 5 €/MWh around average 22.64 €/MWh NG price

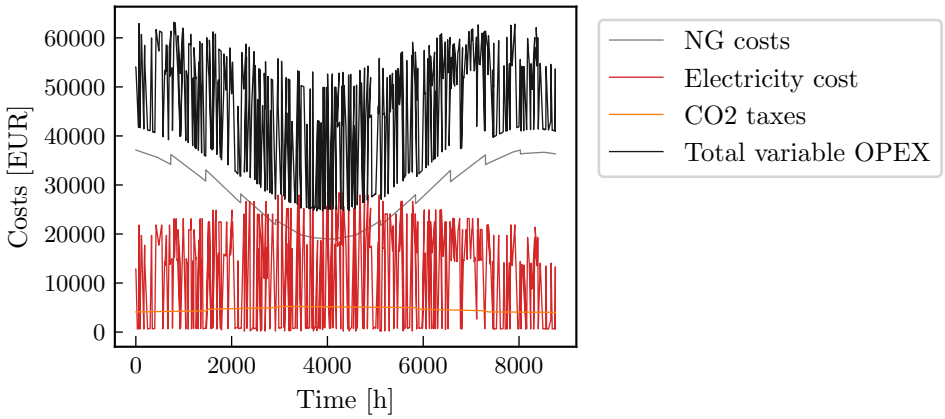

(b) Dynamic operation with seasonal NG price with amplitude 10 €/MWh around average 22.64 €/MWh NG price

Figure F.2: The different hourly Variable OPEX distributions per dynamic pricing scenario